



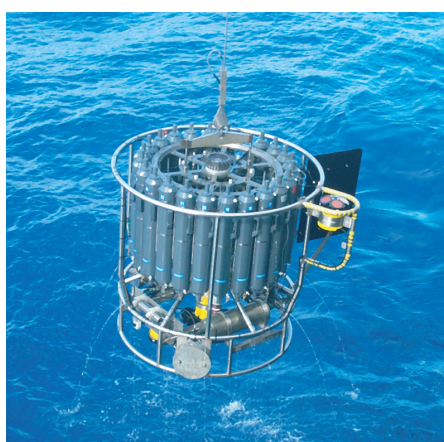
Max-Planck-Institut für Meteorologie  
*Max Planck Institute for Meteorology*



MAX-PLANCK-GESELLSCHAFT

# Interactions between Climate and Land Cover Changes on the Tibetan Plateau

Xuefeng Cui



Berichte zur Erdsystemforschung  $\frac{17}{2005}$

*Reports on Earth System Science*

## Hinweis

Die Berichte zur Erdsystemforschung werden vom Max-Planck-Institut für Meteorologie in Hamburg in unregelmäßiger Abfolge herausgegeben.

Sie enthalten wissenschaftliche und technische Beiträge, inklusive Dissertationen.

Die Beiträge geben nicht notwendigerweise die Auffassung des Instituts wieder.

Die "Berichte zur Erdsystemforschung" führen die vorherigen Reihen "Reports" und "Examensarbeiten" weiter.

## Notice

*The Reports on Earth System Science are published by the Max Planck Institute for Meteorology in Hamburg. They appear in irregular intervals.*

*They contain scientific and technical contributions, including Ph. D. theses.*

*The Reports do not necessarily reflect the opinion of the Institute.*

*The "Reports on Earth System Science" continue the former "Reports" and "Examensarbeiten" of the Max Planck Institute.*



## Anschrift / Address

Max-Planck-Institut für Meteorologie  
Bundesstrasse 53  
20146 Hamburg  
Deutschland

Tel.: +49-(0)40-4 11 73-0  
Fax: +49-(0)40-4 11 73-298  
Web: [www.mpimet.mpg.de](http://www.mpimet.mpg.de)

## Layout:

Bettina Diallo, PR & Grafik

Titelfotos:

vorne:

Christian Klepp - Jochem Marotzke - Christian Klepp

hinten:

Katsumasa Tanaka - Christian Klepp - Clotilde Dubois

# Interactions between Climate and Land Cover Changes on the Tibetan Plateau

Dissertation zur Erlangung des Doktorgrades der Naturwissenschaften  
im Fachbereich Geowissenschaften der Universität Hamburg  
vorgelegt von

**Xuefeng Cui**  
aus China

Hamburg 2005

Xuefeng Cui  
Max-Planck-Institut für Meteorologie  
Bundesstrasse 53  
20146 Hamburg  
Germany

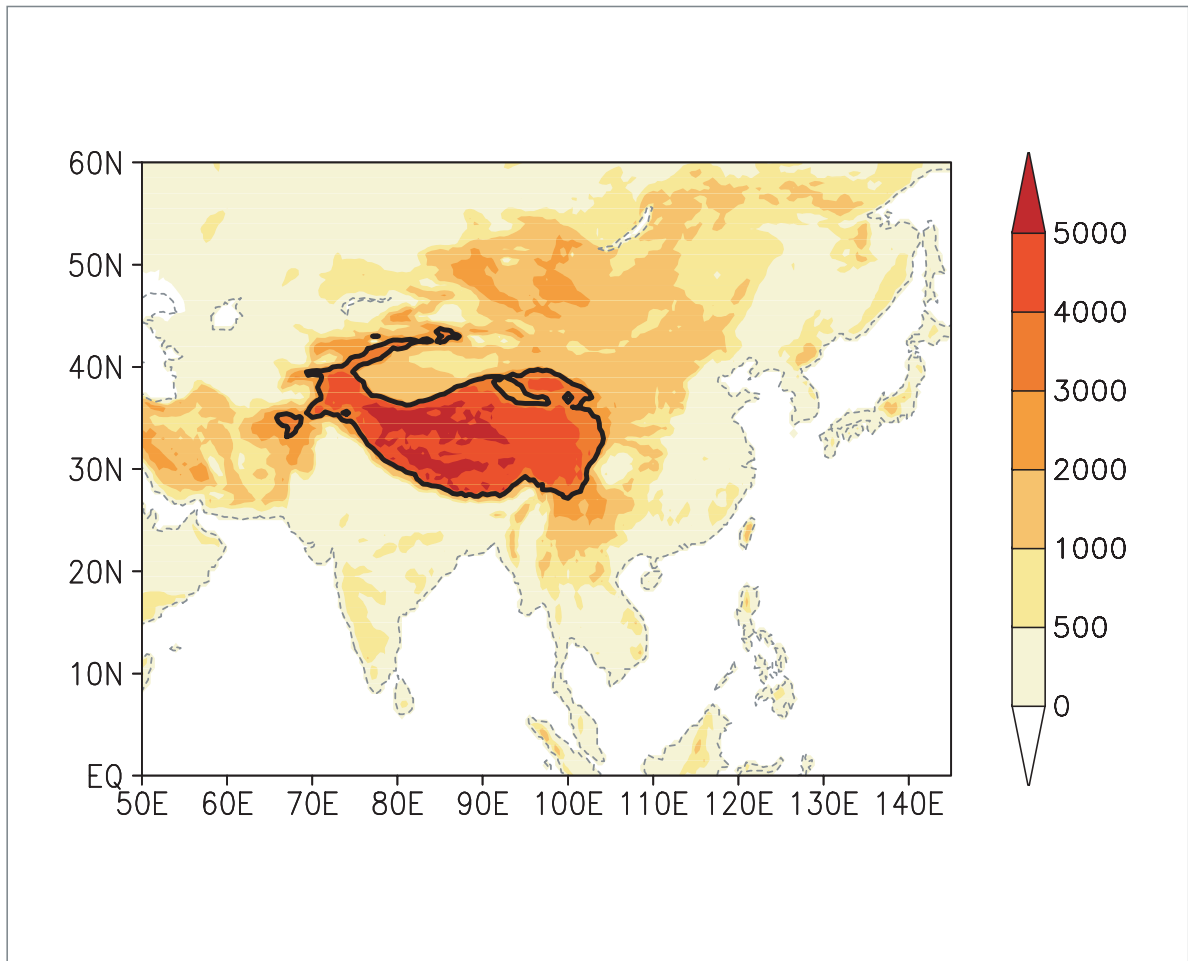
Als Dissertation angenommen  
vom Fachbereich Geowissenschaften der Universität Hamburg

auf Grund der Gutachten von  
Prof. Dr. Hartmut Graßl  
und  
Prof. Dr. Hans Graf

Hamburg, den 12. Dezember 2005  
Professor Dr. Helmut Schleicher  
Dekan des Fachbereiches Geowissenschaften

# Interactions between Climate and Land Cover Changes on the Tibetan Plateau

---



**Xuefeng Cui**

Hamburg 2005



## Contents

### **I. Introduction**

1.1 Atmospheric Implications of the Tibetan Plateau.....	1
1.2 Surface Climate on the Tibetan Plateau.....	6
1.2.1 Surface Temperature.....	6
1.2.2 Precipitation.....	7
1.2.3 Climate Change on the Tibetan Plateau.....	8
1.3 Land Cover Change on the Tibetan Plateau.....	10
1.4 Motivations of the Thesis.....	12
1.5 Outline of the Thesis.....	13
Reference.....	14

### **II. Climate Impacts of Anthropogenic Land Use**

#### **Changes on the Tibetan Plateau.....19**

2.1 Introduction.....	19
2.2 Model and Experiments.....	22
2.3 Results.....	29
2.3.1 ECHAM5 Current Scenario.....	29
2.3.2 ECHAM5 Natural Scenario.....	35
2.4 Conclusion and Discussions.....	46
References.....	47

### **III. Deforestation/Reforestation at the Southeast Tibetan Plateau. Part I: Impacts on Current Climate.....51**

3.1 Introduction.....	51
3.2 Model and Experiments.....	55
3.3. Results.....	59
3.3.1. Evaluation of the ECHAM5 Model.....	59
3.3.2. Impacts of Vegetation Change on Climate.....	64
a) Local and Regional Impacts.....	64
b) Global Perspective.....	67
3.4 Conclusion.....	73
References.....	74

<b>IV. Deforestation/Reforestation at the Southeast Tibetan Plateau. Part II: Compounding Effects with Greenhouse Warming Climate.....</b>	<b>79</b>
4.1 Introduction.....	79
4.2 Model and Experimental Setup.....	81
4.3 Doubled CO <sub>2</sub> Warming Climate.....	82
4.4. Impacts of Deforestation in a Greenhouse-warmed Climate.....	85
4.5 Joint Impacts of Deforestation and Doubled CO <sub>2</sub> Concentration...	90
4.6 Conclusions.....	95
References.....	97
<b>V. Application of the Regional Climate Model REMO on the Tibetan Plateau.....</b>	<b>99</b>
5.1 Introduction.....	99
5.2 Model and Experimental Setup.....	101
5.3 Validation Datasets.....	103
5.4 Results.....	105
5.5 Conclusions and Discussions.....	111
References.....	114
<b>VI. Conclusions and Outlook.....</b>	<b>117</b>
6.1 Conclusions.....	117
6.2 Outlook.....	119
References.....	120
<b>Acknowledgement.....</b>	<b>121</b>

## **Abstract**

Climatic impacts of land cover changes on the Tibetan Plateau, which happened extensively during the last half century, are investigated through numerical simulations with the atmospheric general circulation model ECHAM5. The control simulation demonstrates a reasonable production of the large-scale characteristics of seasonal climate in the Asian region in terms of atmospheric circulation and surface climate. A sensitivity experiment with current land cover over the Tibetan Plateau replaced by non-anthropogenic land cover reveals a drier and warmer climate on the Tibetan Plateau and remote impacts on the Indian and East Asian monsoon. Global implications are small, however with larger regional effects. Another experiment with forest replacement at the southeast Tibetan Plateau is conducted to investigate the climate influences of deforestation. It turns out that evaporation is decreased and precipitation is increased at the deforested areas, pointing to increased runoff and influences downstream. Deforestation at the southeast Tibetan Plateau leads to a warmer Indian continent throughout the year, whereas South China is cooler and wetter in spring. We also found remote impacts of land cover changes on the Tibetan Plateau mainly through teleconnections in atmospheric circulation changes. By simulation of deforestation influences at the southeast Tibetan Plateau under warmer climate conditions assuming doubled atmospheric CO<sub>2</sub> concentration, it is found that the impacts of deforestation are non-linearly modulated by the warmer climate condition.

For downscaling global climate model results the regional climate model REMO is applied over the Tibetan Plateau. Summer 1998 is chosen as a case study and a “double-nesting” technique is implemented. Results reveal that REMO can represent reasonably well the regional characteristics in terms of atmospheric circulation and surface climate when “perfect boundaries” are provided. REMO is able to produce daily precipitation as well as the onset of the monsoonal rainfall on the Tibetan Plateau. For future studies, it is suggested to apply the REMO/ECHAM5 nesting system to understand the climate impacts of land cover changes on the Tibetan Plateau by providing more realistic local responses and transferring global scale information.



# Chapter I: Introduction

## 1.1 Atmospheric Implications of the Tibetan Plateau

One of the cleanest places in the world, the Tibetan Plateau (hereafter referred to as TP) is a huge mountainous area in the Eurasian continent, with  $1 \times 10^6 \text{ km}^2$  area and an averaged altitude of 4000m (see Figure 1.1). Because of its height and size, it plays an important role in determining the formation and variation of regional weather and climate in East and South Asia, as well as the Northern Hemisphere atmospheric circulation in general (e.g. Manabe and Terpestra 1974; Manabe and Broccoli 1990; Tang et al. 1998; Ye and Wu 1998; Zhou et al. 2000). Following Ye and Gao (1979) and other studies, the effects of the TP on the atmosphere are divided into three major categories as follows:

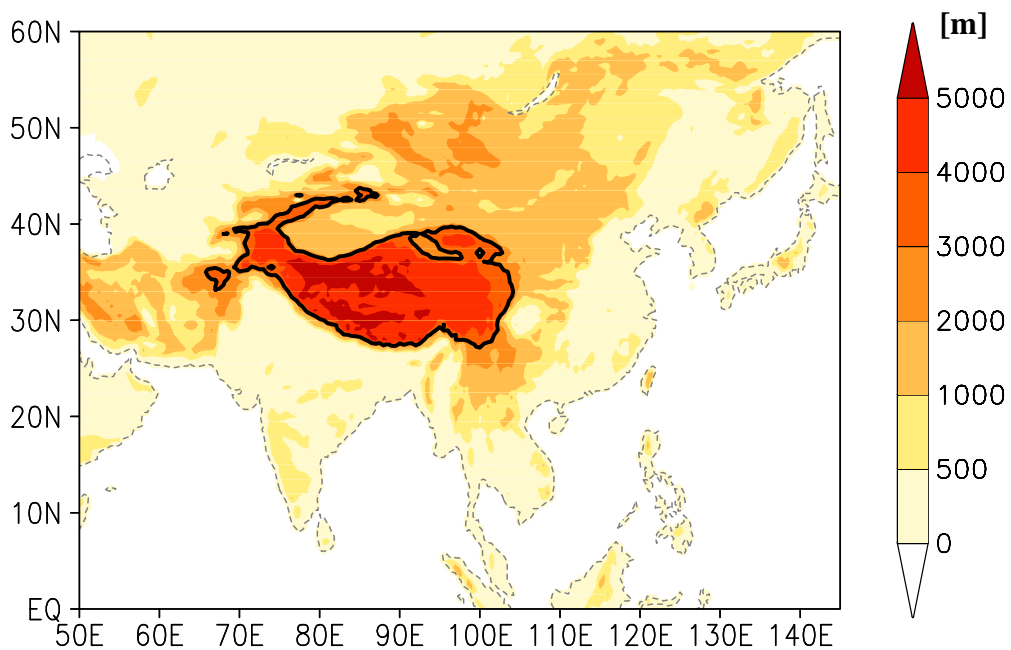


Figure 1.1 Geographic map of the Tibetan Plateau shown from global gridded elevation and bathymetry (ETOPO30) data at 0.5 degree resolution. The Tibetan Plateau is referred to in this study as the area where elevation is higher than 3000m above sea level (a. s. l.) shown as thick black contour line.

**i) Dynamic Effect:** The TP exerts dynamic orographic blocking effects on zonal and meridional air motions by its presence and shape, resulting in strong horizontal and vertical perturbations of atmospheric flows (e.g. Ye and Gao 1979).

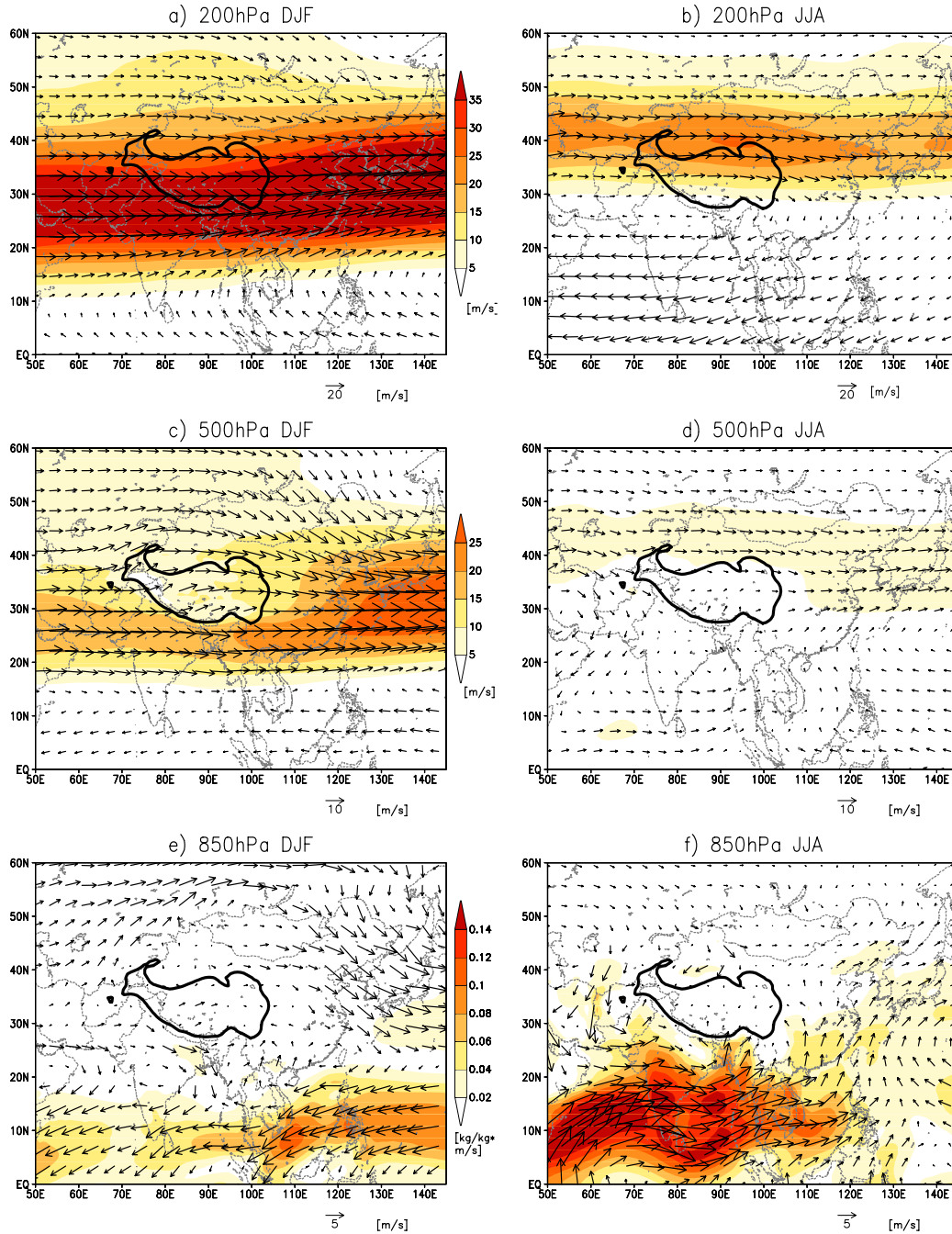
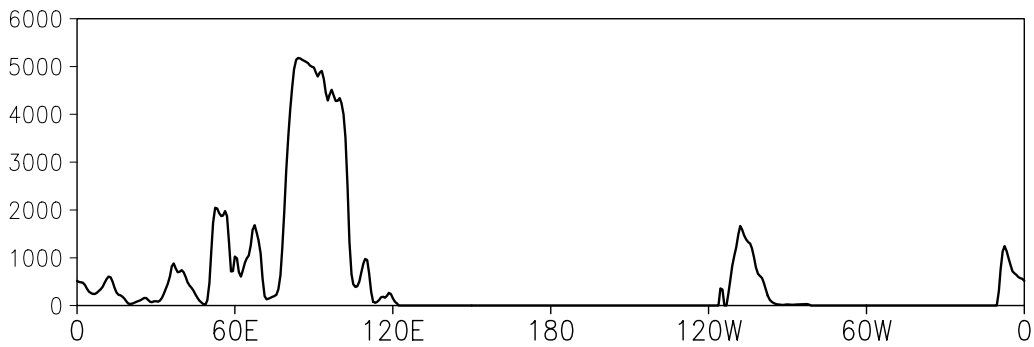
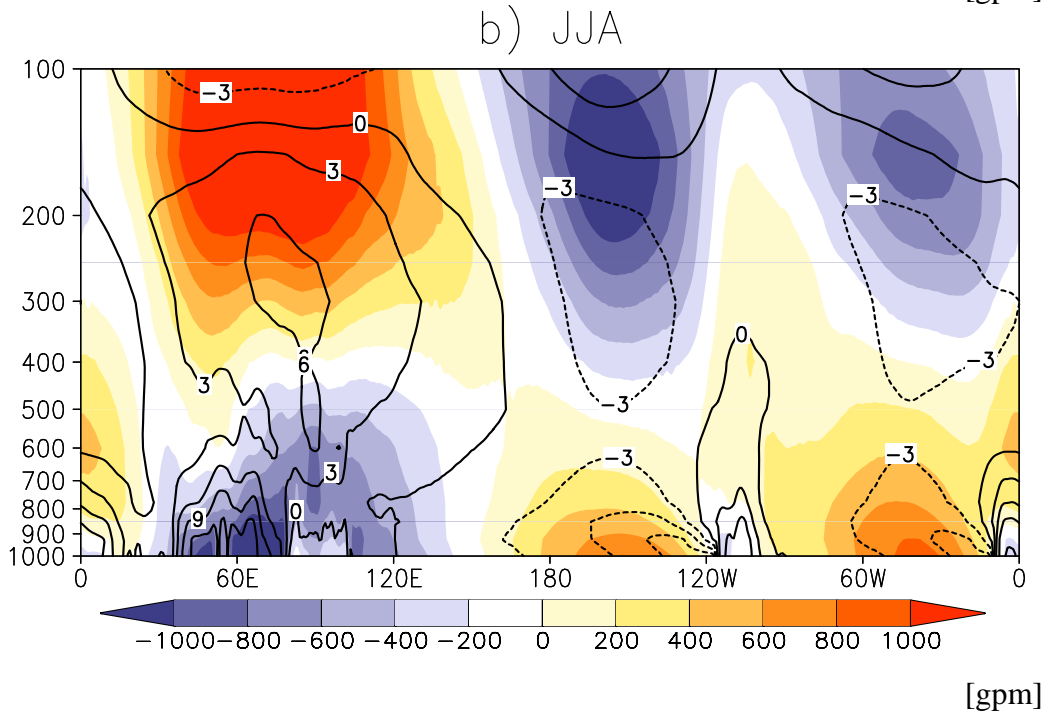
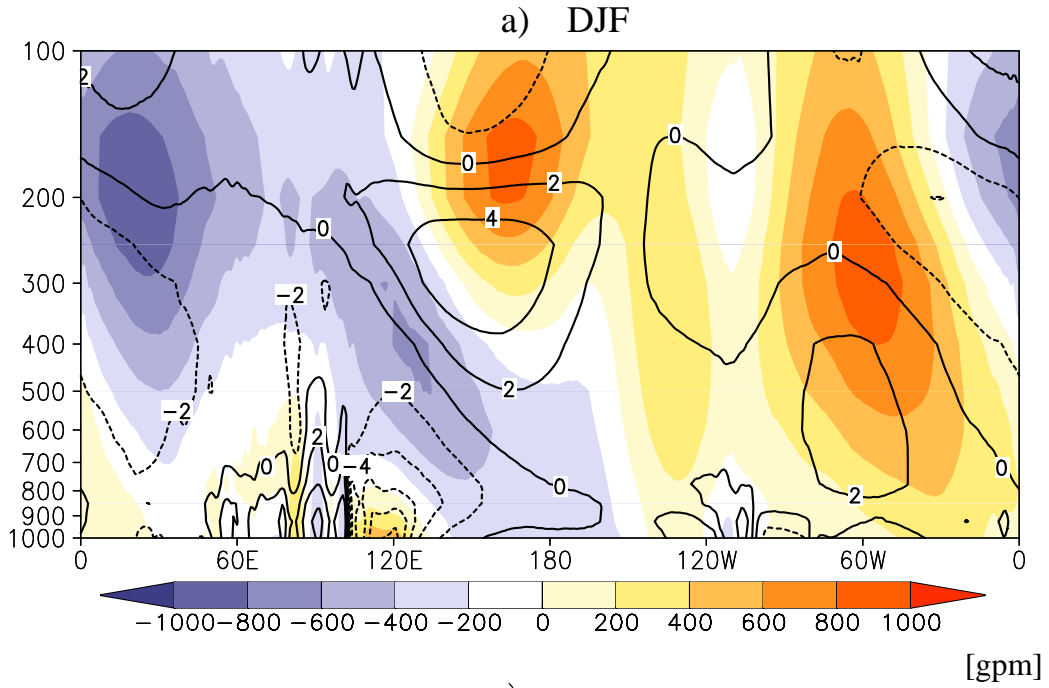


Figure 1.2. Atmospheric circulation in the troposphere (200hPa to 850hPa from top to bottom) during winter (left) and summer (right). Zonal wind components higher than 5 m/s are shaded in a) to d), while convergence of moisture transport at 850hPa is shaded in e) and f).

Figure 1.2 shows the atmospheric circulation in the troposphere during winter and summer. Climatological mean of the ‘modern satellite’ era (Kistler et al. 2001) from 1980-1999 is averaged from the European Centre for Medium-Range Weather Forecasts (ECMWF) reanalysis data (ERA40; Simmons and Gibson 2000). Since the westerly air “flows around” rather than “climbs up” the TP (Trenberth and Chen 1988), they bifurcate at the western plateau and converge in the eastern plateau (Ding 1994), thereby blocking the tropospheric circulation and contributing to the development of the monsoon circulation in summer and the formation of the Siberian high-pressure system in winter (e.g. Manabe and Terpsta, 1974). The shift of the mid-tropospheric westerly jet stream from the south of the TP in winter to the north in early summer is associated with the outburst of the Asian monsoon. Liu and Yin (2002) found by numerical modelling that the seasonal transition of wind distributions would not happen in the northeast Asian monsoon region (east of the TP), if the height of the TP is decreased to less than 1500m.

**ii) Thermodynamic Effect:** In summer, the TP acts as an elevated heat source and moisture sink affecting the atmospheric circulation (e.g. Flohn 1957; Ye and Gao 1979; Yanai et al. 1992; Li and Yanai 1996; Ueda et al. 2003).

Figure 1.3 shows the altitude-longitude sections along 30° N of geopotential height and atmospheric temperature anomalies from global zonal mean during winter and summer. Note that, the warm-anticyclone in the upper troposphere moves from the western Pacific during winter to above the TP during summer. The heating of the TP can warm up the air aloft at a rate of about 3K higher than the zonal mean air temperature found at the same level, thus causing large-scale up-lifting air motions at the TP. This drives lower tropospheric inflow towards the plateau, in favour of the northward march of warm and moisture tropical air current (Figure 1.2f) and the eventual outbreak of the summer monsoon (e.g., Luo and Yanai 1983; Li and Yanai 1996). He et al. (1987) found that the general circulation over Asia experiences two distinct stages of abrupt transitions, resulting in the successive onsets of the early summer rains over Southeast Asia and the Indian summer monsoon. The two transitions are related to similar successive stages of upper-tropospheric warming over longitudes east of 85° E (the eastern TP, south China) and over longitude west of 85° E (Iran, Afghanistan, the western TP). Yanai et al. (1992), by examining the thermodynamic energy equation, showed that the first stage of upper-tropospheric warming (over the eastern Plateau) is primarily caused by diabatic heating and warm horizontal advection, and the second stage (over the western Plateau) is caused by adiabatic warming due to large-scale subsidence. These studies demonstrate that the effects of heating can be felt not only locally but also remotely through advection and wave action. The thermal effects of the TP involve surface sensible heating and latent heating above elevated slopes such as is found at the other main elevated plateaus in the world including the Andes (e.g. Broccoli and Manabe 1992).



**iii) Surface Indirect Effect:** The third effect mainly refers to the active local atmospheric systems (like meso-scale convective system, frontal system, Tibetan vortices) at the TP and along the slope that greatly modify the large-scale circulation. The complex terrain and variable boundary conditions of the TP create a unique weather and climatic system in the middle troposphere over 4000m, which is important to address (e.g. Shimizu 2001). On the TP, observational data demonstrate that the temperature and energy portion experience not only a strong diurnal variation due to intensive solar radiation but also dramatic seasonal variations due to frequent rainfall during the Asian monsoon period (e.g. Ye and Gao 1979; Zhou et al. 2000).

It is worth to mention that the TP is also source for several major rivers in southeastern and eastern Asia, including Huanghe River, Changjiang River, Mekong River, and Salween River. Although the precipitation in the TP is not large, the runoff is considerable due to steep orographic variation and low evaporation limited by low surface temperature (Kondo and Xu, 1997; Xu and Haginoya, 2001). The TP also plays an important role in the variation of the Asian summer monsoon through the atmospheric heating controlled by its hydrological process (Fujii 2001). The variation of summer monsoon rainfall, Meiyu (China), Baiu (Japan), and Changma (Korea) is the most important cause for floods and drought over this region where half of the world population lives. Shifts in the hydrological cycle in the TP, especially precipitation, would heavily impact the river systems originating from it, leading to disruptions of the existing socio-economic structures of populations living on the TP and those living downstream (Beniston et al., 1996).

---

Figure 1.3. Altitude-longitude sections of geopotential height eddies and atmospheric temperature anomalies along 30°N in a) and b). Geopotential height eddies [unit: gpm] are shaded and atmospheric temperature anomalies [unit: K] are shown as contour lines. Topography along 30°N is shown in the bottom for reference of the location of the Tibetan Plateau.

## 1.2 Surface Climate on the Tibetan Plateau

### 1.2.1 Surface Temperature

Figure 1.4 shows the climatological (1980-1999) seasonal near surface atmospheric temperature on the Tibetan Plateau. The data is obtained from Climatic Research Unit (known as CRU; New et al. 2002; available from <http://www.cru.uea.ac.uk/>). Gradients along the TP's periphery are generally very strong; temperature increases from north-west to south-east. During winter the TP is characterized by temperatures around  $-25^{\circ}\text{C}$  in the west and  $-15^{\circ}\text{C}$  in the east. During spring and autumn, the mean temperature in the western TP is about  $-10^{\circ}\text{C}$ , and higher in the eastern TP. In summer, the entire TP's temperature rises above  $0^{\circ}\text{C}$ . The east warms up to  $5\text{-}10^{\circ}\text{C}$ , and the high elevations of the west warm up to  $0\text{-}5^{\circ}\text{C}$ . The deserts north of the TP as well as regions to the east warm up to  $25^{\circ}\text{C}$ . Areas south of the TP are hot ( $30\text{-}35^{\circ}\text{C}$ ).

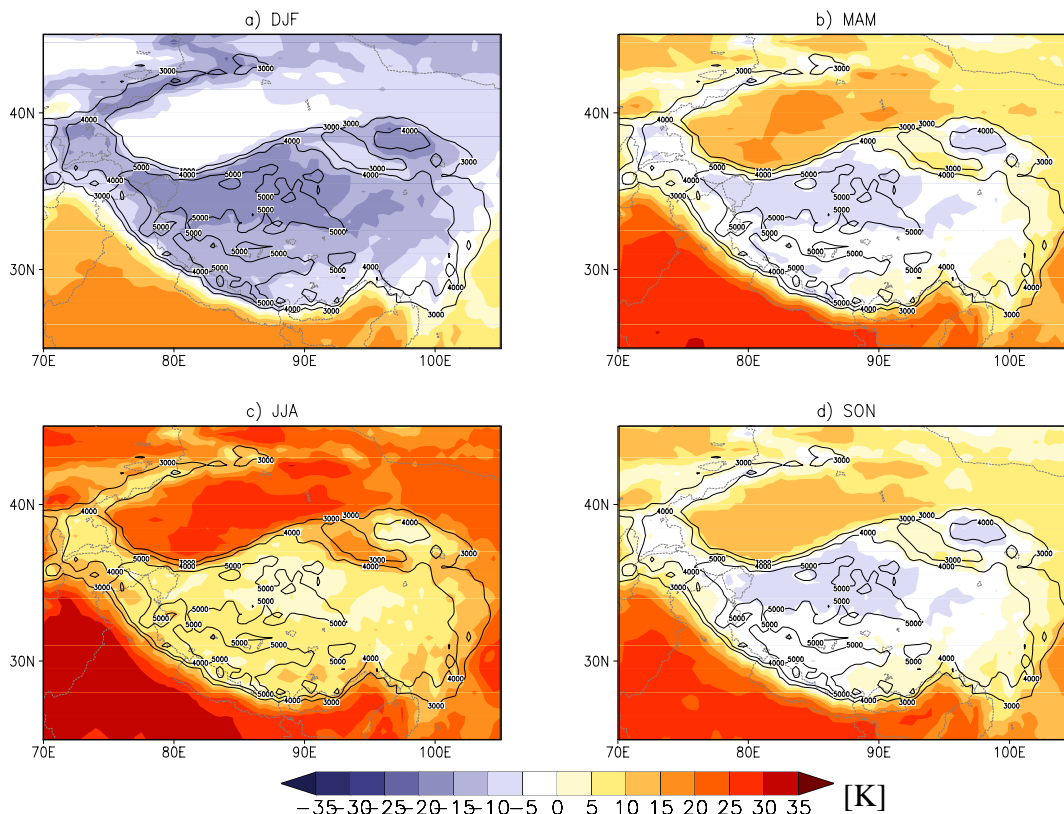


Figure 1.4. Seasonal climatological mean surface temperature of the Tibetan Plateau during a) DJF, b) MAM, c) JJA, and d) SON, respectively, from 20-year (1980-1999) averages of CRU observation data (details in text).

Despite the seasonal variations, near surface air temperatures over the TP also have strong diurnal variations because of the strong incoming solar radiation during the daytime. The diurnal change of the surface soil temperature can be up to  $50^{\circ}\text{C}$  in spring and sensible heat flux is dominant to heat the near surface

atmosphere. As the summer monsoon progresses, the surface becomes wet due to frequent precipitation. The diurnal variation of surface temperature is reduced to about 20°C and the latent heat flux and the soil heat capacity also increase gradually. The rising surface temperature is accordingly restricted and the sensible heat flux becomes lower (Tanaka et al. 2003).

### 1.2.2 Precipitation

Figure 1.5 shows the seasonal precipitation on the TP calculated from CRU during 1980-1999. The amount of precipitation on the TP is small and extremely variable in time and space (Ueno et al. 2001), resulting in a large spatial variability of soil-water content, as well as sensible-heat flux and water-vapour flux from the surface (Xu and Haginoya, 2001). Summer precipitation (Figure 1.5c) accounts for more than 60% of the total annual precipitation. Summer precipitation, therefore, is important to many ecological processes as well as human activities in this region. Precipitation gradually decreases from southeast to northwest, from approximately 700mm to lower than 50 mm annually (Liu and Yin 2001). Satellite observations reveal some rainfall during the pre-onset period even on the western plateau especially along the western slope of the plateau (see Figure 1.5a; b). The lower limit of snowfall elevation with a 50% probability is estimated at around 5000m a.s.l., as determined by the constant nighttime temperature in conjunction with monsoon cloud development (Ueno et al. 2001).

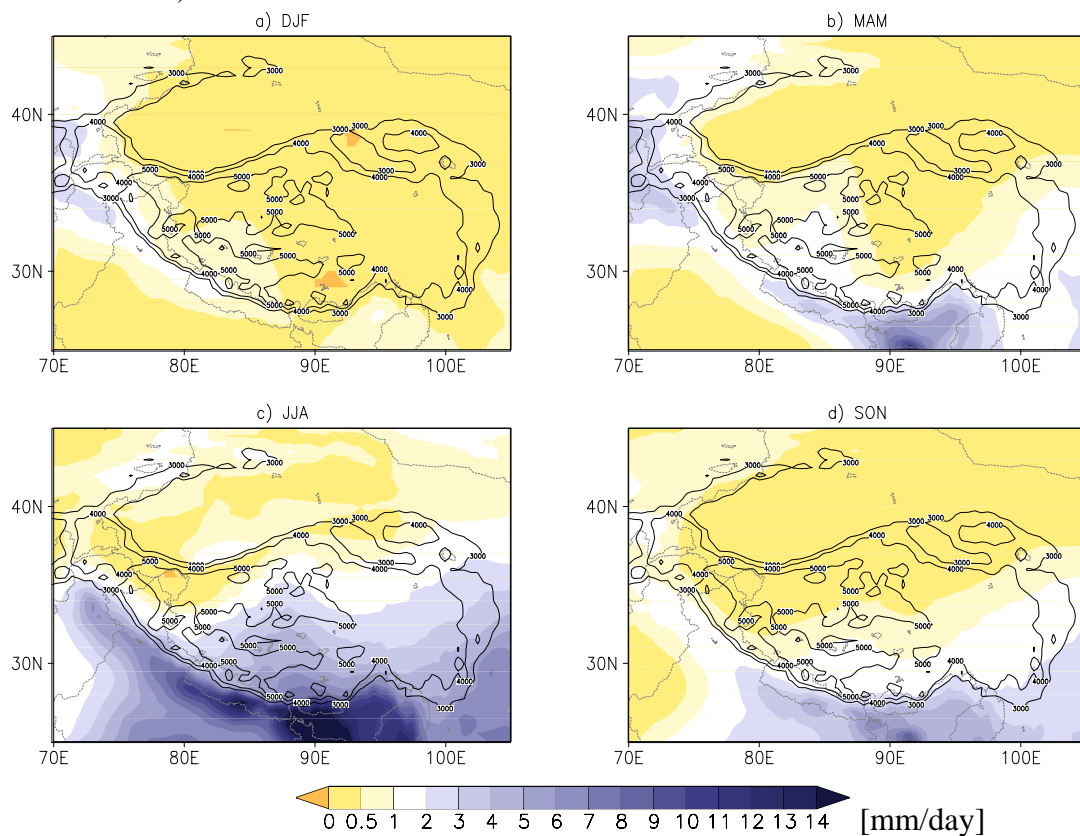


Figure 1.5. Same as Figure 1.4, but for precipitation.

There are motivations for using rainfall as a basis for monsoon assessments, as well as a number of challenges posed by its use. For example, precipitation is a very difficult meteorological variable to monitor, involving complex spatial and temporal gradients. Correction of precipitation measurements on the TP is highly recommended and necessary (Ueno and Ohata 1996).

### 1.2.3 Climate Change on the Tibetan Plateau

There is little disagreement about the significant influence of the TP on regional and global atmospheric conditions, but the mechanisms of this influence are still poorly understood, especially the aforementioned third influence. One of the big obstacles is that the knowledge of the water cycle and energy budget over the TP and its vicinity is still very limited. This is mainly because of its very short meteorological observation history (since the 1950s) and sparse observation stations (Figure 1.6). Weather stations are mostly located in the eastern lower elevated region along the valleys. The short history and low density of observation on the TP also complicate the assessment of climate change.

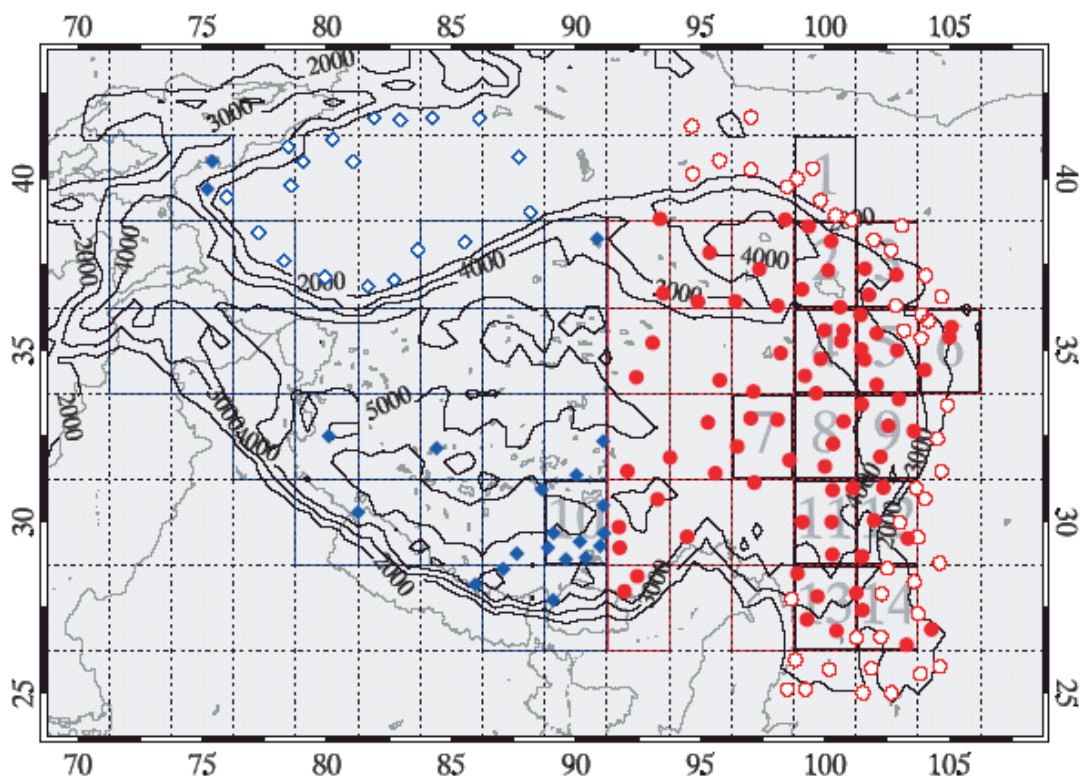


Figure 1.6. Map of the observation sites on and near the Tibetan Plateau. In total, there are 161 meteorological stations; open circles denote stations below 2000m, and solid symbols denote those above 2000m. The red and blue colors distinguish between eastern and western Tibetan Plateau stations, respectively. Elevation contours are defined as in Figure 1.1 [from Frauenfeld et al. 2005].

Although it is difficult to capture climate change on the TP due to the lack of observations, several studies have been conducted, recently. Tang et al. (1998) found temperature change trends on the TP are consistent with trends that occurred in other regions in China over the past 40 years (from 1950 to 1990), but at a higher rate. Other studies based on the same observation data also revealed regional variations of the warming trends (Liu and Chen 2000; Wu and Liu 2004). For example, the southeast TP has become warmer and drier during the last 40 years (Niu et al. 2004), which is also indicated from tree ring records (Braeuning and Mantwill 2004). Lin and Zhao (1996) divided the TP into nine subregions in terms of precipitation regimes and found that some subregions became drier and others wetter. Spring precipitation increases in the western Himalayas and the India region since the 1970s (Singh and Yadav, 2005). Tang et al. (1998) suggested that the spatial distribution of the precipitation anomaly over the Tibetan Plateau and its neighboring areas is controlled by the variation in the regional atmospheric circulation of the so-called “Plateau Monsoon” on the decadal timescale. Liu and Yin (2001) also suggested that the interannual variations of precipitation on the TP are closely associated with the North Atlantic Oscillation (NAO).

By making optimal use of the few available observations, there is great hope that meteorological analyses and forecasts can provide a more complete and reliable picture of the climate in this region. However, reanalysis is also controlled by the performances of the assimilation and modeling tools (Bengtsson et al. 2004). Temperature and precipitation, as type B or type C variable in reanalysis data (Kistler et al. 2001), are highly dependent on the model performance (Bengtsson et al. 2004). Unfortunately, the TP is not the region which benefits from large development and validation efforts. Frauenfeld et al. (2005) found that the observed climate trends of temperature are not represented by the ERA40 reanalysis data. As a result, the climate of the Tibetan Plateau remains highly uncertain. More observation stations need to be built on the TP and longer periods of observation are necessary to remedy this.

The GAME-Tibet project, launched in 1996, is an international land-atmosphere interaction field experiment implemented on the Tibetan Plateau both at the plateau scale and meso-scale under the framework of the Global Energy and Water-cycle Experiment (GEWEX) Asian Monsoon Experiment (GAME) within the World Climate Research Program (WCRP). The overall goal of GAME-Tibet is to clarify the interactions between land surface and atmospheric processes over the Tibetan Plateau in the context of the Asian Monsoon system. To achieve this goal, the scientific objective of GAME-Tibet is to improve the quantitative understanding of land-atmosphere interactions over the Tibetan Plateau, to develop process models and methods to apply them over large spatial

scales, and to develop and validate satellite-based retrieval methods, which shall greatly improve our understanding of the effects of the Tibetan Plateau summarized above. During GAME phase I, GAME-Tibet progressed through two experimental phases, the pre-phase observation period (POP) in 1997 and the intensive observation period (IOP) in 1998 in close cooperation with the second Tibetan Plateau Experiment of Atmospheric Science (TIPEX) led mainly by Chinese scientists (Tao et al. 2000). It contributed to international research activities in the related science fields by providing all data obtained through the GAME-Tibet Data Information System (DIS) in 2000. GAME-Tibet is one of nine Continental Scales Experiments (CSEs) together with the Lena River Basin, GAME-HUBEX, and GAME-Tropics in Asia, the Mackenzie, Mississippi, and Amazon River Basins over the Americas, and the Baltic Sea catchment in Europe (Masuda 2004). More information can be found at <http://monsoon.t.u-tokyo.ac.jp/Tibet/>.

### **1.3 Land Cover Change on the Tibetan Plateau**

The TP is a unique natural landscape, with broad areas of intricate physiognomic types. Thus, remote sensing data sets are very powerful tools to evaluate land cover changes for this region (Suh and Lee, 2004). Figure 1.7 shows the dominant land cover types on the TP in the year 1950 and 2000. The data for 1950 is obtained from the International Satellite Land Surface Climatology Project (ISLSCP) initiative II data collection (Klein Goldewijk, 2001). Tundra is the major land cover type in the central TP. There are forests located at the southeastern part and grassland/Steppe on the northern and western boundaries. The data for 2000 is obtained from the Global Land Cover 2000 database (GLC2000 2003). Vegetation distribution on the plateau has been shown to be very sensitive and vulnerable to environmental change due to the high altitude of the plateau, where growth and distribution of plants depend heavily on the local climate conditions (Zhang et al. 1996). Due to the steady decrease in average temperature and annual rainfall from the south-east to the north-west of the TP, the biomass and biodiversity is decreasing correspondingly from south-east to north-west. It shows a clear horizontal and vertical transformation of vegetation patterns caused by temperature and humidity trends, and a vertical transformation due to the combined effects of topography and atmospheric circulation (Song et al. 2004). In 2000, the vegetation type changes gradually from cropland at the southeast region to temperate shrubland/meadow in the middle region to temperate desert, alpine desert, ice/polar desert in the northwest region. Figure 1.7 clearly demonstrates that the land cover on the Tibetan Plateau changed strongly during the last 50 years. Tundra was generally replaced by shrubland in the central Plateau. Warm and conifer forests at the southeastern TP almost disappeared and changed mainly into cropland. Bare land shows up at the western border of the Plateau replacing the original grassland/Steppe found there.

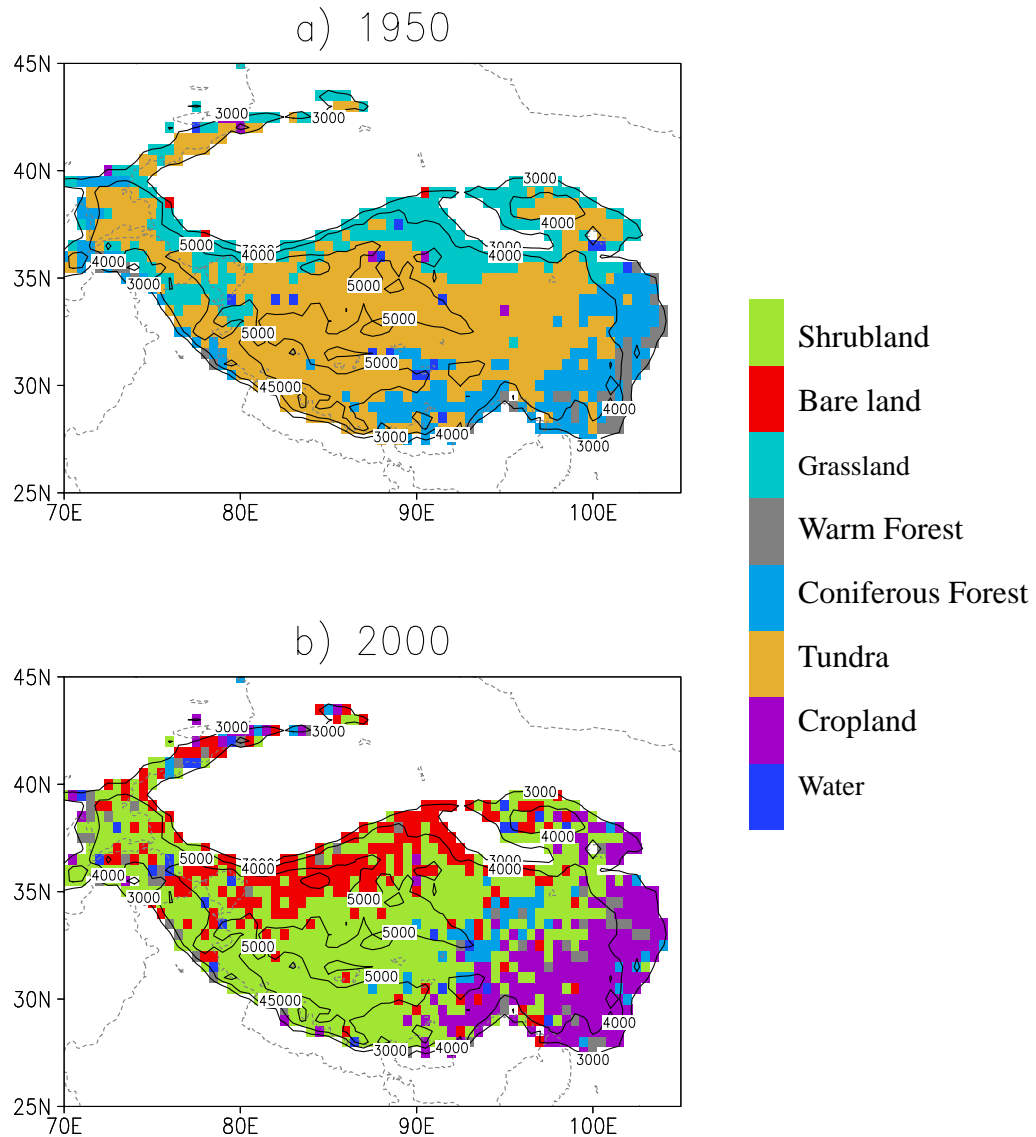


Figure 1.7. Land cover distributions on the Tibetan Plateau in a) 1950 and b) 2000. Elevation levels of 3000, 4000, and 5000m are shown for reference. Data sources are given in the text.

The permafrost area on the TP is about  $1.5 \times 10^5 \text{ km}^2$  (Zhang et al. 1996). Permafrost plays a very important role in determining vegetation distribution and dynamics and in indicating changes and fluctuations in climate. Forests and some shrubland/meadow occur in the no-permafrost areas. Temperate steppe, desert, and some shrubland/meadow occur on the seasonal frozen ground. Alpine steppe, desert, and ice/polar desert occur in the continuous permafrost areas. The development of the vegetation and environment went through several transitions responding to climate changes (Tang et al. 1998).

## **1.4 Motivations of the Thesis**

Climate change influences vegetation distribution, and land cover changes (LCC) influence climate (e.g. Charney 1975) by affecting the water and energy cycles through dynamic and thermodynamic processes. Extensive local and regional land use changes during the second half of the last century might be a potential explanation (Kalnay and Cai 2003) for the difference between reanalysis data and station trend on the TP (Frauenfeld et al. 2005). LCC not only affect local and regional weather and climate but also impact the global climate (e.g. Avissar and Werth 2005). However, quantitative evaluations of climate changes induced by land cover change are very difficult because of limitations in meteorological or land surface observational data, and because land-atmosphere interactions are highly nonlinear (Suh and Lee, 2004). Global climate models (GCMs) are powerful tools for land cover change studies (e.g. Nobre et al. 1991; Mabuchi et al. 2005). An atmospheric general circulation model ECHAM5 (Roeckner et al. 2003; 2004) has been applied in this thesis to simulate the climate impacts of land cover changes on the Tibetan Plateau.

The distribution of vegetation on the TP is determined by environmental conditions as well as human disturbance, which is usually extreme in terms of spatial heterogeneity (Ni 2000). The great expansion in human activity on the TP is causing significant changes of natural conditions (Ni 2000). Currently, about 17% of the Tibet Autonomous Region's total land is desertified and this land is always found in the densely populated regions, where human activities are intensive (Zou et al. 2002). Desertification on the TP is caused by both natural and human factors (Zou et al. 2002). Therefore, the impacts of anthropogenic land cover changes on the TP will be separately addressed in Chapter 2, where I will address the questions: How have human-induced land cover changes on the Tibetan Plateau impacted the local, regional, and even global climate? Are these changes corresponding with the observed climatic trends?

Deforestation is an important part of land surface changes and has been extensively studied during the last two decades. Tropical deforestation, such as in the Amazon (e.g. Shukla et al. 1990), Africa (e.g. Snyder et al. 2004), and southeast Asia (e.g. Xue et al. 2004) was extensively studied. The forest of the southeastern TP has merely disappeared and been replaced mainly by cropland and built-up areas during the last 50 years with much less study (Houghton and Hackler 2003; see Figure 1.7). It is important from both a scientific and administrative view to study the climate impact of deforestation/reforestation at the southeastern Tibetan Plateau. Chapter 3 will address this topic.

Ecological and biogeochemical processes are highly sensitive to climatic variability and disturbances. Climate warming greatly affected the environment of the TP, such as by the degradation of the permafrost (Yang et al. 2004). The response of life zones on the TP to climate changes as predicted by Zhang et al (1996) showed that the natural vegetation would shift northwards and westwards from the present position due to climate warming. Natural vegetation such as tropical and sub-tropical forests, coniferous forests, and alpine meadows would increase, but decrease on alpine steppe, alpine desert, and polar desert is expected (Ni 2000). The climate scenario analysis shows that most of the dominant tree species would shift northwards and westwards as the climate gets warmer for a scenario of CO<sub>2</sub> concentration of 500 ppmv (Song et al. 2004). Ni (2000) also concluded from their model simulation that the continuous permafrost areas of the TP would mostly disappear, while the no-permafrost area would greatly increase under future global warming climate. They also pointed out that the disappearance of permafrost and the expansion of no-permafrost areas would accelerate the desertification of the Tibetan Plateau. However, all these projections of land use changes are based on future possible surface temperature and/or precipitation produced by GCMs scenario simulations. As always, it is difficult to determine whether or not the models are “good enough” to be trusted when used to make predictions for the future (Covey et al. 2003), in addition to the high uncertainty existing when reproducing climate over the Tibetan Plateau by GCMs. In chapter 4, we aim to investigate how the impact of deforestation at the southeast TP is modulated under a different climate background condition, projected with doubled atmospheric CO<sub>2</sub> concentration.

The reliability of GCM predictions over the Tibetan Plateau is low due to the difficulty of representing the complex terrain by the coarse horizontal resolution of these models (hundreds kilometers; Houghton et al. 2001). Regional climate models (RCM) have become a powerful tool for downscaling the climate information originating from GCMs to a regional scale (Giorgi and Mearns 1999). A regional climate model REMO (Jacob and Podzun 1997) has been applied over the Tibetan Plateau and a “double-nesting” experiment has been conducted for 1998 summer. A summary will be given in chapter 5. In the future, a nesting model system of REMO/ECHAM5 may be applied, aiming not only to specify the local response to land cover changes but also to transfer or downscale the information from global scale.

## **1.5 Outline of the thesis**

This thesis is cumulatively organized with four major chapters basing on publications or manuscripts to be submitted to journals.

1. Climatic impact of anthropogenic land cover changes on the Tibetan Plateau. Accepted by *Global and Planetary Change*;
2. Deforestation/reforestation at the Southeast Tibetan Plateau. Part I: impacts on current climate. To be submitted to *J. Climate*;
3. Deforestation/reforestation at the Southeast Tibetan Plateau. Part II: compounding effects with greenhouse warming on climate. To be submitted to *J. Climate*;
4. Evaluation of regional climate model REMO simulation over the Tibetan Plateau. In preparation.

These chapters 2 to 5 are presented with a separate abstract and conclusion. Chapter 1 gives the overall climate background of the Tibetan Plateau and the motivations of this thesis. Conclusions and an outlook are given in Chapter 6. In order to keep the chapters 2 to 5 integrated as scientific papers, some points might be repeated in the thesis and they are referred to in each chapters with the paper's name, not the chapter number.

**Reference:**

- Avissar, R., and D. Werth, 2005: Global hydroclimatological teleconnections resulting from tropical deforestation. *J. Hydrometeorology*, **6**, 134-145.
- Bengtsson, L., S. Hagemann, and K. I. Hodges, 2004: Can climate trends be computed from reanalysis data? *J. Geophys. Res.*, **109**, D11111, doi: 10.1029/2004JD004536.
- Beniston, M., D. G. Fox, and et al., 1996: The impacts of climate change on mountain regions, *Second assessment report of Intergovernmental Panel on Climate Change (IPCC)*, Chapter 5, Cambridge University Press, Cambridge, pp. 191-213.
- Braeuning, A., and B. Mantwill, 2004: Summer temperature and summer monsoon history on the Tibetan Plateau during the last 400 years recorded by tree rings. *Geophys. Res. Lett.*, **31**, L24205, doi:10.1029/2004GL020793.
- Broccoli, A.J., and S. Manabe, 1992: The effect of orography on middle latitude northern hemisphere dry climates, *J. Climate*, **5**, 1181-1201.
- Charney, J.G., 1975. Dynamics of deserts and droughts in the Sahel. *Qrtly. J. Roy. Meteor. Soc.*, **101**, 193-202.
- Covey, C., K. M. AchutaRao, U. Cubasch, P. Jones, S. J. Lambert, M. E. Mann, T. J. Philips, and K. E. Taylor, 2003: An overview of results from the Coupled Model Intercomparison Project (CMIP). *Glob. Planet. Change*, **37**, 103-133.
- Ding, Y., 1994: Monsoon of China. Kluwer Academic, 550PP.
- Flohn, H., 1957: Large-scale aspects of the “summer monsoon” in South and East Asia. *J. Meteor. Soc. Japan*, **75<sup>th</sup>** Ann., 180-186.
- Frauenfeld, O.W., T. Zhang, and M. C. Serreze, 2005: Climate change and variability using European Centre for Medium-Range Weather Forecasts reanalysis (ERA40) temperatures on the Tibetan Plateau. *J. Geophys. Res.*, **110**, D02101, doi: 10.1029/2004JD005230.
- Fujii, H. and T. Koike, 2001: Development of a TRMM/TMI algorithm for precipitation in the Tibetan Plateau by considering effects of land surface emissivity. *J. Meteor. Soc. Japan*, **79(1B)**, 475-483.
- Giorgi, F., and L. O. Mearns, 1999: Introduction to special section: Regional climate modeling revisited. *J. Geophys. Res.*, **104 (D6)**, 6335-6352.
- GLC2000, 2003: European Commission, Joint Research Center, available at: <http://www.gvm.jrc.it/glc2000>
- He, H., J. W. McGinnis, X. Song, And M. Yanai, 1987: Onset of the Asian summer monsoon in 1979 and the effect of the Tibetan Plateau. *Mon. Wea. Rev.*, **115**, 1966-1995.
- Houghton, J. T., L. G. Meria Filho, B. A. Callender, H. Harris, A. Kattenberg, and K. Maskell (eds.), 1996: *The Science of Climate Change: Contribution of Working Group I to the Second Assessment of the Intergovernmental Panel on Climate Change*, Cambridge University Press, Cambridge, U. K., p. 572.

- Houghton, J. T., Y. Ding, D. J. Griggs, M. Noguer, P. J. van der Linden, X. Dai, K. Maskell, and C. A. Johnson, Eds., 2001: *Climate Change 2001: The Scientific Basis*. Cambridge University Press, 881 pp.
- Houghton, R. A., and J. L. Hackler, 2003: Sources and sinks of carbon from land-use change in China. *Global Biogeochemical Cycles*, **17(2)**, 1034, doi:10.1029/2002GB001970.
- Jacob, D. and R. Podzun, Sensitivity studies with the regional climate model REMO, *Meteorl. Atmos. Phys.*, **63**, 119-129, 1997.
- Kalnay, E., and M. Cai, 2003: Impact of urbanization and land-use change on climate, *Nature*, **423(6939)**, 528-531.
- Kistler, R., E. Kalnay, W. Collins, S. Saha, G. White, J. Woollen, M. Chelliah, W. Ebisuzaki, M. Kanamitsu, V. Kousky, H. van den Dool, R. Jenne, and M. Fiorino, 2001: The NCEP-NCAR 50-year reanalysis: Monthly means CD-ROM and documentation. *Bull. Amer. Meteor. Soc.*, **82**, 247-267.
- Klein Goldewijk, K., 2001: Estimating global land use change over the past 300 years: The HYDE database. *Global Biogeochemical Cycles*, **15(2)**, 417-433.
- Kondo, J. and J. Xu, 1997: Seasonal variations in the heat and water balances for nonvegetated surfaces. *J. Appl. Meteor.*, **36**, 1676-1695.
- Li, C., and M. Yanai, 1996: The onset of the Asian summer monsoon in relation to land-sea thermal contrast., *J. Climate*, **9**, 358-375.
- Liu, X-D and B. Chen, 2000: Climate warming in the Tibetan Plateau during recent decades. *Int. J. Climatol.* 20: 1729-1742.
- Liu, X., and Z. Y. Yin, 2002: Sensitivity of East Asian monsoon climate to the Tibetan Plateau uplift, *Palaeogeogr. Palaeoecol.*, **183**: 223-245.
- Mabuchi, K., Y. Sato, and H. Kida, 2005: Climatic impact of vegetation change in the Asian tropical region. Part I: Case of the Northern Hemisphere summer. *J. Climate*, **18**, 410-428.
- Manabe, S., and T. B. Terpsta, 1974: The effects of mountains on the general circulation of the atmosphere as identified by numerical experiments. *J. Meteor. Soc. Japan*, **31**, 3-42
- Manabe, S., and A. J. Broccoli, 1990: Mountains and arid climate of middle latitudes. *Science*, **247**, 192-195.
- Masuda, K., 2004b: GAME's contribution to GEWEX water and energy balance study. *Extended abstract of the 6<sup>th</sup> International Study Conference on GEWEX in Asia and GAME*, Dec. 3-5, 2004, Kyoto, Japan.
- New, M., D. Lister, M. Hulme, and I. Markin, 2002: A high resolution data set of surface climate over global land areas. *Clim. Res.*, **21**, 1-25.
- Ni, J., 2000: A simulation of biomes on the Tibetan Plateau and their responses to global climate change. *Mountain Research and Development*, **20(1)**, 80-89.
- Niu, T., Chen, L., Zhou, Z., 2004. The characteristics of climate change over the Tibetan Plateau in the last 40 years and the detection of the climate jumps. *Advances in Atmospheric Sciences*, **21(2)**, 193-203.

- Nobre, C.A., Sellers, P.J., Shukla, J., 1991. Amazonian deforestation and regional climate change. *J. Climate*, **4**, 975-988.
- Roeckner, E., G. Bauml, L. Bonaventura, R. Brokopf, M. Esch, M. Giorgetta, S. Hagemann, I. Kirchner, L. Kornblueh, E. Manzini, A. Rhodin, U. Schlese, U. Schulzweida, and A. Tompkins, 2003: The atmospheric general circulation model ECHAM5. Part I: Model description. *Report No. 349, Max-Planck-Institut fuer Meteorologie*, Hamburg, pp. 5-6. available at <http://www.mpimet.mpg.de>
- Roeckner, E., R. Brokopf, M. Esch, M. Giorgetta, S. Hagemann, L. Kornblueh, E. Manzini, U. Schlese, and U. Schulzweida, 2004: The atmospheric general circulation model ECHAM5. Part II: Sensitivity of simulated climate to horizontal and vertical resolution. *Report No. 354, Max-Planck-Institut fuer Meteorologie*, Hamburg, pp 18-20. available at <http://www.mpimet.mpg.de>
- Shimizu, S., K. Ueno, H. Fujii, R. Shiroyaka and L. Liu, 2001: Mesoscale characteristics and structures of stratiform precipitation on the Tibetan Plateau. *J. Meteor. Soc. Japan*, **79(1B)**, 435-461.
- Simmons, A.J., and J. K. Gibson, 2000: The ERA40 Project Plan. *ERA40 Project Report Series No.1*, ECMWF, Reading, UK, pp. 63.
- Singh, J., Yadav, R.R., 2005. Spring precipitation variations over the western Himalaya, India, since A.D. 1731 as deduced from tree rings. *J. Geophys. Res.*, **110**, D01110, doi:10.1029/2004JD004855.
- Snyder, P. K., J. A. Foley, M. H. Hitchmann, and C. Delire, 2004: Analyzing the effects of complete tropical forest removal on the regional climate using a detailed three-dimensional energy budget: An application to Africa. *J. Geophys. Res.*, **109**, D21102, doi:10.1029/2003JD004462.
- Song, M. H., C. P. Zhou, and Q. Y. Hua, 2004: Distributions of dominant tree species on the Tibetan Plateau under current and future climate scenarios. *Mountain Research and Development*, **24(2)**, 166-173.
- Suh, M.S., Lee, D.K., 2004. Impacts of land use/cover changes on surface climate over east Asia for extreme climate cases using RegCM2. *J. Geophys. Res.*, **109**, D02108, doi: 10.1029/2003JD003681.
- Tanaka, K., I. Tamagawa, H. Ishikawa, Y. Ma, and Z. Hu, 2003: Surface energy budget and closure of the eastern Tibetan Plateau during the GAME-Tibet IOP 1998. *J. Hydro.*, **283**, 169-183.
- Tang, M.-C., G.-D. Cheng, and Z.-Y., Lin, Eds, 1998: *Contemporary climatic variations over the Qinghai-Xizang (Tibet) Plateau and their influences on Environments* (in Chinese). Guangdong Science and Technology Press, Guangzhou, 229pp.
- Tao, S., L. Chen, X. Xu, and Y. Xiao: *The Second Tibetan Plateau Experiment of Atmospheric Sciences (TIPEX): Theoretical studies process I; II; III*. China Meteorological Press. 2000.
- Trenberth, K. E., and C.J. Guillemot, 1998: Evaluation of the atmospheric moisture and hydrological cycle in the NCEP/NCAR reanalysis. *Clim. Dyn.*, **14**, 213-231.

- Ueda, H., H. Kamahori, and N. Yamazaki, 2003: Seasonal contrasting features of heat and moisture budgets between the eastern and western plateau during the GAME IOP. *J. Climate*, **16**, 2309-2324.
- Ueno, K., and T. Ohata, 1996: The importance of the correction of precipitation measurements on the Tibetan Plateau. *J. Meteor. Soc. Japan*, **74**, 211-220.
- Ueno, K., H. Fujii, H. Yamada and L. Liu, 2001: Weak and frequent monsoon precipitation over the Tibetan Plateau. *J. Meteor. Soc. Japan*, **79(1B)**, 419-434.
- Wu, Q., Liu, Y., 2004. Ground temperature monitoring and its recent change in Qinghai-Tibet Plateau. *Cold regions Science and Technology* 38, 85-92.
- Xu, J., and S. Haginoya, 2001: An estimation of heat and water balances in the Tibetan Plateau. *J. Meteor. Soc. Japan*, **79(1B)**, 485-504.
- Xue, Y., H. H. Juang, W. P. Li, S. Prince, R. DeFries, Y. Jiao, and R. Vasic, 2004: Role of land surface processes in monsoon development: East Asia and West Africa. *J. Geophys. Res.*, **109**, D03105, doi:10.1029/2003JD003556.
- Yanai, M., C. Li, and Z. Song, 1992: Seasonal heating of the Tibetan Plateau and its effects on the evolution of the summer monsoon. *J. Meteor. Soc. Japan*, **70**, 319-351.
- Yang, M., S. Wang, T. Yao, X. Gou, A. Lu, and X. Guo, 2004: Desertification and its relationship with permafrost degradation in Qinghai-Xizang (Tibet) plateau. *Cold Regions Science and Technology*, **39**, 47-53.
- Ye, D. and Y. Gao, 1979: *The meteorology of the Qinghai-Xizang (Tibet) Plateau*, Sciences Press, Beijing, 278 pp (in Chinese).
- Ye, D., and G.-X., Wu, 1998: The role of the heat source of the Tibetan Plateau in the general circulation. *Meteor. Atmos. Phys.*, **67**, 181-198.
- Zhang X. S., D. A. Yang, G. S. Zhou, C. Y. Liu, and J. Zhang, 1996: Model expectation of impacts of global climate change on biomes of the Tibetan Plateau. In Omasa K., K. Kai, H. Taoda, Z. Uchijima, and M. Yoshino, (Eds.) *Climate Change and Plants in East Asia*. Tokyo: Springer-Verlag, pp. 25-38.
- Zhang, P., Shao, G., Zhao, G., Master, D.C. Le, Parker, G.R., Dunning, J.B. Jr., Li, Q., 2000: China's forest policy for the 21th century. *Science*, **288**, 2135-2136 (in policy forum).
- Zhou, M. And Staff Members of Chinese Academy of Meteorological Science, 2000: *Observational Analysis and Dynamic study of Atmospheric Boundary Layer on Tibet Plateau*. Meteorology Press, Beijing, 125 pp (in Chinese).
- Zou, X., S. Li, C. Zhang, G. Dong, Y. Dong, and P. Yan, 2002: Desertification and control plan in the Tibet Autonomous Region of China. *J. Arid Environments*, **51**, 183-198.

# **Chapter II:**

## **Climate Impacts of Anthropogenic Land Use Changes on the Tibetan Plateau**

### **Abstract**

A general atmospheric circulation model (ECHAM5) has been applied to investigate the impact of land use changes on the Tibetan Plateau (TP) on local and global climate. The “control” simulation with current land cover reasonably represents the large-scale circulation and state of the atmosphere over the Tibetan Plateau and the surrounding region. Modifying the land cover to a hypothetical non-anthropogenically-influenced vegetation cover shows significant modifications to the local and remote climate. Compared to this scenario, the TP is warmer and drier under present conditions. The Indian summer monsoon is intensified and the East China summer monsoon is weakened due to human-induced land cover change on the TP. The mean global temperature has almost no variation, whereas precipitation slightly increases. Our study indicates that human-induced land use changes on the Tibetan Plateau have had a significant impact on local to regional, and to a lesser extent global, climate.

Key words: Tibetan Plateau; Land use change; Monsoon; GCM

### **2.1 Introduction**

Land use changes (LUC) by human activities, such as deforestation, urbanization, and agricultural practice, have long been known to influence climate (e.g. Charney 1975). Land surface conditions affect the dynamics and thermodynamics of the atmosphere by influencing the water cycle and energy budget. LUC may affect local, regional, and possibly global weather and climate (e.g. Werth and Avissar 2002). Previous studies of the impact of LUC on climate have mostly investigated the effects of tropical deforestation (e.g. Shukla et al. 1990; Nobre et al. 1991; Henderson-Sellers et al. 1993) and the impacts of Saharan desertification (e.g. Xue 1997; Clark et al. 2001; Snyder and Foley 2004). Recently, some studies have focused on the interaction of LUC and climate in East Asia (e.g. Yatagai and Yasunari 1995; Xue 1996; Fu 2003). To our knowledge, no such study has been performed investigating LUC/climate interactions over the Tibetan Plateau (TP) region so far. A limitation of most

performed studies has been that they investigated distinct local and regional responses to LUC. Regional responses, however, are highly variable from one location to another (e.g. Govindasamy et al. 2001), and even within the same region, responses vary depending on the prevailing climatic conditions (e.g. Pan et al. 1999). A solution to this high variability is to perform detailed regional studies to assess specific responses of LUC in different parts of the world (Xue et al. 2001), permitting greater insight into the impacts of LUC on global climate.

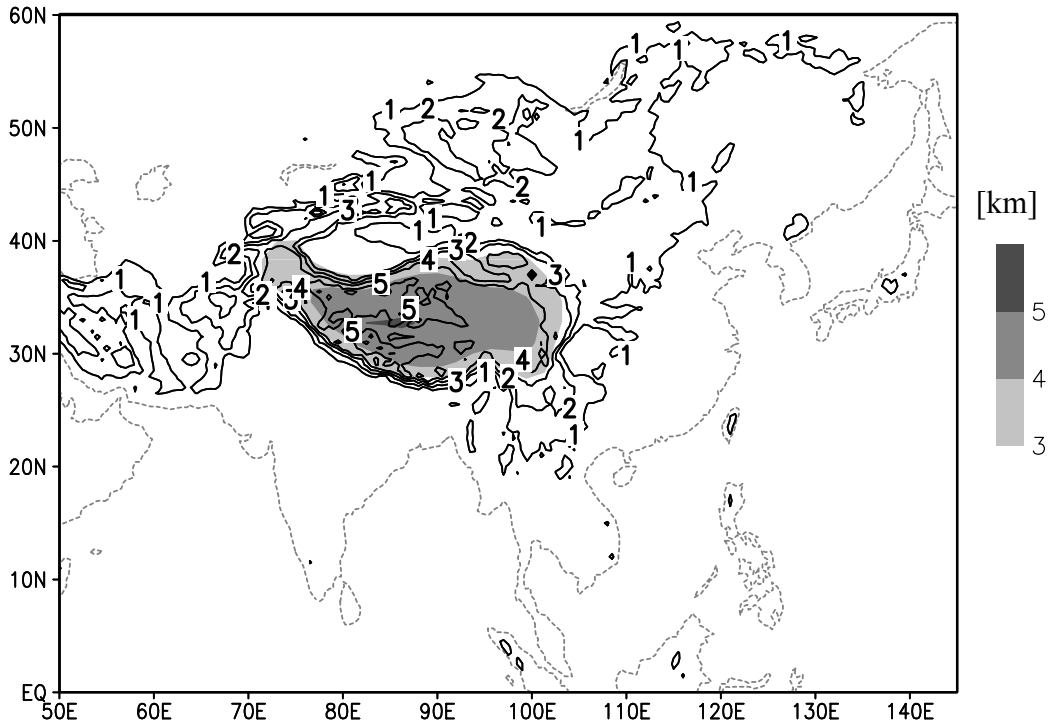


Figure 2.1. The main topography over the Tibetan Plateau and its vicinity. The Tibetan Plateau is shown as the shaded region where elevation is higher than 3000m a.s.l. at T63 resolution. Black contour lines show topography at 0.5° resolution with an interval of 1000m.

Mountainous and high-elevated regions, such as the TP, are very vulnerable to climate change (e.g. Beniston 2003). As referred to in this paper, the TP is the geographic region with elevation higher than 3000m, including the Tibet Autonomous Region, Qinghai province, parts of Sichuan and Gansu provinces, and part of the Xinjiang Uygur Autonomous region (shaded region in Figure 2.1). Because of its height (average elevation of 4200m) and size (about  $1 \times 10^6$  square kilometers), the TP plays an important role in forming and inducing variations of regional weather and climate in east and south Asia, as well as the Northern Hemisphere atmospheric circulation in general (e.g. Ye and Gao 1979). Analyses of temperature series of 97 stations showed that most of the TP has experienced statistically significant warming since the mid-1950s, especially in

winter. The linear rate of the temperature increase over the TP during the period of 1955-1996 was about 0.16° C/decade for the annual mean and 0.32° C/decade for the winter mean, exceeding those for the Northern Hemisphere and the same latitudinal zone in the same period (Liu and Chen 2000). Frauenfeld et al. (2005) confirmed such warming trends on the TP during the period of 1957-2000 based on the analysis of 161 station records. As a result of the rising air temperature, the lower altitude limit of permafrost has risen by 40-80m on the TP (Li and Cheng 1999) and the permafrost area on the TP has decreased by 10,000 km<sup>2</sup> in the recent years (Wang et al. 2000). The southeast of the TP was also growing wetter during the last 40 years shown for the station records (Niu et al. 2004). Tree ring records show a positive trend of late summer rainfall in the southeast TP for the period of 1961-1990 (Braeuning and Mantwill 2004) and an increase of spring precipitation since the 1970s over the western Himalayan region (Singh and Yadav 2005). Despite these wetter conditions, the level of Qinghai Lake, the largest lake on the TP, has fallen dramatically and shrunk in area since the beginning of 20th century, mainly due to the decrease of precipitation in the catchment (Qin and Huang 1998). As the TP is characterized by very complex terrain and weather stations are biased to the eastern, lower-elevation, populated areas, observational data is not ideal for assessing long-term trends on the TP (Frauenfeld et al. 2005). The results obtained from the studies described above can only represent the available data sources they used. They indicate an obvious warming climate on the TP in recent decades. Frauenfeld et al. (2005), however, found that there are no significant trends on the TP in its 2m temperature from European Centre for Medium-Range Weather Forecasts (ECMWF) Reanalysis (ERA40; Simmons and Gibson 2000). Kalnay and Cai (2003) suggested the extensive local and regional land use changes during recent decades as a potential explanation for the difference between reanalysis and station trend.

Grassland occupies about 50% of the TP and is mostly used for livestock grazing. Over the last 30 years, livestock numbers across the TP have increased more than 200% due to inappropriate land management practices (Du et al. 2004). Land use represents the most substantial human alteration of the Earth system for a long period (Vitousek et al. 1997). Population in the Autonomous Region has increased rapidly from 1960 (1.2 million) to 1990 (2.2 million) (Chinese national statistics reports), contributing to both urbanization and changing landscape. For instance, Lhasa, the capital of the Tibet Autonomous Region, has grown 2400% in the last 50 years (Du et al. 2004). Zou et al. (2002) found from observational data that desertified land is about 17.03% of the Tibet Autonomous Region's total land, and has been always mainly found in densely populated regions. Desertification on the TP most likely resulted from human-induced LUC (Zou et al. 2002).

Quantitative evaluation of climate changes by LUC is very difficult because long term meteorological and land surface observational data are not available. A further complication is that the land-atmosphere interactions are highly nonlinear. An approach to overcoming these difficulties is to utilize regional climate models (RCM) and global circulation models (GCM) in the study of LUC/climate change interactions (Suh and Lee 2004). GCMs have long been used to study the TP, e.g. the comparison of climates under conditions with and without topography of the Tibetan Plateau (e.g. Murakami 1958; Manabe and Terpestra 1974; Broccoli and Manabe 1992; Liu and Yin 2002) although it is known that climatic modelling of the TP is especially difficult because of the steep orographic profile and heterogeneous surface conditions (Cole et al. 1994). All GCMs involved in the AMIP (Gates et al. 1999), AMIP II, and CLIVAR/Monsoon GCM Intercomparison Project (Kang et al. 2002) have large systematic errors in simulating the mean Asian monsoon climate and circulation. With model development, the performances of GCMs to reasonably reproduce the seasonal mean monsoon precipitation and circulation in the magnitude and pattern of flow have been improved although biases still exist (e.g. Rajendran et al. 2004). Evaluation of model performance in representing the mean circulation and surface climate, especially in the Asian region are strongly recommended before assessing model results of sensitivity experiments.

In this study, a general atmospheric circulation model has been applied to investigate the impact of LUC on the TP on regional and global climate. We have specifically examined: 1) how human-induced LUC impact the local climate on the TP, 2) whether the modeled climate changes correspond to the observed trends in recent decades, 3) whether the local effects are transmitted to further regions, and 4) how transmitted effects affect the weather and climate in other regions. The paper is organized as follows: in section 2.2, the model and experimental set-ups are introduced. In section 2.3, model performance on seasonal mean circulation and surface climate are evaluated with observations and sensitivity study results are presented as well. Finally, a discussion of the results, possible implications as well as conclusions are given in section 2.4.

## **2.2 Model and experiments**

### **2.2.1 Model introduction**

The most recent version of the Max Planck Institute for Meteorology atmospheric general circulation model, ECHAM5 (Roeckner et al. 2003) is used in this study. Duemenil Gates and Liess (2001) used the previous version ECHAM4 to study the sensitivity of the local and global climate during a full annual cycle to deforestation and afforestation in the Mediterranean region at T42 horizontal resolution. Their results agreed with other similar studies, but

they also pointed out that the assumptions of vegetation cover and surface parameterization need to be improved in future studies. Compared to ECHAM4, ECHAM5 includes new surface processes, land surface data sets derived from satellite observations (Hagemann 2002) and a seasonal cycle of vegetation ratio and leaf area index, which may have detectable impact on the simulation of the seasonal cycle of precipitation and evaporation (van den Hurk et al. 2003). Additionally, a sub-grid scale orographic parameterization developed by Lott and Miller (1997) and Lott (1999) is implemented in ECHAM5 aiming to represent the effects of orographic variations on smaller scales than the typical horizontal resolution of a climate model (Roeckner et al. 2003). Lott (1999) concluded that such parameterization schemes are beneficial to GCMs by decelerating significantly the low level flow, which is expected to improve the performance in mountainous regions, like the TP.

A hybrid 19 level coordinate system is used in the vertical direction: the sigma system at the lowest model levels gradually transforms into a pressure system in the lower stratosphere. Roeckner et al. (2004) concluded that some individual processes, like the Indian and East Asian monsoon evolution, are better captured by ECHAM5 at higher horizontal resolution, although there is little evidence for convergence to a more realistic global climate state at higher resolution. Given the restriction of computational resource, the simulations in this study are performed at T63 resolution, corresponding to a grid size of about 1.875° in longitude and latitude. In the Tibetan Plateau region, this is equal to about 150 km in the longitudinal and 200 km in the latitudinal directions. While some of the realism of summer precipitation in terms of intensity of single events is missing in such a coarse resolution GCM, the use of the global model enables us to see global climate sensitivity of the model simulation to the land use/land cover change, to observe the propagation of atmospheric effects from the area where the local changes were applied, and may reveal global teleconnections.

### **2.2.2 Experiment design**

Assessment of land use changes on the TP is extremely difficult due to the scarcity of observational data at both spatial and temporal scales. Remote sensing data sets are very powerful tools to evaluate the LUC for this region (Suh and Lee 2004). Figure 2.2a shows the current land cover type also obtained from the International Satellite Land Surface Climatology Project (ISLSCP) initiative II data collection (Loveland et al. 2001). Currently, the TP has a western shrubland and an eastern grassland part, with bare land appearing at the northern boundary. This vegetation distribution responds to the dry west and wet east (Ye and Gao 1979).

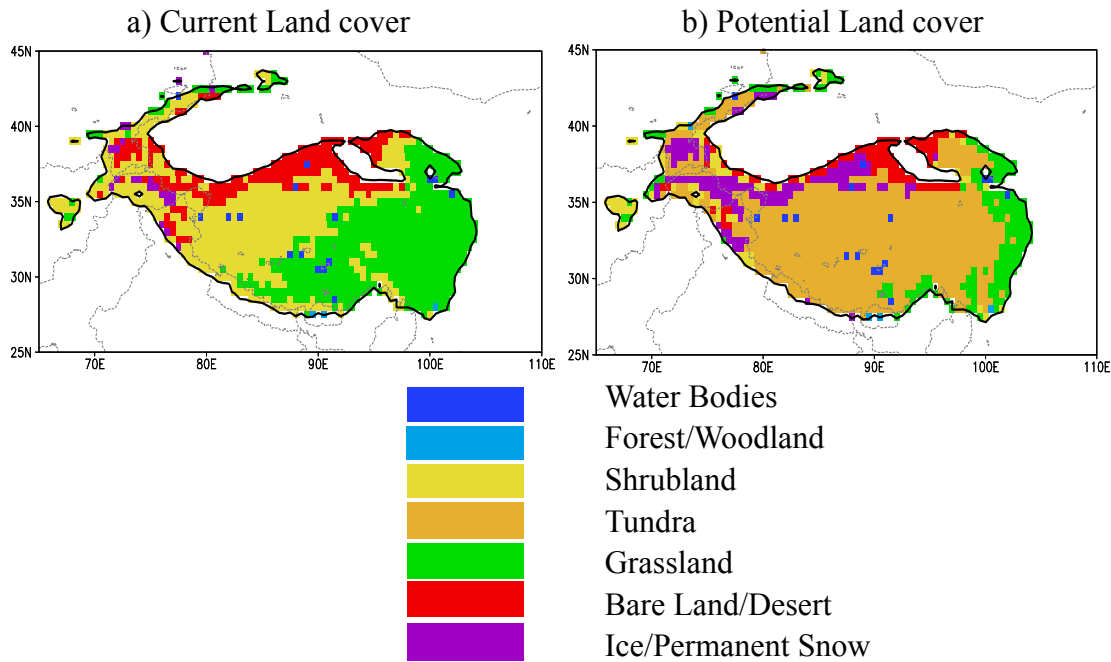


Figure 2.2. Dominant a)current, and b)“natural” non-anthropogenically-influenced land cover on the Tibetan Plateau at 0.5° resolution. Data are obtained from the International Satellite Land Surface Climatology Project (ISLSCP) initiative II data collection.

The “natural” distribution of vegetation types in a region should be in equilibrium with climate, water and nutrient availability, but, in reality, the distribution of vegetation is always modified by anthropogenic influences. Reconstruction of the non-anthropogenically influenced vegetation other than by modelling is rather difficult. However, it is feasible to specify the equilibrium climate vegetation, called Potential Natural Vegetation (PNV), which represents the vegetation cover that would most likely exist now in equilibrium with present-day climate and natural disturbance, in the absence of human activities (Ojima et al. 2000). The PNV data used in this paper is based on the ISLSCP initiative II data collection and it is not necessarily representative of pre-human settlement vegetation in non-human dominated regions, such as the TP (Ramankutty and Foley 1999). Without human influences and with present-day climate, almost the whole TP would be covered by tundra (Figure 2.2b). Compared with the current land cover (Figure 2.2a), a much smaller region (Figure 2.2b) is covered with grassland on the east part and less bare land on the northern boundary. Ice and permanent snow would be located in the northwest part of the TP. More accurate estimates of the land cover changes on the TP should be developed. However, the current estimates enable us to begin exploring the issues addressed in the modelling experiments conducted in this study.

The control experiment run called “current scenario” used a standard ECHAM5 simulation to represent the “real” climate system with the modern day land cover. The sensitivity experiment, called “natural scenario”, replaced the current land cover on the TP (Figure 2.2a) with the natural land cover without anthropogenic influences (Figure 2.2b). In ECHAM5, vegetation is characterized by the ratio of the leaf area to the projection area and the fractional area covered by plants (Leaf Area Index (LAI) and Vegetation Fraction (VGR), respectively; see Hagemann (2002) for more details). The land surface parameters are allocated to each ecosystem type based on the 1-km resolution global land cover characteristics database derived from 1-km Advanced Very High Resolution Radiometer (AVHRR) data (available from U.S. Geological Survey 2001). Table 2.1 lists the main surface parameters applied in ECHAM5 for major land cover types on the TP. For snow-free land surfaces, the annual mean background albedo derived from satellite data only depends on the ecosystem type. Figure 2.3 shows the yearly means of LAI and VGR used in the current and natural experiment, respectively. In the central and western part of the TP, current LAI and VGR are lower than the natural case, and they are higher mainly in the southeastern part. High LAI values correspond to high canopy conductance values, resulting in a relatively large portion of available energy being used for evapotranspiration (van den Hurk et al. 2003). The annual cycle of LAI and VGR (Figure 2.4) shows that the main differences occur in the boreal summer. In the winter, current VGR is larger than the natural one, while current LAI is always smaller than natural LAI.

Table 2.1: Surface parameters for major land cover types on the Tibetan Plateau. It includes background surface albedo  $\alpha$ , surface roughness length due to vegetation  $Z_{0,veg}$ , fractional vegetation cover VGR, leaf area index (LAI) for the growing (g) and dormancy season (d) and the volumetric wilting point  $f_{pwp}$ . (from Hagemann 2002).

Global Ecosystems Legend	Albedo $\alpha$	$Z_{0,veg}$	VGR <sub>g</sub>	VGR <sub>d</sub>	LAI <sub>g</sub>	LAI <sub>d</sub>	$f_{pwp}$
Water	0.07	0.0002	0.	0.	0.	0.	0.
Shrubland	0.2	0.1	0.44	0.	1.5	0.1	0.50
Tundra	0.17	0.03	0.51	0.	2.2	0.4	0.34
Grassland	0.16	0.03	0.9	0.1	4.5	0.	0.49
Bare Land	0.28	0.005	0.	0.	0.	0.	0.
Ice/Permanent Snow Cover	0.7	0.005	0.	0.	0.	0.	0.

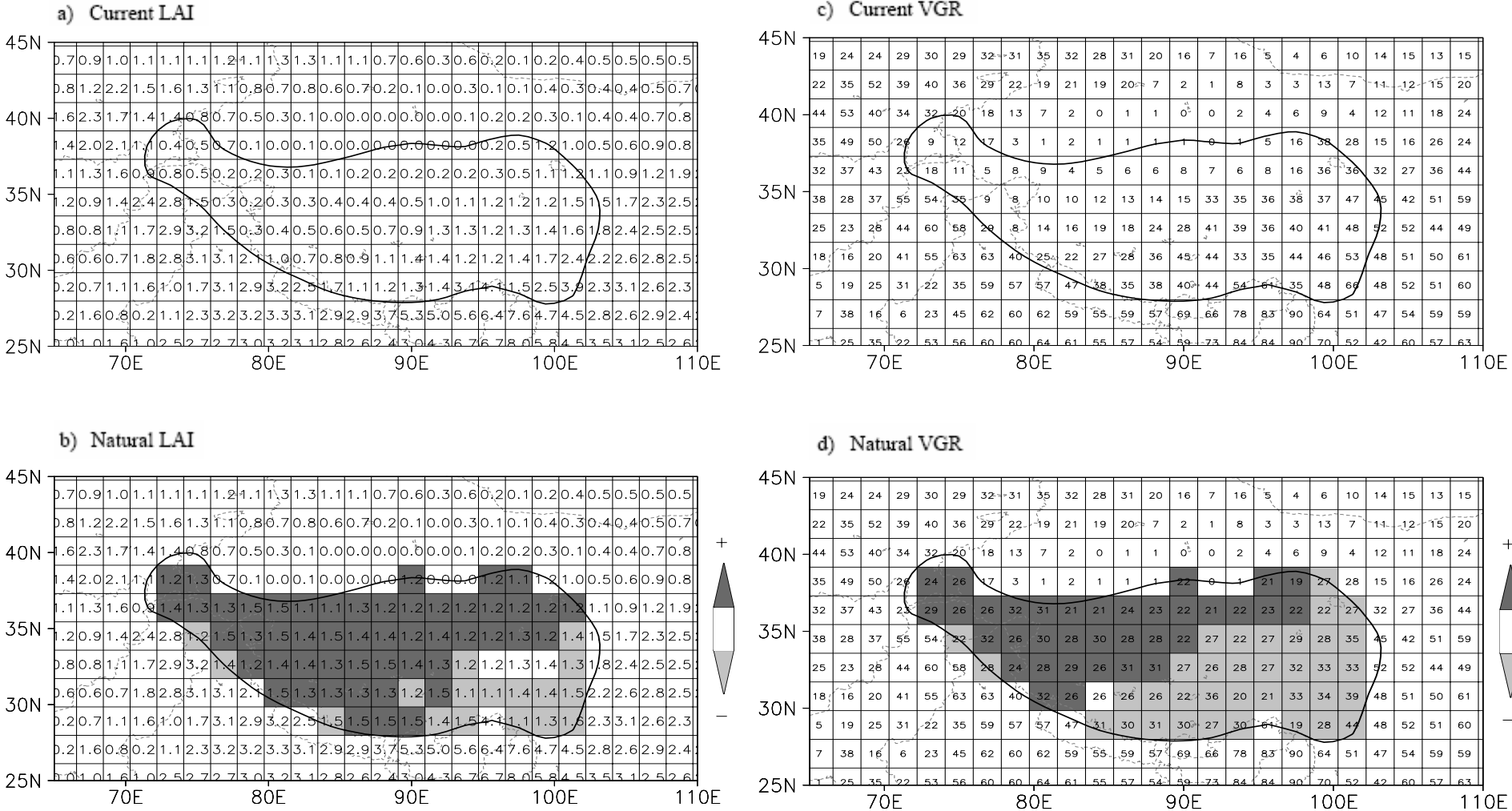


Figure 2.3. Leaf area index (LAI;) and vegetation fraction (VGR, unit: %) distribution on the Tibetan Plateau for current and natural scenarios. Grids are shaded where changes (current-natural) are greater than 0.01 or 1%.

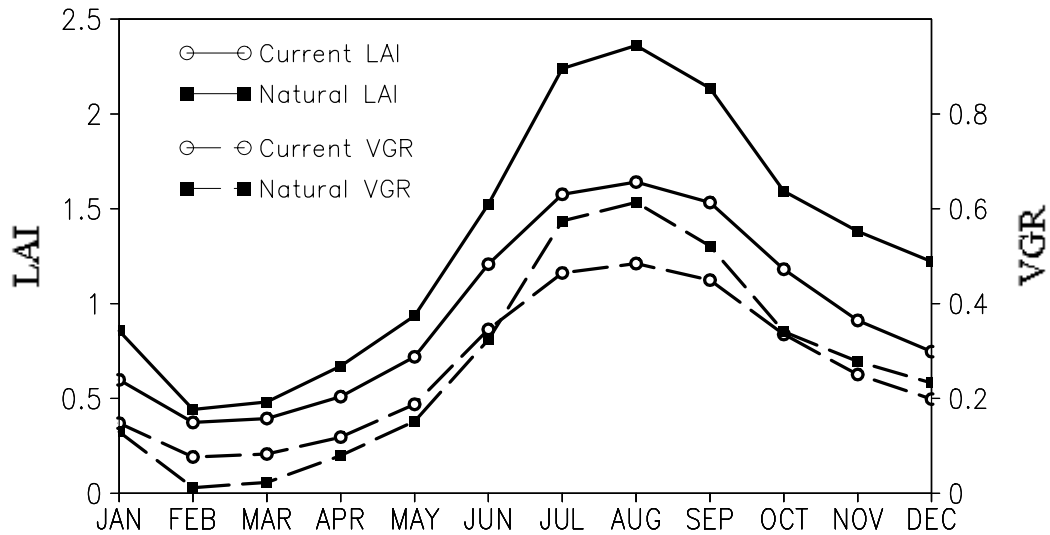


Figure 2.4. Seasonal variations of the area averaged Leaf Area Index (LAI, left) and vegetation fraction (VGR, right, unit: %) on the Tibetan Plateau from the current and natural scenarios.

Both experiments are integrated for 22 years, driven with climatological global sea surface temperature (SST) and sea ice averaged over the period 1979-1988 to eliminate additional inter-annual variability. The atmospheric variability represented in such integrations is generally less than that in simulations with inter-annually varying boundary conditions of SST and sea ice (Bengtsson et al. 1996). The results presented in this paper are the mean values over the last 10 years of the model simulations, discarding the first 12 years to eliminate the effects of model spin-up. In this paper, we restricted ourselves on the seasonal mean characteristics. The calendar monthly mean is calculated by a normal mean of the corresponding months of the 10 years. To evaluate the model performances, especially for the TP and its vicinity, results from the control run are compared with several observational datasets, listed in Table 2.2. Kistler et al. (2001) named the period from 1979 to present as “modern satellite” era, and also pointed out that the reanalysis data are most reliable in this period. Thus in this study, the present climate to evaluate the ECHAM5 simulation is calculated from all the datasets as the 20 years mean from 1980 to 2000. The calendar monthly mean is calculated with the normal mean of the corresponding months of the 20 years.

The natural vegetation cover simulation is compared with the current vegetation cover simulation to show the effects of land use change on the regional and global climate. In this paper, we restricted ourselves to showing the comparisons of means. Since both experiments start from the same initial condition except the land cover on TP and the integrations are short, the results from the two experiments are not independent from each other. Therefore the t test, also known as Student’s t test, is not appropriate for testing the null hypothesis that the change of land cover on the TP has no effect on the state of the modeled atmosphere (von Storch and Zwiers 1999). Von Storch and Zwiers (1999)

proposed a so-called ‘Paired Difference Test’ to test the null hypothesis that the mean difference is zero using a one-sample t test. The distributional assumptions are that the differences have a normal distribution and that all the differences come from the same distribution. This method is applied to each grid point to assess statistical significance. At the 5% (10%) significance level, one would expect 5% (10%) of the grid points to show statistically significant differences merely by chance. However, physical insight is required to ascertain the statistical significance is physical significance (von Storch and Zwiers 1999). Statistical significance is determined using seasonal (December, January, February; March, April, May; June, July, August; September, October, November) or annual rather than monthly averages to include less of the year-to-year variability (Bonan 1997). Each year of model output represents one seasonal or annual ‘sample’. The analyzed duration of both experiments (10 years) means that there are only 9 degrees of freedom when testing for the difference between two means with the method applied here.

Table 2.2. Observational datasets used: CPC Merged Analysis of Monthly Precipitation (CMAP); Climate Research Unit (CRU); Global Precipitation Climatology Project (GPCP) and reanalysis (NCEP-DOE Atmospheric Model Intercomparison Project (AMIP II) Reanalysis (NCEP-R2). Variables include monthly precipitation (P), 2 m temperature (T), zonal wind (U), meridonal wind (V), and geopotential height (H).

Dataset	Parameters	Horizontal resolution	References	Source
CMAP	P	2.5° × 2.5°	Xie and Arkin, 1997	<a href="http://www.cdc.noaa.gov/cdc/data.cmap.html">http://www.cdc.noaa.gov/cdc/data.cmap.html</a>
CRU	P; T	0.5° × 0.5°	New et al., 2002	<a href="http://www.cru.uea.ac.uk">http://www.cru.uea.ac.uk</a>
GPCP	P	2.5° × 2.5°	Adler et al., 2003	<a href="http://lwf.ncdc.noaa.gov/oa/wmo/wdcamet-ncdc.html">http://lwf.ncdc.noaa.gov/oa/wmo/wdcamet-ncdc.html</a>
NCEP- R2	T; U; V; H	2.5° × 2.5°	Kanamitsu et al., 2002	<a href="http://wesley.ncep.noaa.gov/products/wesley/reanalysis2/kan/reanl2-1.html">http://wesley.ncep.noaa.gov/products/wesley/reanalysis2/kan/reanl2-1.html</a>
ERA40	T; U; V; H	T159 (0.75°)	Simmons and Gibson, 2000	<a href="http://www.mad.zmw.de">http://www.mad.zmw.de</a>

## 2.3 Results

### 2.3.1 ECHAM5 Current Scenario

Evaluation in the Asian region is discussed in detail focusing on the summer (June July August (JJA)) rainy season and the winter (December January February (DJF)) season. Wind and geopotential height are “type A” variables in reanalysis data, which are generally strongly influenced by the available observations and are therefore the most reliable products of the reanalysis (Kistler et al. 2001). Figure 2.5 shows a comparison of wind and geopotential height anomalies from zonal mean at 200 hPa between ERA40 and the ECHAM5 current scenario. The NCEP R2 data is very similar to the ERA40, so we have only shown the ERA40 dataset. ECHAM5 reproduces the major meteorological

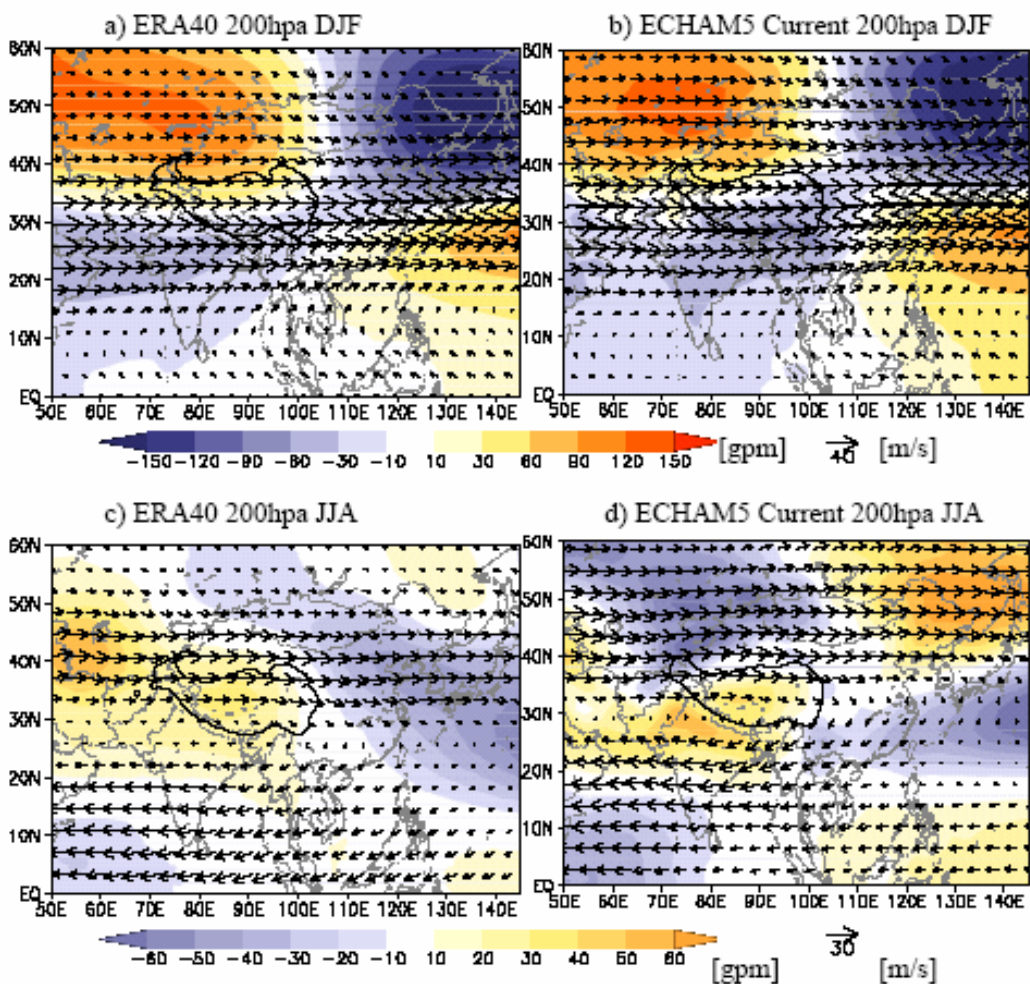


Figure 2.5. Wind circulation and geopotential height anomalies derived from the zonal mean of the whole region (50° E-140° E) at 200 hPa from ERA40 and ECHAM5 current simulations for JJA (below) and DJF (up). The thick black contour line shows the Tibetan Plateau. Coastlines and political boundaries are shown in grey contours.

features: the dominant westerlies move northward from winter to summer and an anticyclone centered on the TP appears in summer. There are also discrepancies between the model simulation and the observations. The simulation shows higher wind speed in both seasons and unrealistic pressure systems in summer: too high over India and northeast China while too low over the Indian Ocean and the northwest side of the TP. Differences may be decreased if more realistic SSTs are applied, like in AMIP experiments, rather than the climatological mean values that are used in current simulation. Figure 2.6 and Figure 2.7 are the same as Figure 2.5 but for the 500 hPa and 850 hPa levels, respectively. The model reasonably simulates the large-scale features. The westerly jet still dominates the circulation at 500 hPa in winter similar to 200 hPa level and it also shifts from the south of the TP to the north in summer.

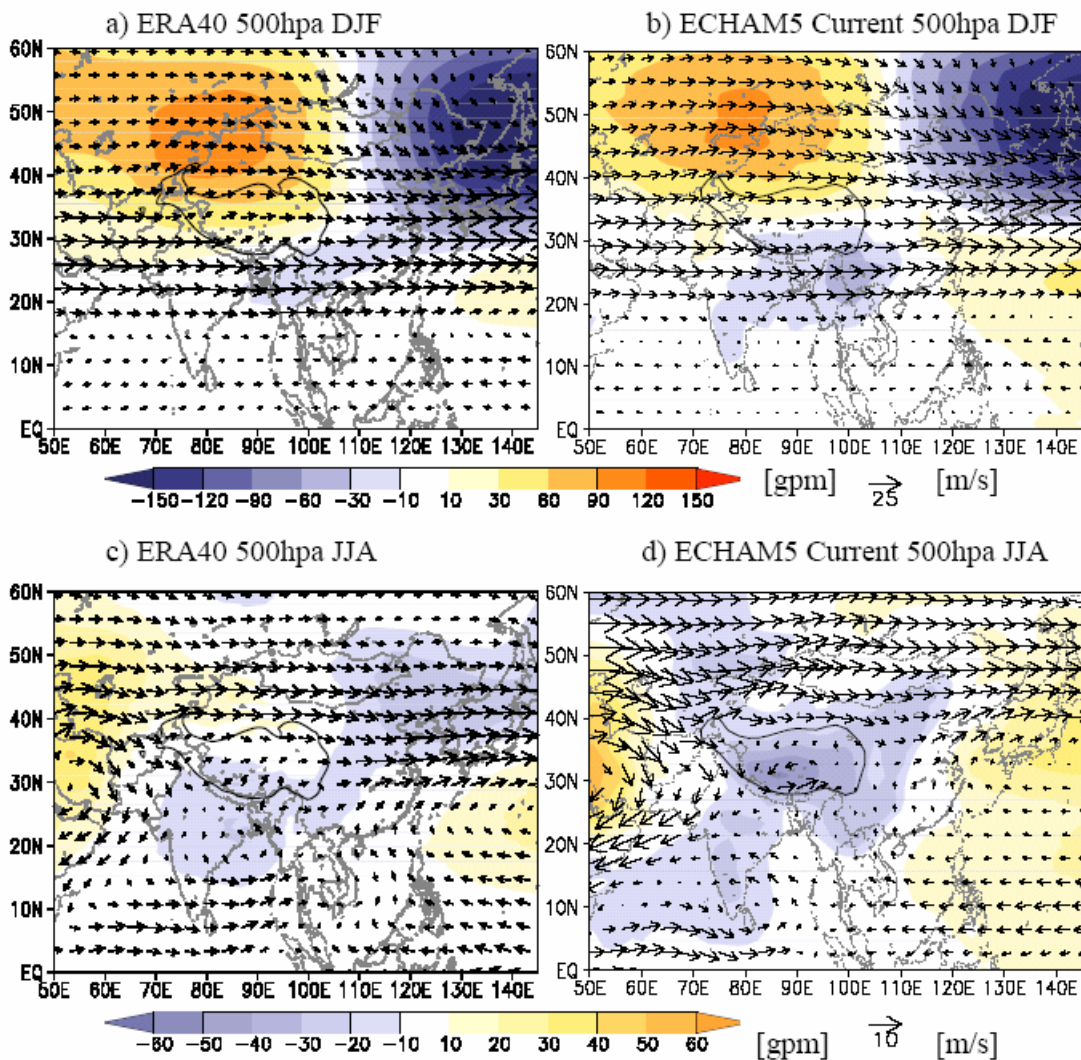


Figure 2.6. Same as Figure 2.5, but for 500 hPa.

A low pressure area is located over the TP and its vicinity at 500 hPa and 850 hPa level, while it is a high pressure area at 200 hPa. This is a very special pressure system on the TP in summer. At 850 hPa, the wind follows the landmass distribution more closely. In summer it blows from the Indian Ocean to India and from the Pacific Ocean to the East Asian continent, laden with warm and moist air mass, thus producing summer monsoon rainfall in these regions. In the winter, the wind blows from the central Eurasian continent to East Asia, transporting cold and dry air. Such circulations produce the winter monsoon for these regions. The model simulates well the deep trough centered at 140° E, 50° N, existing from 850 hPa to 200 hPa in winter, that disappears in summer and becomes a high. There is always a small trough in the lower mid troposphere that moves from the east of India in winter to the west of India in summer and gets stronger. In general, ECHAM5 realistically reproduces the major features of the circulation system in this region with somewhat higher wind speed and least realistic geopotential heights in summer. The model performs better at lower troposphere and in winter.

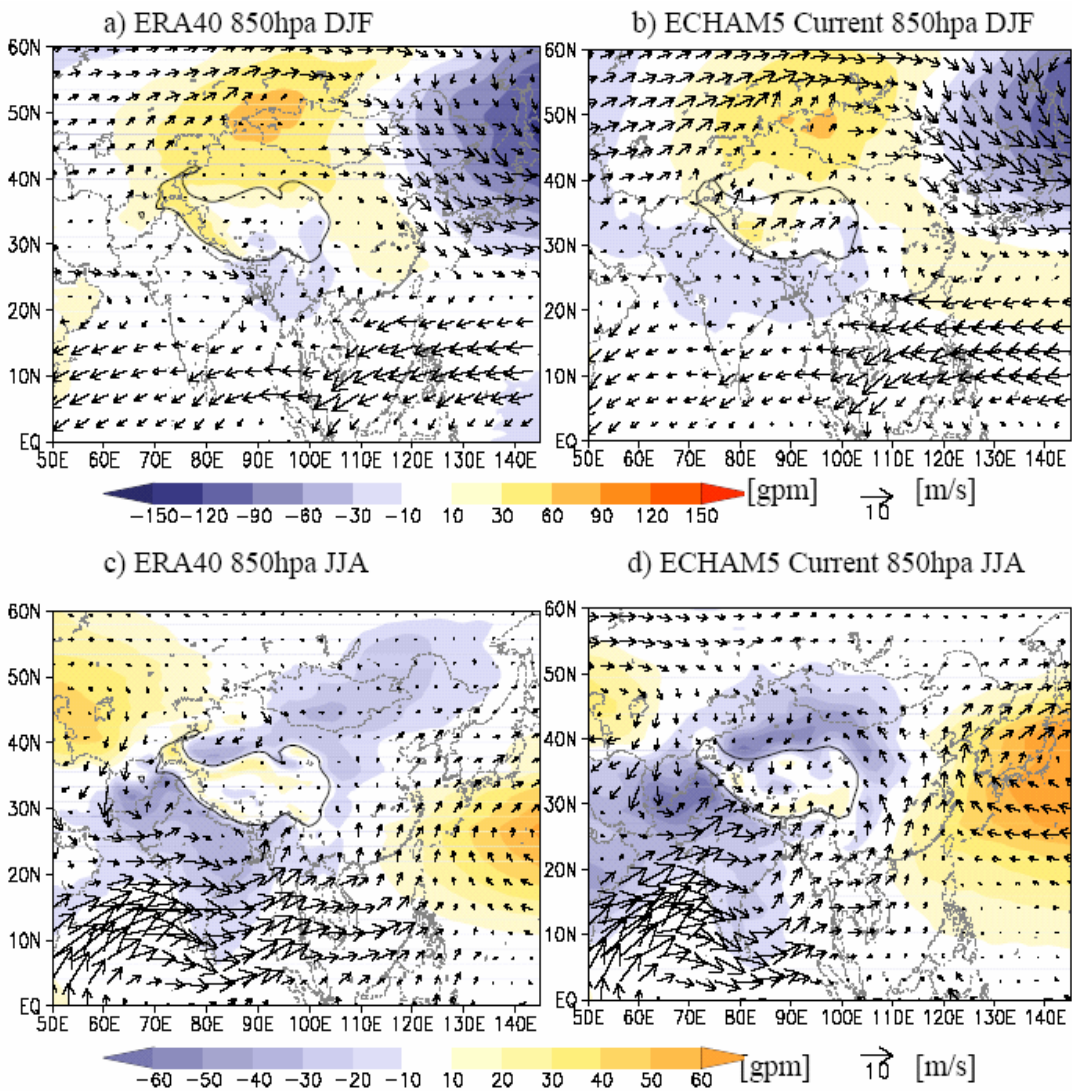


Figure 2.7. Same as Figure 2.5, but for 850 hPa. Geopotential height and wind on the TP are only for reference.

Figure 2.8 and Figure 2.9 present the 2 m air temperature in summer (JJA) and in winter (DJF) from observations (CRU), reanalysis data (ERA40 and NCEP-R2), and from our ECHAM5 current simulation, respectively. For the ERA40 and NCEP-R2 reanalysis data, 2 m temperature is a “type B” variable, partly influenced by the model parameterization, and is therefore less reliable (Kistler et al. 2001). Compared with station measurements where grid cells contain at least four stations, the reanalysis temperatures from ERA40 are consistently lower, by as much as 7° C (Frauenfeld et al. 2005). On the TP, such a topographically complex, data-sparse area, it is not surprising to see the spatial difference among ERA40, NCEP R2 and CRU data, further exaggerated by the

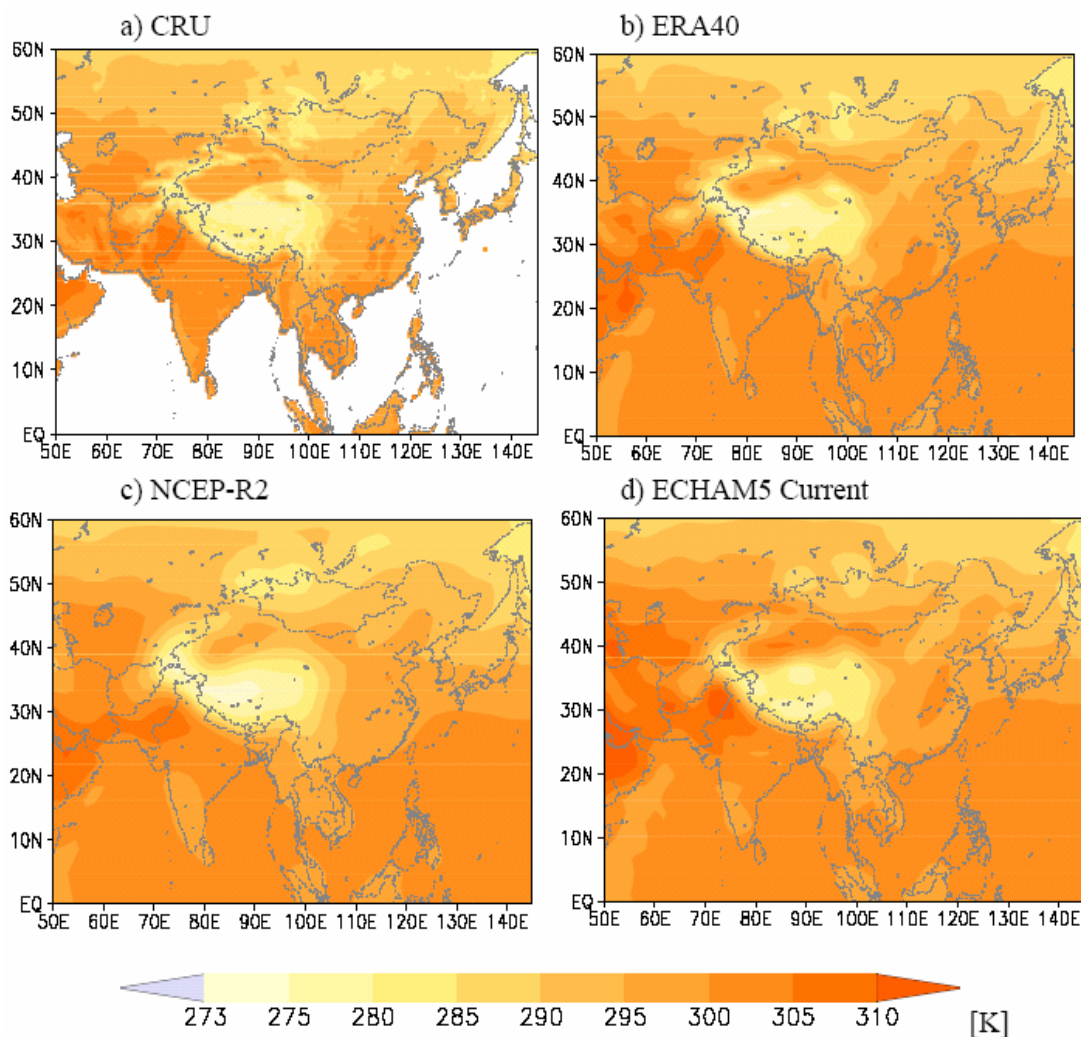


Figure 2.8. Intercomparison of summer (JJA) 2 m air temperature from a) CRU, b) ERA40, c) NCEP-R2, and d) ECHAM5 current simulation. Data information listed in Table 2.1.

different horizontal resolutions. To better represent the real surface parameters on the TP, we suggest that higher horizontal resolution data sets that resolve the steep topographic variations should be developed in the future. In general, ECHAM5 simulates well the major patterns and temperatures year round. During winter, 2 m temperatures on the TP are below  $0^{\circ}\text{C}$  on the entire plateau, with summer values of only  $0^{\circ}\text{C}$  in the west and about  $10^{\circ}\text{C}$  in the east. ECHAM5 also reproduces well the heating contrast between landmass and ocean, which is generally considered to be the most important driving mechanism for the monsoon system (e.g. Webster et al. 1998).

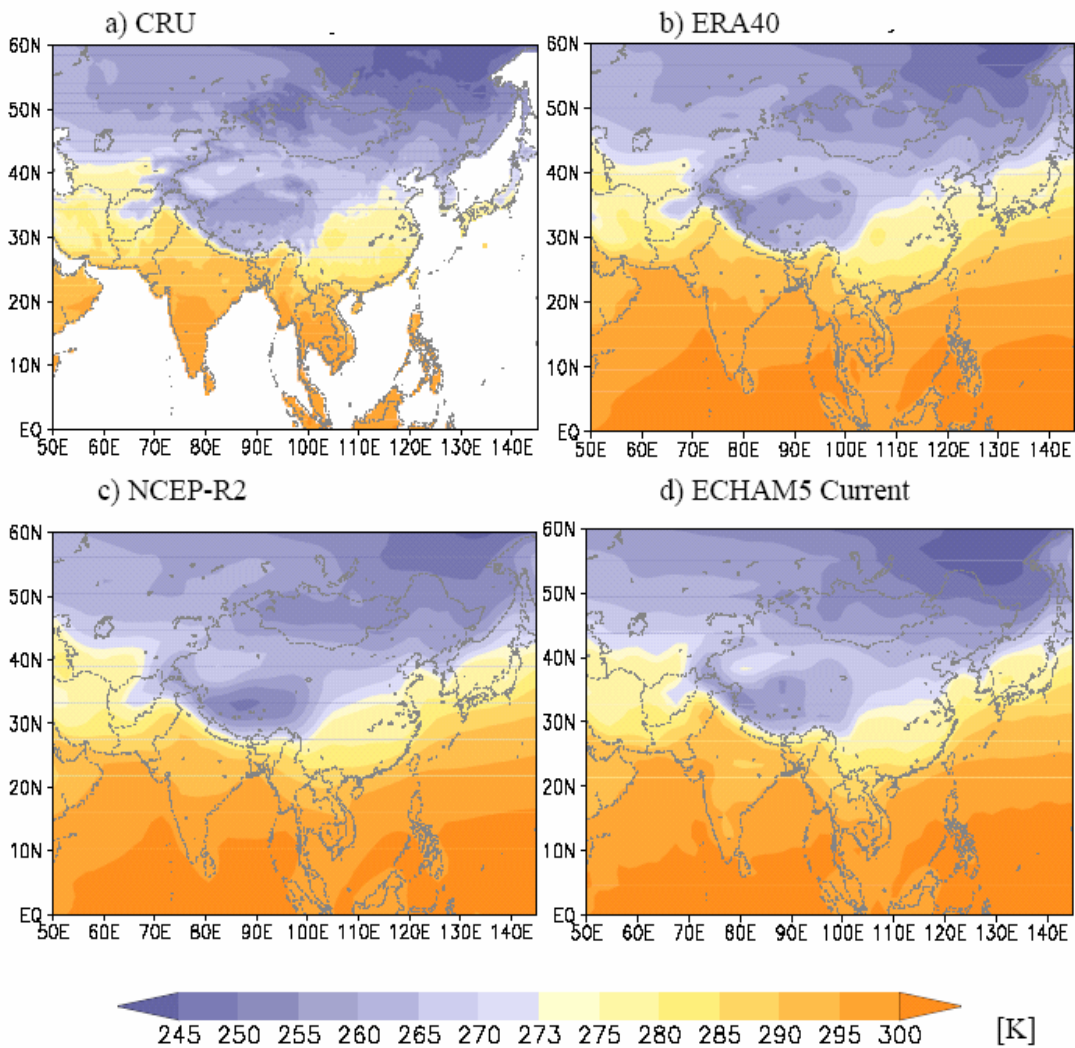


Figure 2.9. Same as Figure 2.8, but for DJF.

ECHAM5 also reproduces well the summer monsoon rainfall belt from the Indian continent to southern China (Figure 2.10), except too high (more than 20 mm/day) rainfall at the south of the Himalayas in summer. This effect may be caused by too much convective rainfall parameterized by the model at that steep topographic barrier. ECHAM5 simulates very realistically the rain belt moving back to the Tropics in winter (Figure 2.11). As mentioned in section 2.1, almost all current GCMs have very large systematic errors in simulating the mean monsoon climate and circulation (Kang et al. 2002). Due to the uncertainties of the model related to the simulation of the Asian monsoon, the values of the monsoon rainfall produced by the model should be cited with high caution. This does not, however, obstruct this study, because our main aim is to qualitatively, not quantitatively, investigate the climatic response to the land use changes on the TP.

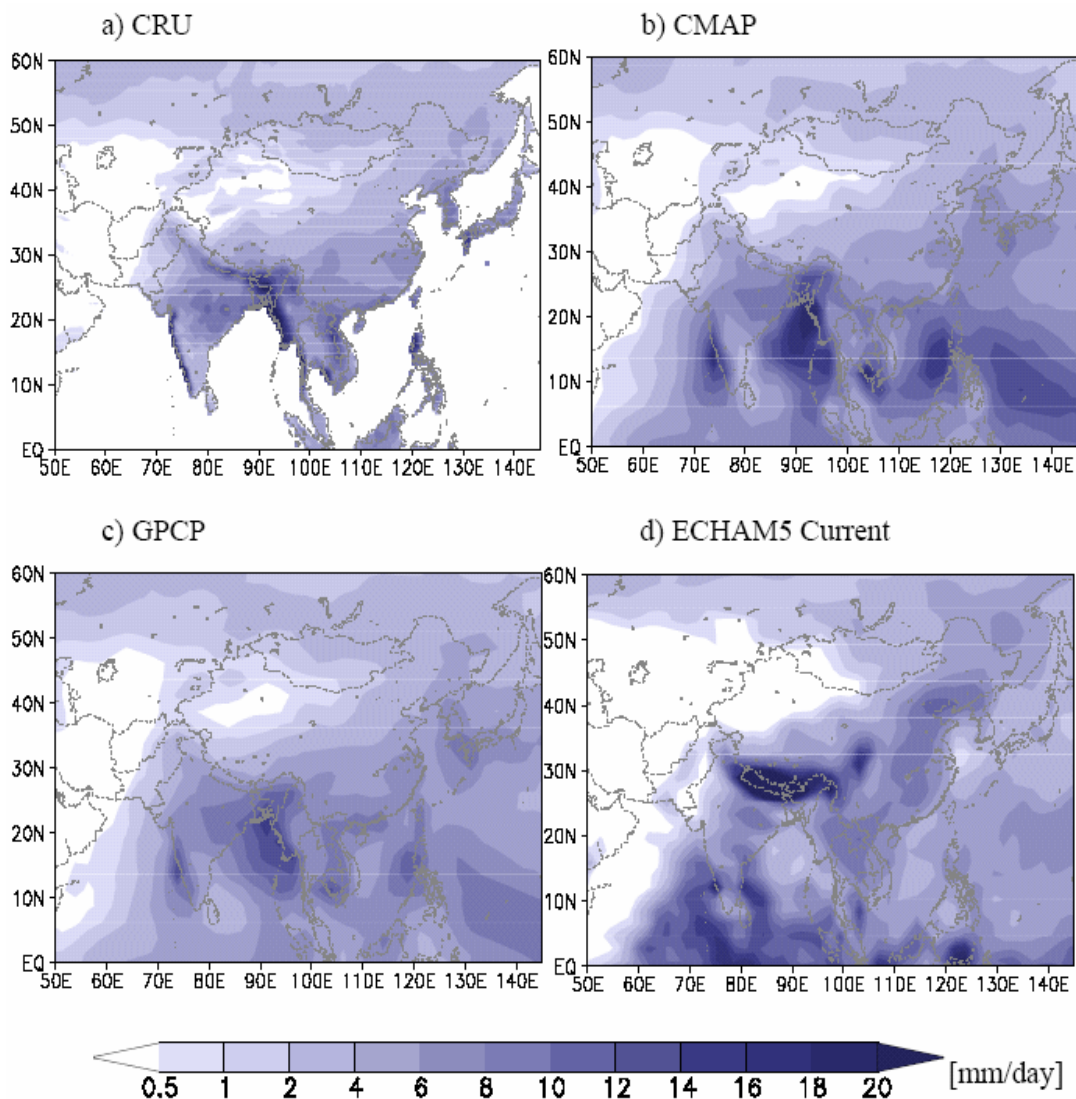


Figure 2.10. Intercomparison of summer (JJA) monthly precipitation from a) CRU, b) ERA40, c) NCEP-R2, and d) ECHAM5 current simulation. Data information listed in Table 2.1.

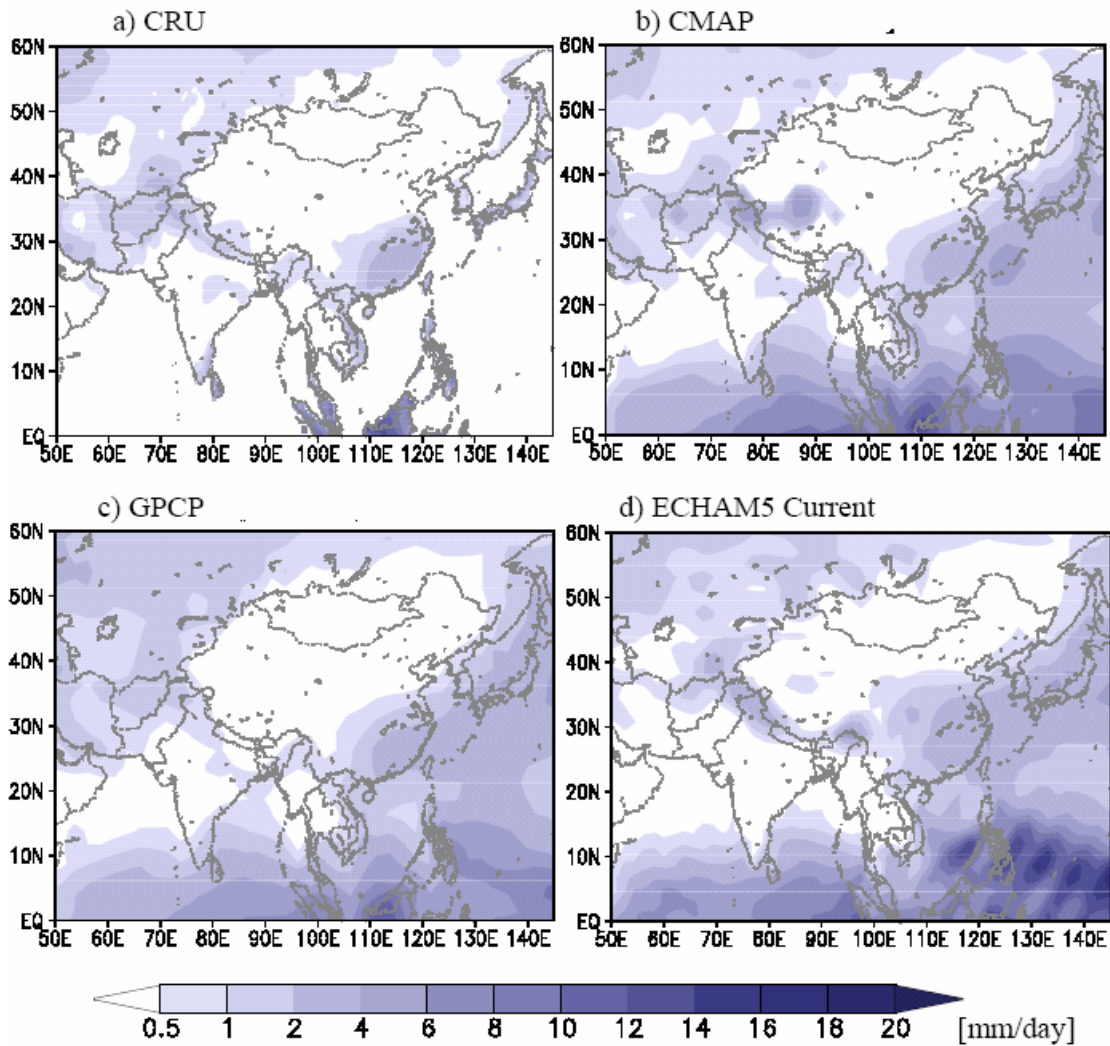


Figure 2.11. Same as Figure 2.10, but for DJF.

### 2.3.2 ECHAM5 Natural Scenario

One of the direct effects of LUC is the modification of surface albedo, and thus an influence on solar radiation absorbed at the surface. In ECHAM5, for snow-free land surfaces, an annual mean background albedo derived from satellite data is allocated to the major ecosystems shown in Table 2.1 for the TP. For land surface, the grid-mean albedo depends on a number of parameters including fractional forest area, leaf area index, bare-soil land, snow albedo calculated as a linear function of surface temperature, and the fractional snow cover (Hagemann 2002). Over water surfaces the albedo is set to a constant value of 0.07. Figure 2.12 shows the difference between the current and natural scenarios of a) albedo, b) net surface solar radiation, c) 2 m air temperature, d) soil moisture, e) evaporation, and f) precipitation. The current albedo is larger (less) in the north (south) of the TP compared to the natural one, and thus decreases (increases) the solar radiation absorbed by the surface. The modification of the radiation budget will change the surface fluxes and, thus, the local climate. Temperature is higher almost for the whole TP with its largest values in the west, mainly because there is more ice/snow covering these surfaces when assuming natural land cover. On average, the area averaged temperature of the TP increased by  $0.17^{\circ}\text{C}$  due to human induced land use change (Table 2.3).

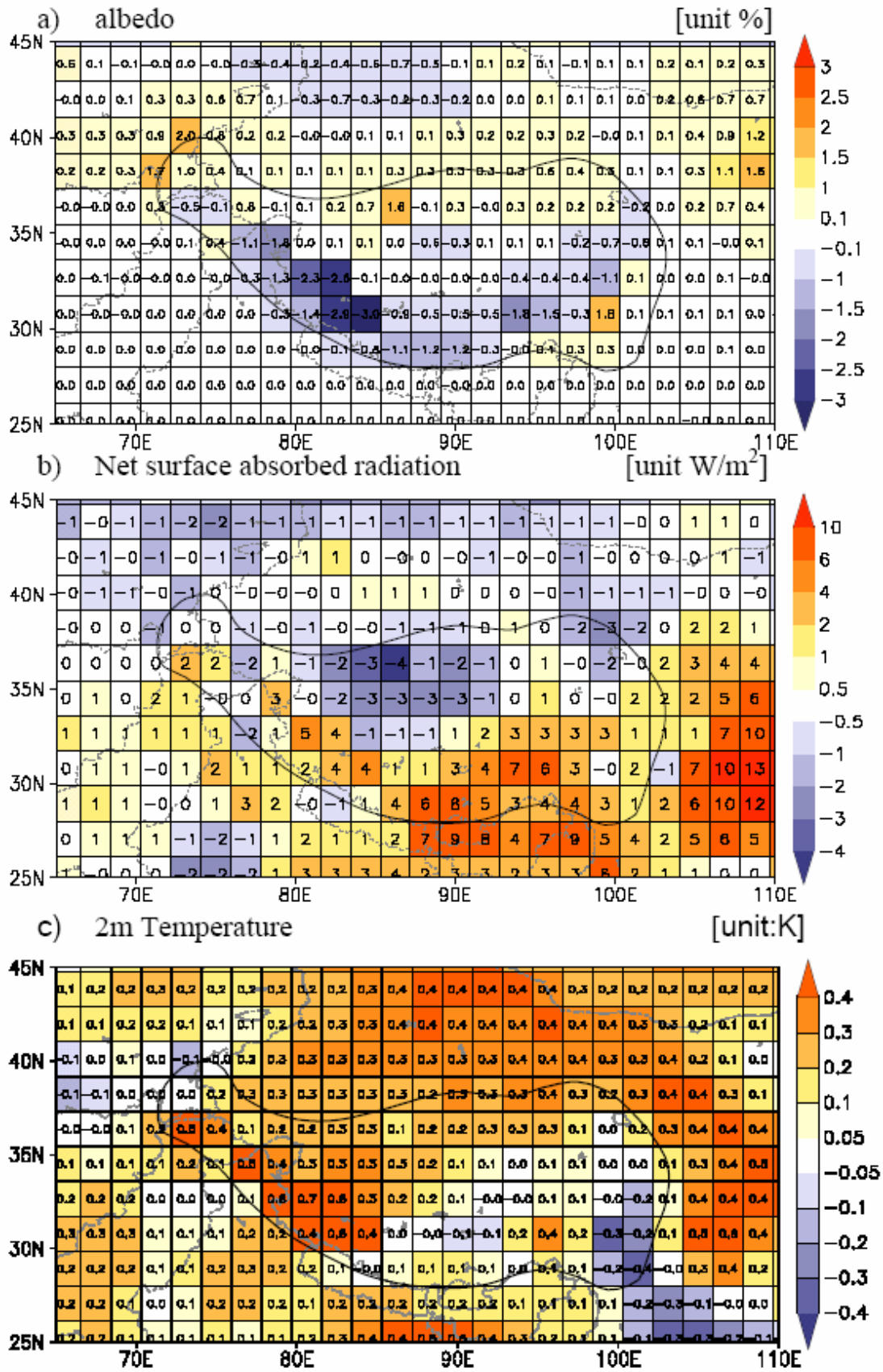


Figure 2.12. The difference (current minus natural) of a) albedo, b) net surface solar radiation, c) 2 m temperature, d) soil moisture, e) evaporation, f) precipitation.

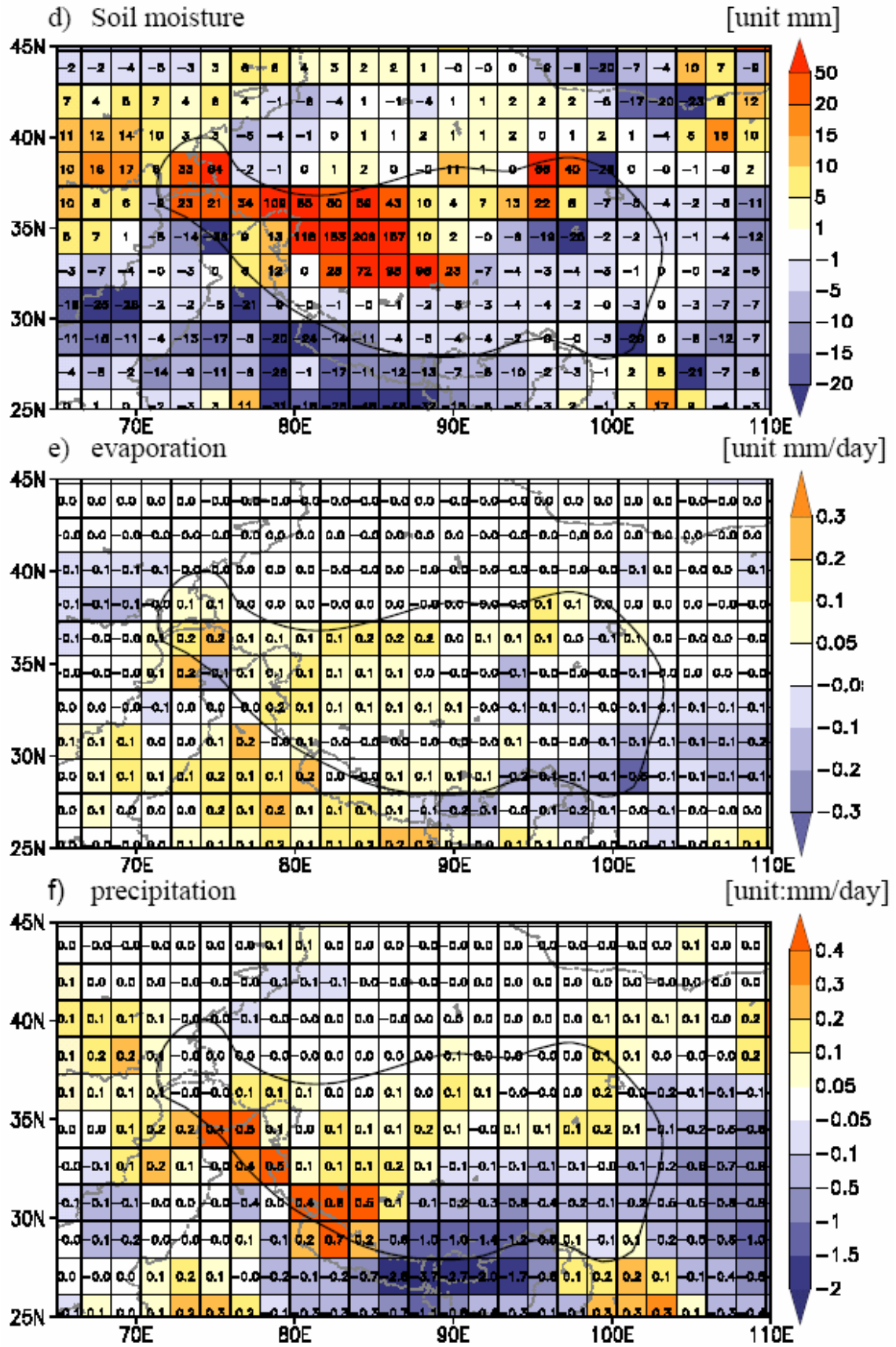


Figure 2.12. (continued)

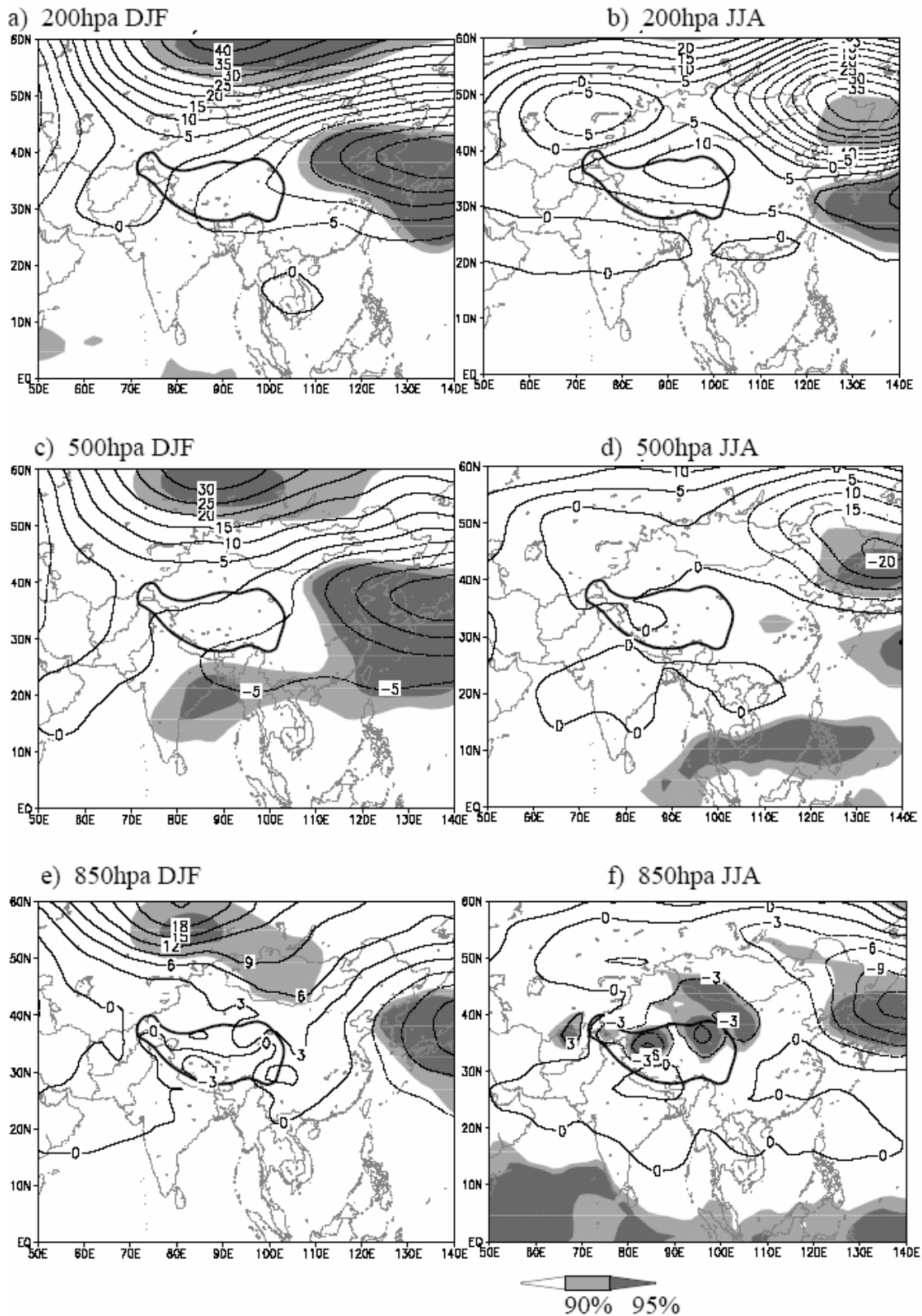


Figure 2.13. The difference (current minus natural) of geopotential heights at 200, 500, and 850 hPa (from top to bottom) in DJF (left) and JJA (right), respectively. The thick black contour line shows the Tibetan Plateau. Statistical significant changes are shaded at 90% and 95% levels. The values of geopotential height at 850 hPa on the Tibetan Plateau are only for reference.

Another direct effect of LUC on local climate is the modification of the local water cycle. The parameterization of soil hydrology in ECHAM5 comprises budget equations for the amount of snow on the surface, the amount of water intercepted by the vegetation, and the soil water storage. Only a maximum value of 10 cm is accessible for evaporation in the non-vegetated part of a grid point (bare soil). In the vegetated part the difference between actual soil moisture and the wilting point, assigned differently according to the type of vegetation (listed in Table 2.1; Hangmann 2002), is accessible for evaporation. Figure 2.12d-f shows more active water exchange in the west of the TP, with higher precipitation, soil moisture, and thus higher evaporation in the current scenario than in the natural one. In the east of the TP, the climate is modified in the opposite direction, with annual mean soil moisture content, evaporation and precipitation all decreased to different extents. The area average change of yearly mean precipitation on the TP is decreased by 9 mm (Table 2.3). It is interesting to see that precipitation is decreased dramatically to the south of the Himalayas. We do not yet know what mechanisms are contributing to the observed changes. The observed changes are not limited locally to the TP. To study the remote impact of LUC on the TP, the analysis in the following section focuses on the Asian monsoon region.

Figure 2.13 shows the changes (current minus natural scenario) of geopotential height in winter (DJF) and summer (JJA) at 200 hPa, 500 hPa and 850 hPa, respectively. Significance levels of 90% and 95% are shaded. In winter, the geopotential heights are increased to the north of the TP at all levels, which will weaken the westerlies in this region, while the geopotential heights decrease to the east of the TP. The trough centered at 140° E, 50° N is strengthened and deeper, intensifying the winter monsoon in East Asia. In summer, the anticyclone over the TP at 200 hPa gets stronger, however it does not pass the 90% significance level. The geopotential height gets lower in the lower troposphere, which will intensify the special pressure system over the TP and thus strengthen summer monsoon on the TP. There is a weakening centre of pressure to the northeast of Asia at all levels in summer, strengthening the Northwest Pacific anticyclone. However, this decreasing centre also prevents the wind blowing further from the Pacific to north China, suggesting that the East Asia summer monsoon in North China is weakened. The circulation changes provide the dynamical basis for the impact of LUC transmitting to remote regions.

Figure 2.14 presents the temperature changes (current minus natural scenario) for the Asian region. In spring temperature increases in central Siberia and also in the south of the Himalayas and India. Temperature also increases at the western TP, however, it does not pass the 90% significance level. In southern China, the temperature decreases along the coastal regions. The warming trends at northern China, India, and the western TP last till summer and autumn. In winter, the temperature decreases in entire East Asia, centered at south-central China.

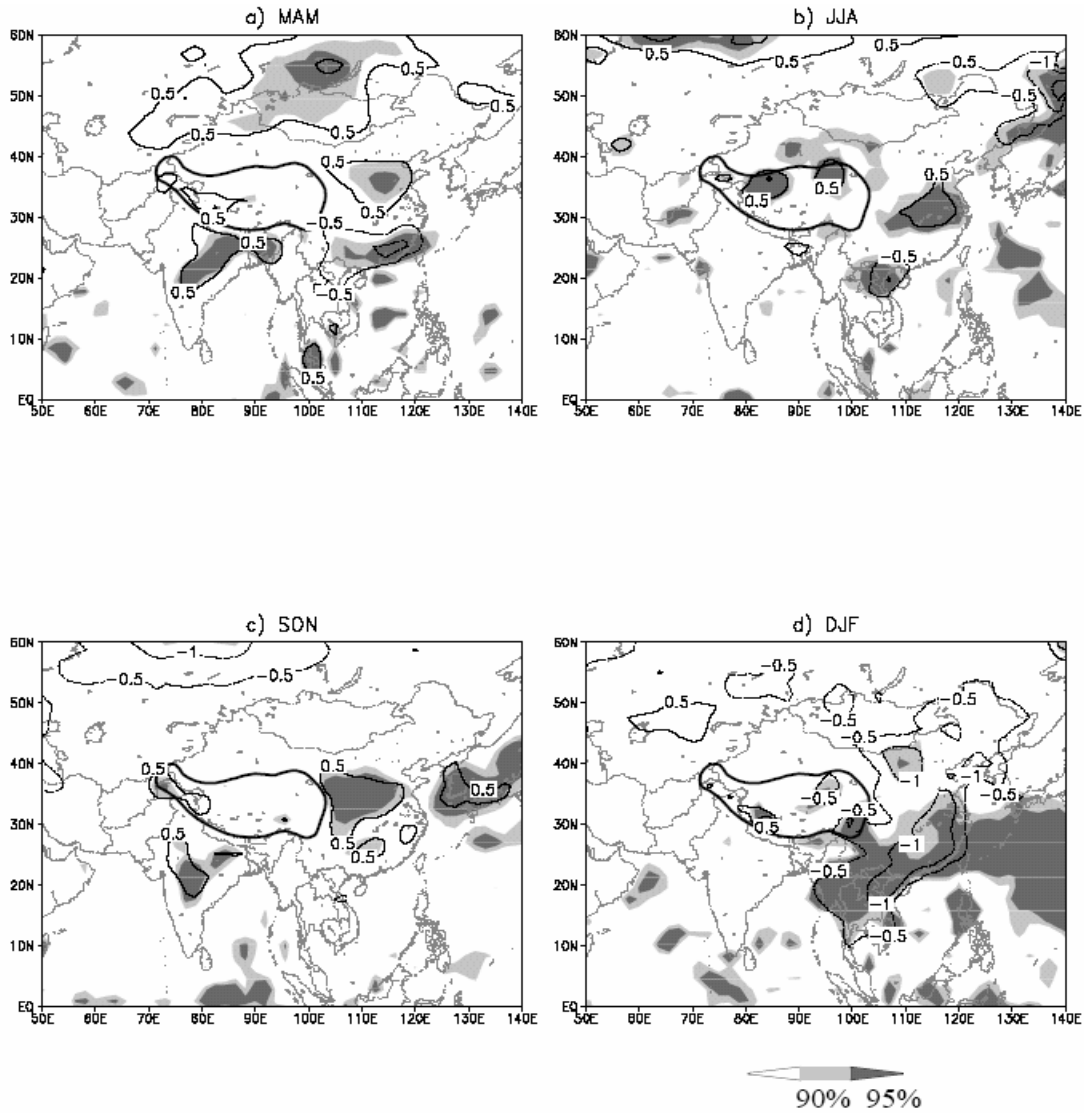


Figure 2.14. The difference (current minus natural) of daily 2 m temperature [K] in four seasons. The thick black contour line shows the Tibetan Plateau.

In tropical deforestation studies, it was found that the conversion of tropical forests into croplands significantly affected mean precipitation and evaporation due to local changes in tropical convection (e.g. Shukla et al. 1990). In mid-latitude deforestation studies, little change in the global scale hydrological cycle is found due to land use change (e.g. Govindasamy et al. 2001), suggesting that the precipitation dynamics in the mid latitudes are less affected by local convection but dominated by large-scale condensation associated with baroclinically driven storms. The effect of LUC on the TP on rainfall over the Asian region is shown in Figure 2.15. In spring, rainfall in the western Himalayas is intensified, which agrees well with the measurements from tree ring discussed in section 2.1. The rainfall is intensified in the South China Sea region and lasts almost all year round, although it is not always statistically significant. In central China, north of the Yangtze River valley, rainfall is weakened dramatically and this decrease lasts until summer with the center

shifted southerly. In summer, the rainfall in India is intensified, but it is not statistically significant and it changes its sign in autumn. Considering that the TP is the source for several major rivers in Asia, including Huanghe River, Yangtze River, Mekong River, and Salween River, the remote effects found in this study suggest that the land use changes on the TP should be considered when assessing flood/drought studies in India and China. Discussions in section 2.3.1 show that there are high uncertainties in the evaluation of the mean precipitation on the TP not only in the global observation datasets but also in our model simulation. More accurate simulation of the regional climate, especially the precipitation, on the Tibetan Plateau should be addressed in the future.

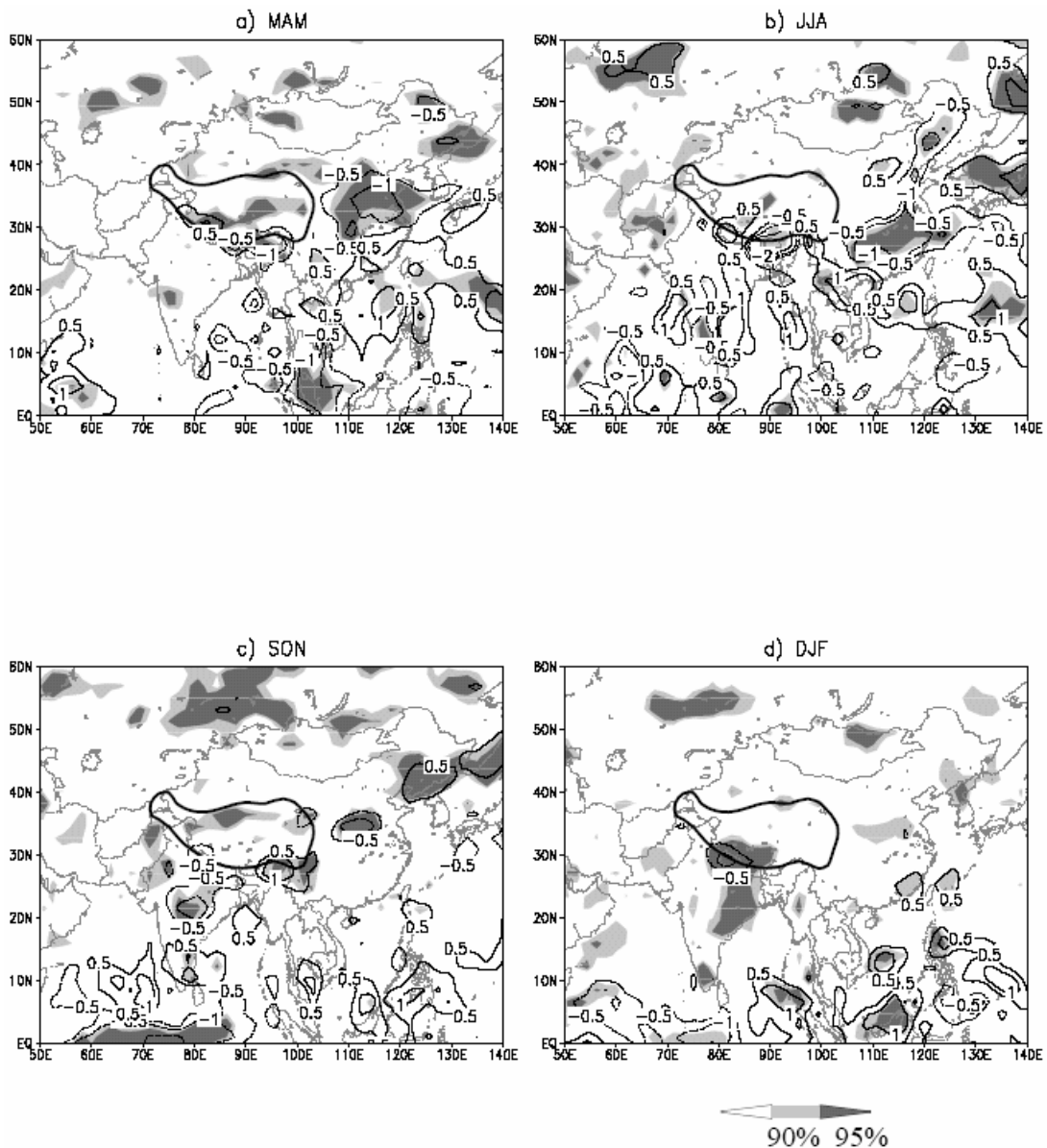


Figure 2.15. Same as Figure 2.14, but for precipitation [mm/day].

A summary of the annual mean difference between natural and current scenarios for the area averaged values over the TP region is given in Table 2.3. The current area average LAI and fractional vegetation are lower than is the potential vegetation cover, leading to a decreasing surface albedo. The land surface changes lead to higher pressure and temperature at 200 hPa and 500 hPa levels. The large-scale circulation changes will result in surface temperature and surface evaporation increasing and rainfall decreasing. It can be concluded that the TP is warmer (0.17 K) and drier under current than non-anthropogenically influenced land cover.

Table 2.3. Summary of annual mean difference between current and natural scenarios for the area averaged parameters over the TP including the leaf area index (LAI), fraction of vegetation (VGR), surface albedo, geopotential height (H, unit: gpm) and atmospheric temperature (T, unit: K) at 200 hPa and 500 hPa, daily precipitation (P, unit: mm/day), Evaporation (E, unit: mm/day), and atmospheric temperature at 2m ( $T_{2m}$ , unit: K).

	LAI	VGR	Albedo	H <sub>200</sub>	H <sub>500</sub>	T <sub>200</sub>	T <sub>500</sub>	P	E	T <sub>2m</sub>
Current scenario	0.95	0.26	0.2798	12247	5776.1	219.98	263.69	3.05	-1.24	271.70
Natural Scenario	1.32	0.27	0.2830	12241	5774.1	219.73	263.57	3.08	-1.26	271.53
Diff	-0.37	-0.01	-0.0002	6	2.0	0.25	0.12	-0.03	0.02	0.17

Figure 2.16 shows the global response of geopotential heights at 200 hPa and 500 hPa to the land cover change on TP, respectively. The circulation changes mainly in the middle and high latitude regions. There are several enhanced centres, e.g., Siberia, southwest America, south Indian Ocean, and southeast Australia, and south Brazil mainly at 200 hPa level and several weakening centers as well, e.g., Canada, Drake Passage between South America and Antarctica, and a small region located in the North Pacific Ocean centered at 35°N, 160°W area. All these changes of circulation will reflect the changing patterns of temperature, as seen later. The mechanisms of such changes of circulation are complicated and cannot be well explained by only one scenario run in the present paper. More studies concerning this point should be performed in future.

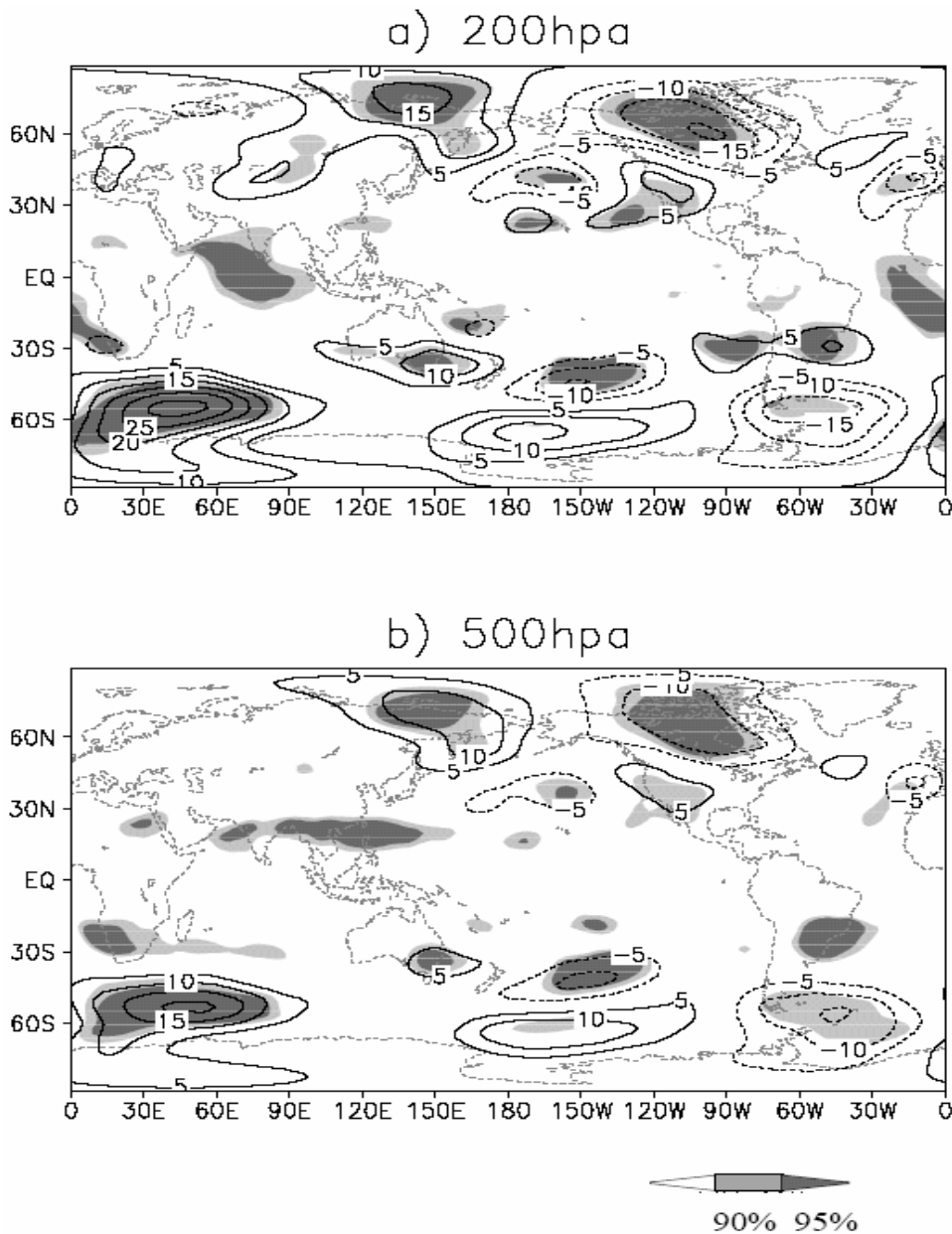


Figure 2.16. Difference (current minus natural, contour line) of annual mean geopotential heights at a) 200 hPa and b) 500 hPa, respectively. Significant changes are shaded at 90% and 95% levels, respectively.

Figure 2.17 shows the global change of the 10-year mean daily temperature and yearly precipitation due to LUC on the TP. Significance levels are also provided at 90% and 95%. The distributions of temperature changes are highly related to the changes of circulation shown in Figure 2.16. Several regions including Siberia, USA, and South America are warmer, while Europe, Canada and Africa are colder as a result of human-induced LUC on the TP. Asia, northwest China, Mongolia and India are getting warmer while northeast China, Southeast Asia are getting colder with current land cover on TP. However, not all changing centers pass the significant levels. Changes in Siberia, North America, Brazil, Southeast Asia are statistically significant. It is interesting to find that the changes in the Polar Regions are also statistically significant. As discussed in

section 2.2, the statistical significance still needs to be ascertained by further physical insight. Figure 2.17c shows that rainfall is intensified over Southeast Asia, Sea of Japan, west Pacific centered at 20° N, 180° area, the Gulf of Mexico, and southwest of the Indian Ocean. Decreases of rainfall can also be found in several regions including central China, northeast of the Indian Ocean, the western Pacific along the Equator and Brazil. As shown in Figure 2.17d, only small proportions of these changes are statistically significant. Since precipitation is highly related to the local or regional processes, remote impacts should be treated cautiously. We suggest more scenario experiments including land surface boundary changes to be performed for the TP in future. There is strong warming, but only relatively small changes of precipitation in the Polar Regions. This response of the polar climate to LUC on the TP may shed some light on the poor ability of most GCMs to accurately represent Arctic Climate (Randall et al., 1998). The area averages for large parts of the Northern Hemisphere (0° -70° N), the Southern Hemisphere (0° -70° S) and the globe (70° S-70° N) are listed in Table 2.4.

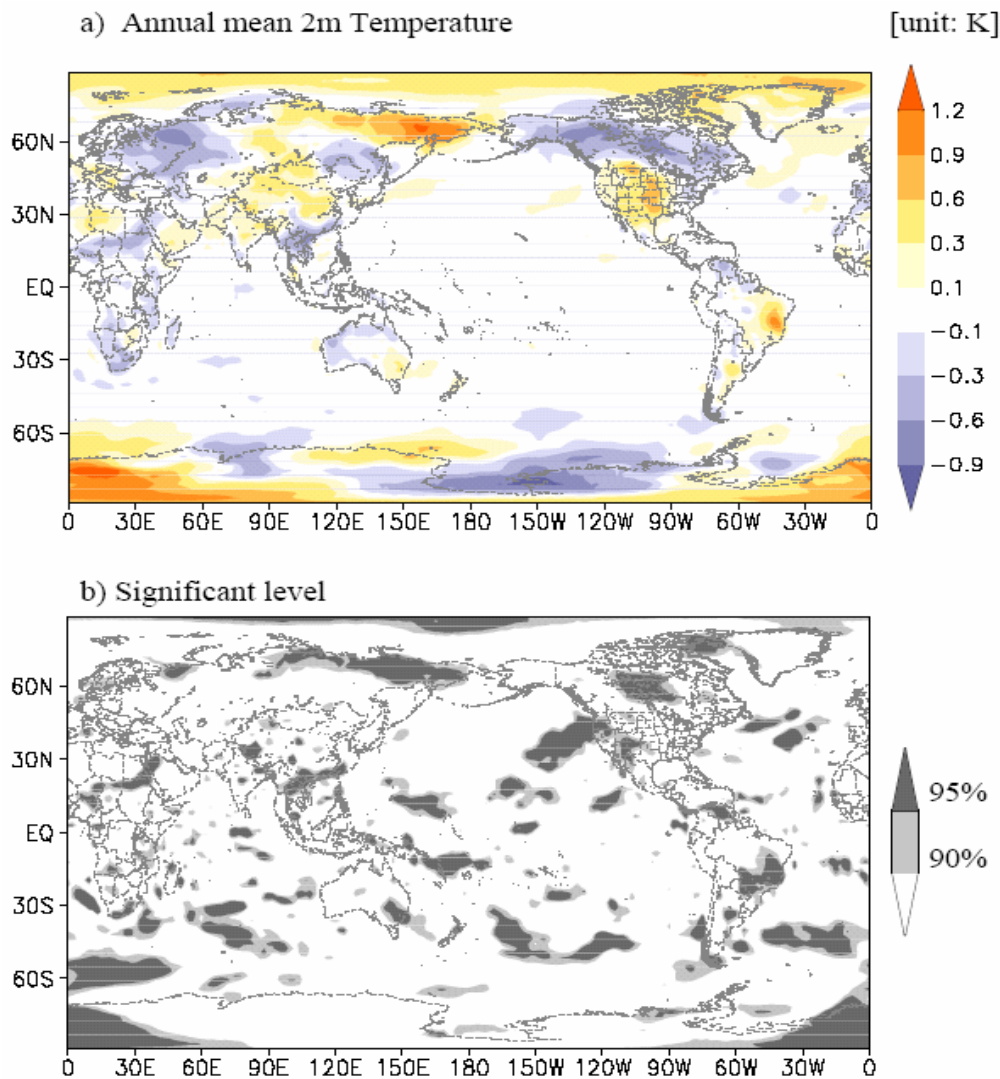


Figure 2.17. Difference (current minus natural) of a) daily 2 m temperature and c) yearly mean precipitation and corresponding significance levels for b) and d) at 90% and 95%, respectively.

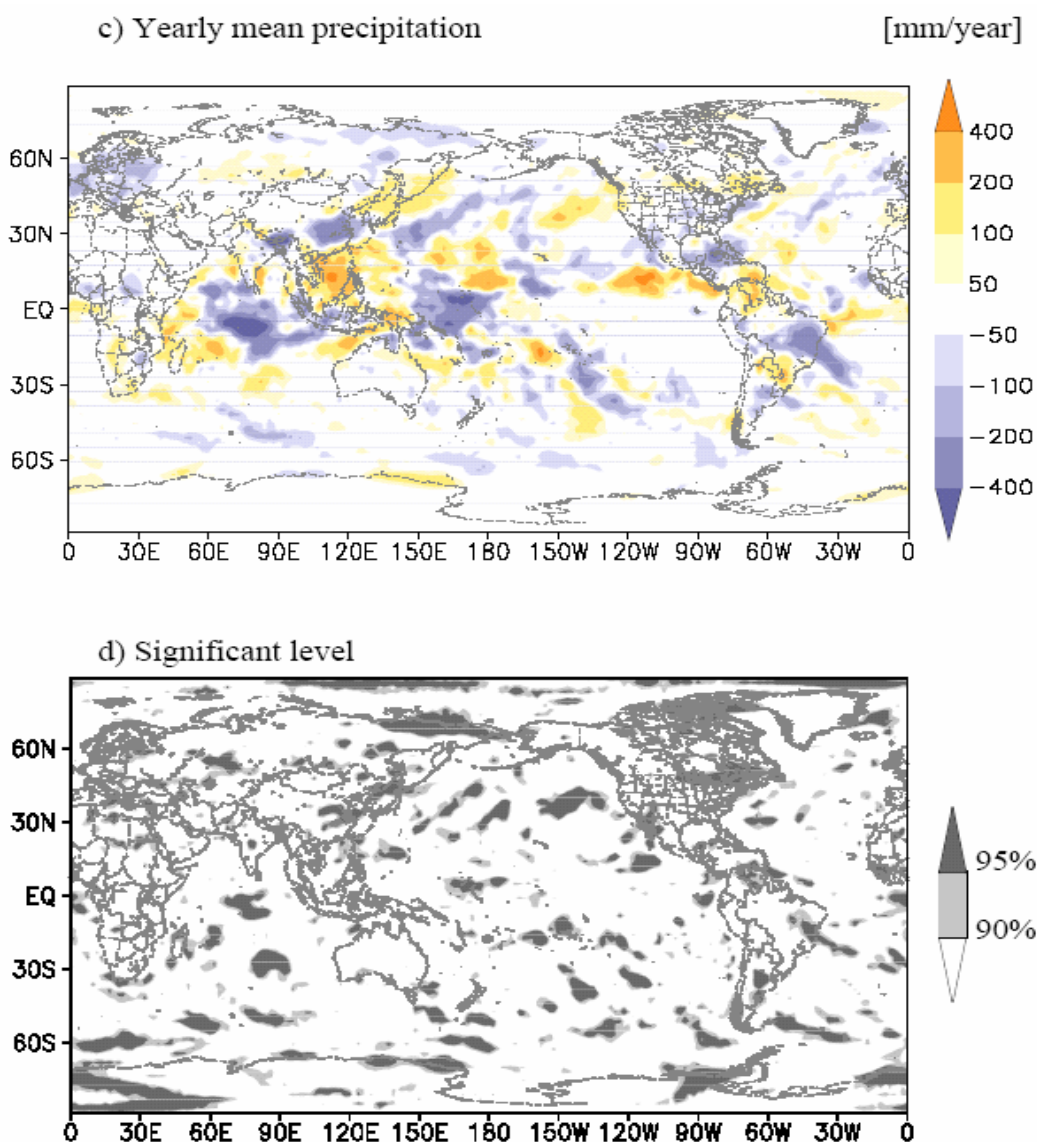


Figure 2.17. (continued)

Table 2.4. Comparison of 10 years daily mean temperature and yearly mean precipitation from current and natural simulation for large parts of the Northern Hemisphere (NH; Equator-70° N), the Southern Hemisphere (SH; 70° S-Equator), and the globe (70° S-70° N).

Regions	Temperature [K]			Precipitation [mm/year]		
	Current	Natural	Current minus Natural	Current	Natural	Current minus Natural
NH	290.113	290.104	0.009	1135.70	1128.12	7.58
SH	289.587	289.585	0.002	1089.27	1094.72	-5.45
Globe	289.850	289.845	0.005	1112.49	1111.42	1.07

## **2.4 Conclusion and discussions**

We have performed “equilibrium” climate simulations using the most recent version of the Max Planck Institute for Meteorology atmospheric general circulation model, ECHAM5. Our analysis shows that anthropogenic land use changes (LUC) on the Tibetan Plateau (TP) influence the local and remote climate. Specifically, the TP is warmer (0.17° C) and drier (-9 mm/year) than it would be without anthropogenic LUC. The TP has been observed to warm over recent decades, corresponding with a concurrent human-induced LUC towards urban and desertified areas. This trend towards warming is shown in our model experiments. We hypothesize that at least some of the observed TP temperature increase is due to the human-induced LUC. More observational studies of the characteristics of precipitation changes on the TP will help to validate or refute this hypothesis. Human-induced LUC on the TP results in an intensification of the Indian summer monsoon and a weakening of the East Asia monsoon in China. The latter helps to explain the weakening of the East Asia monsoon in the last 120 years (Fu 2003). The global climate due to LUC on the TP is slightly wetter (+1mm per year), but no distinct temperature changes in the model simulations are observed.

It should be kept in mind that the results mentioned above are obtained from the response of only one simulation to local LUC on the TP and, therefore, should be treated qualitatively but not quantitatively. One potential source of uncertainty that we have not completely accounted for is our ability to simulate the local climate system on the TP. The detailed local response is uncertain because we have not precisely resolved either the terrain or individual storms. However, the large-scale patterns match well with observations. It is possible that other GCMs would yield quantitatively different results, because the results may be highly sensitive to the formulation of the model and the parameterization of various physical processes. As an example, the evaluations of impacts of deforestation in the Amazonian River basin from different studies diverge considerably in magnitude and even the sign of the impacts (Lean and Rowntree 1997). Experience with global (AMIP; Gates et al. 1999) and regional (Project to Intercompare Regional Climate Simulations (PIRCS); Gutowski et al. 1998) climate modelling has demonstrated the usefulness of intercomparing model results. It is suggested therefore that more studies evaluating impacts of land use changes on the Tibetan Plateau would supplement the results reported here.

The goal of this study was to highlight the response of the climate system to changes in land cover. SST and sea ice are prescribed to isolate the influence of the land use change. In the future, it will be valuable to perform simulations with an interacting ocean, allowing for the effects of El Niño-Southern Oscillation. Grassland currently occupies about 50% of the TP and may act as a carbon sink nowadays (Du et al. 2004). It will be interesting to perform future scenario experiments that include effects of greenhouse gas, like CO<sub>2</sub>, when assessing the impact of the future land cover change on the TP.

Additionally, an improved parameterization of convection suitable for steep topography and a higher resolution could increase the reliability of the model simulations. Regional or meso-scale models embedded within GCMs may be able to assess more realistically the consequences of LUC on local scales, especially when they occur with high spatial heterogeneity. Cui et al. (2004) concluded that a regional model might improve the local climate simulation on the TP. Such a nested model system may help not only to specify the local response to LUC but also transfer or downscale the information from global models. Generally very high resolution or locally adjusted grids will be necessary to fully account for the effects of TP ecological modifications on large scale and global climate.

## References

- Adler, R.F., J. Susskind, G. J. Huffman, D. Bolvin, E. Nelkin, A. Chang, R. Ferraro, A. Gruber, P. Xie, J. Janowiak, B. Rudolf, U. Schneider, S. Curtis, and P. Arkin, 2003: The version 2 Global Precipitation Climatology Project (GPCP) monthly precipitation analysis (1979-present). *J. Hydrometeor.* **4**(6), 1147-1167.
- Bengtsson, L., K. Arpe, E. Roeckner, and U. Schulzweida, 1996: Climate predictability experiments with a general circulation model. *Clim. Dyn.*, **12**, 261-278.
- Beniston, M., 2003: Climatic change in mountain regions: A review of possible impacts. *Climatic Change*, **59**, 5-31.
- Bonan, G. B., 1997: Effects of land use on the climate of the United States. *Climatic Change*, **37**, 449-486.
- Braeuning, A., and B. Mantwill, 2004: Summer temperature and summer monsoon history on the Tibetan Plateau during the last 400 years recorded by tree rings. *Geophys. Res. Lett.*, **31**, L24205, doi:10.1029/2004GL020793.
- Broccoli, A. J., and S. Manabe, 1992: The effect of orography on middle latitude northern hemisphere dry climates, *J. Climate*, **5**, 1181-1201.
- Charney, J. G., 1975: Dynamics of deserts and droughts in the Sahel. *Q. J. R. Meteor. Soc.*, **101**, 193-202.
- Clark, D., Y. Xue, P. Valdes, and R. Harding, 2001: Impact of land surface degradation over different subregions in Sahel on climate in tropical North Africa. *J. Climate*, **14**, 1809-1822.
- Cole, J. E., D. Rubd, and R. G. Faurbanks, 1994: Isotopic response to international climate variability simulated by an atmospheric general circulation model, *Quat. Sci. Rev.*, **12**, 387-406.
- Cui, X. F., H. F. Graf, B. Langmann, W. Chen, and R. H. Huang, 2004: Evaluation of daily precipitation in 1998 summer over the Tibetan Plateau using REMO. *Proceedings of the 4<sup>th</sup> international symposium on the Tibetan Plateau*, Aug. 4-7, Lhasa, China, pp.146.
- Du, M., S. Kawashima, S. Yonemura, X. Zhang, and S. Chen, 2004: Mutual influence between human activities and climate change in the Tibetan Plateau during recent years. *Global and Planetary Change*, **41**, 241-249.
- Duemenil Gates, L. D., and S. Liess, 2001: Impacts of deforestation and afforestation in the Mediterranean region as simulated by the MPI

- atmospheric GCM. *Global and Planetary Change*, **30**, 309-328.
- Frauenfeld, O. W., T. Zhang, and M. C. Serreze, 2005: Climate change and variability using European Centre for Medium-Range Weather Forecasts reanalysis (ERA40) temperatures on the Tibetan Plateau. *J. Geophys. Res.*, **110**, D02101, doi: 10.1029/2004JD005230.
- Fu, C. B., 2003: Potential impacts of human-induced land cover change on East Asia monsoon. *Global and Planetary Change*, **37**, 219-229.
- Gates, W. L., J. S. Boyle, C. Covey, C. G. Dease, C. M. Doutriaux, R. S. Drach, M. Fiorino, P. J. Gleckler, J. J. Hnilo, S. M. Marlais, T. J. Philips, G. L. Potter, B. D. Santer, K. R. Sperber, K. E. Taylor, and D. N. Williams, 1999: An overview of the results of the Atmospheric Model Intercomparison Project (AMIP). *Bull. Am. Meteorol. Soc.*, **80**, 29-55.
- Govindasamy, B., P. B. Duffy, and K. Caldeira, 2001: Land use changes and Northern Hemisphere cooling. *Geophys. Res. Lett.*, **28(2)**, 291-294.
- Gutowski, W. J., E. S. Takle, and R. W. Arritt, 1998: Project to intercompare regional climate simulations, Workshop II, 5-6 June, 1997. *Bull. Am. Meteorol. Soc.*, **79**, 657-659.
- Hagemann, S., 2002: An improved land surface dataset for global and regional climate models. *Report No. 336, Max-Planck-Institut fuer Meteorologie, Hamburg*, pp. 10.
- Henderson-Sellers, A., R. E. Dickinson, T. B. Durbidge, P. J. Kennedy, K. McGuffie, and A. J. Pitman, 1993: Tropical deforestation – Modeling local-scale and regional-scale climate change. *J. Geophys. Res.*, **98**, 7289-7315.
- Jones, P. D., and A. Moberg, 2003: Hemispheric and large-scale surface air temperature variation: An extensive revision and an update to 2001. *J. Climate*, **16**, 206-223.
- Kalnay, E., and M. Cai, 2003: Impact of urbanization and land-use change on climate, *Nature*, **423(6939)**, 528-531.
- Kanamitsu, M., W. Ebisuzaki, J. Woolen, J. Potter, J., and M. Fiorino, 2002: NCEP/DOE AMIP-II Reanalysis (R-2), *Bull. Am. Meteorol. Soc.*, **83**, 1631-1643.
- Kang, I. S., K. Jin, B. Wang, K. M. Lau, J. Shukla, V. Krishnamurthy, S. D. Schubert, D. E. Wailser, W. F. Stern, A. Kitoh, G. A. Meehl, M. Kanamitsu, V. Y. Galin, V. Satyan, C. K. Park, and Y. Liu, 2002: Intercomparison of the climatological variations of Asian summer monsoon precipitation simulated by 10 GCMs. *Clim. Dyn.*, **19**, 383-395.
- Kistler, R., E. Kalnay, W. Collins, S. Saha, G. White, J. Woollen, M. Chelliah, W. Ebisuzaki, M. Kanamitsu, V. Kousky, H. van den Dool, R. Jenne, and M. Fiorino, 2001: The NCEP-NCAR 50-year reanalysis: Monthly means CD-ROM and documentation. *Bull. Amer. Meteor. Soc.*, **82**, 247-267.
- Klein Goldewijk, K., 2001: Estimating global land use change over the past 300 years: The HYDE database. *Global Biogeochemical Cycles*, **15(2)**, 417-433.
- Lean, J., and P. R. Rowntree, 1997: Understanding the sensitivity of a GCM simulation of Amazonian deforestation to the specification of vegetation and soil characteristics. *J. Climate*, **10(6)**, 1216-1235.
- Li, X., and G. D. Cheng, 1999: A GIS aided response model of high altitude permafrost to global change. *Science in China, Series D* **42(1)**, 72-79.
- Liu, X.D., and B. Chen, 2000: Climate warming in the Tibetan Plateau during recent decades. *Int. J. Climatol.*, **20**, 1729-1742.

- Liu, X., and Z. Y. Yin, 2002: Sensitivity of East Asian monsoon climate to the Tibetan Plateau uplift, *Palaeogeogr. Palaeoecol.*, **183**, 223-245.
- Lott, F., and M. Miller, 1997: A new subgrid scale orographic drag parameterization: its testing in the ECMWF model. *Q. J. Roy. Meteorol. Soc.*, **123**, 101-127.
- Lott, F., 1999: Alleviation of stationary biases in a GCM through a mountain drag parameterization scheme and a simple representation of mountain lift forces. *Mon. Wea. Rev.*, **127**, 788-801.
- Loveland, T. R., B. C. Reed, J. F. Brown, D. O. Ohlen, J. Zhu, L. Yang, and F. Lott, 1999: Alleviation of stationary biases in a GCM through a mountain drag parameterization scheme and a simple representation of mountain lift forces. *Mon. Wea. Rev.*, **127**, 788-801.
- Manabe, S., and T. B. Terpsta, 1974: The effects of mountains on the general circulation of the atmosphere as identified by numerical experiments. *J. Meteor. Soc. Japan*, **31**, 3-42.
- Murakami, T., 1958: The sudden change of upper westerlies near the Tibetan Plateau at the beginning of summer season. *J. Meteor. Soc. Japan*, **36**, 239-247.
- New, M., D. Lister, M. Humle, and I. Makin, 2002: A high-resolution data set of surface climate over global land areas. *Clim. Res.*, **21**, 1-25.
- Niu, T., L. Chen, and Z. Zhou, 2004: The characteristics of climate change over the Tibetan Plateau in the last 40 years and the detection of the climate jumps. *Advances in Atmospheric Sciences*, **21(2)**, 193-203.
- Nobre, C. A., P. J. Sellers, and J. Shukla, 1991: Amazonian deforestation and regional climate change. *J. Climate*, **4**, 975-988.
- Ojima, D., et al., 2000: Land use/land cover change in temperate East Asia: current status and future trend. *International START secretariat*, Washington DC, USA, p. 228.
- Pan, Z., T. Eugene, M. Segal, and R. Arritt, 1999: Simulation of potential impacts of man-made land use changes on U.S. summer climate under various synoptic regimes. *J. Geophys. Res.*, **104**, 6515-6528.
- Qin, B., and Q. Huang, 1998: Evaluation of the climatic change impacts on the inland lake – A case study of Lake Qinghai, China. *Climatic Change*, **39(4)**, 695-714.
- Ramankutty, N., and J. A. Foley, 1999: Estimating historical changes in global and cover: croplands from 1700 to 1992. *Global Biogeochemical Cycles*, **13(4)**, 997-1027.
- Randall, D., J. Curry, D. Battisti, G. Flato, R. Grumbine, S. Hakkinen, D. Martinson, R. Preller, J. Walsh, and J. Weatherly, 1998: Status of and outlook for large-scale modeling of atmosphere-ice-ocean interactions in the Arctic. *Bull. Amer. Meteor. Soc.*, **79(2)**, 197-219.
- Roeckner, E., G. Bauml, L. Bonaventura, R. Brokopf, M. Esch, M. Giorgetta, S. Hagemann, I. Kirchner, L. Kornblueh, E. Manzini, A. Rhodin, U. Schlese, U. Schulzweida, and A. Tompkins, 2003: The atmospheric general circulation model ECHAM5. Part I: Model description. *Report No. 349, Max-Planck-Institut fuer Meteorologie, Hamburg*, pp. 5-6.
- Roeckner, E., R. Brokopf, M. Esch, M. Giorgetta, S. Hagemann, L. Kornblueh, E. Manzini, U. Schlese, and U. Schulzweida, 2004: The atmospheric general circulation model ECHAM5. Part II: Sensitivity of simulated climate to horizontal and vertical resolution. *Report No. 354, Max-Planck-Institut fuer*

- Meteorologie*, Hamburg, pp 18-20.
- Shukla, J., C. Nobre, and P. J. Sellers, 1990: Amazon deforestation and climate change. *Science*, **247**, 1322-1325.
- Simmons, A. J., and J. K. Gibson, 2000: The ERA40 Project Plan. *ERA40 Project Report Series No.1*, ECMWF, Reading, UK, pp. 63.
- Singh, J., and R. R. Yadav, 2005: Spring precipitation variations over the western Himalaya, India, since A.D. 1731 as deduced from tree rings. *J. Geophys. Res.*, **110**, D01110, doi:10.1029/2004JD004855.
- Snyder, P. K., and J. A. Foley, 2004: Analyzing the effects of complete tropical forest removal on the regional climate using a detailed three-dimensional energy budget: An application to Africa. *J. Geophys. Res.*, **109**, D21102, doi:10.1029/2003JD004462.
- Suh, M. S., and D. K. Lee, 2004: Impacts of land use/cover changes on surface climate over east Asia for extreme climate cases using RegCM2. *J. Geophys. Res.*, **109**, D02108, doi: 10.1029/2003JD003681.
- U.S. Geological Survey, 2001. *Global land cover characteristics data base version 2.0*. [http://edcdaac.usgs.gov/glcc/globdoc2\\_0.html](http://edcdaac.usgs.gov/glcc/globdoc2_0.html).
- Vitousek, P. M., H. A. Mooney, J. Lubchenco, and J. M. Melillo, 1997: Human domination of Earth's ecosystems, *Science*, **277**, 494-499.
- van den Hurk, B. J. J. M., P. Viterbo, and S. O. Los, 2003: Impact of leaf area index seasonality on the annual land surface evaporation in a global circulation model. *J. Geophys. Res.*, **108(D6)**, 4191, doi:10.1029/2002JD002846.
- von Storch, H., and F. W. Zwiers, 1999: *Statistical Analysis in Climate Research*. Cambridge University Press. p113.
- Wang, S. L., H. J. Jin, S. X. Li, and L. Zhao, 2000: Permafrost degradation on the Qinghai-Tibet Plateau and its environmental impacts. *Permafrost Peroglac. Process*, **11**, 43-53.
- Webster, P. J., V. O. Magaña, T. N. Palmer, J. Shukla, R. A. Tomas, M. Yanai, and T. Yasunari, 1998: Monsoons: Processes, predictability, and the prospects for prediction. *J. Geophys. Res.*, **103(C7)**, 14451-14510.
- Werth, D., and R. Avissar, 2002: The local and global effects of Amazon deforestation. *J. Geophys. Res.*, **107(D20)**, 8087, doi: 10.129/2001JD000717.
- Xie, P., and P. A. Arkin, 1997: Global precipitation: A 17-year monthly analysis based on gauge observation, satellite estimates and numerical model outputs. *Bull. Amer. Meteor. Soc.*, **78**, 2539-2558.
- Xue, Y., 1996: The impact of desertification in the Mongolian and the Inner Mongolian grassland on the regional climate. *J. Climate*, **9**, 2173-2189.
- Xue, Y., 1997: Biosphere feedback on regional climate in tropical North Africa. *Qrtly. J. Roy. Meteor. Soc.*, **123(B)**, 1483-1515.
- Yatagai, A., and T. Yasunari, 1995: Interannual variations of summer precipitation in the arid/semi-arid region in China and Mongolia. *J. Meteor. Soc. Japan*, **73**, 909-923.
- Ye, D. and Y. Gao, 1979: *The meteorology of the Qinghai-Xizang (Tibet) Plateau*, Sciences Press, Beijing, pp. 278 (in Chinese).
- Zou, X., S. Li, C. Zhang, G. Dong, Y. Dong, and P. Yan, 2002: Desertification and control plan in the Tibet Autonomous Region of China. *Journal of Arid Environments*, **51**, 183-198.

## **Chapter III:**

# **Deforestation/Reforestation at the Southeast Tibetan Plateau**

## **Part I: Impacts on Current Climate**

### **Abstract**

Numerical simulations were performed using a global atmospheric circulation model to investigate the climatic impacts of forest removal in the southeast Tibetan Plateau. A control simulation considering the current vegetation, and a forest replacement sensitivity experiment were performed. The effects of deforestation are revealed by examining the differences between the forest replacement and control experiments. The model results show that deforestation at the southeastern Tibetan Plateau creates decreased transpiration and increased precipitation locally. The deforested area and the whole Tibetan Plateau are wetter in summer. This may produce more runoff into the rivers originating from the Tibetan Plateau and impact downstream areas, where precipitation increases in spring and decreases in summer. The numerical experiments also show that the deforestation of the southeast Tibetan Plateau impacts on Asian climate, by contributing to a warmer Indian continent and a cooler southern China in spring. The remote impacts on the surface climate due to deforestation of the southeastern Tibetan Plateau on the Asian and even global climate are induced by modifications of the atmospheric circulation.

Key Words: Deforestation, Tibetan Plateau, GCM

### **3.1. Introduction**

Deforestation occurs when forest is converted to another land cover type or when the forest fraction falls below a minimum percentage threshold – 10% from the United Nations (U.N.) Food and Agriculture Organization (FAO 2001). Large-scale land cover changes in general can result in dramatic climate changes (e.g. Charney et al. 1975) and can affect hydrological cycle intensity (e.g. Avissar and Werth 2005) and atmospheric chemistry (e.g. Ganzeveld and

Lelieveld 2004). During the last two decades, tropical deforestation (e.g. Henderson-Sellers and Gornitz 1984), such as in the Amazon (e.g. Shukla et al. 1990), Africa (e.g. Snyder et al. 2004), and southeast Asia (e.g. Xue et al. 2004; Mabuchi et al. 2005a;b), were studied extensively with global atmospheric circulation models (GCMs; e.g. Nobre et al. 1991; Werth and Avissar 2002), regional climate models (e.g. Roy and Avissar 2002; Sen et al. 2004), satellite data analysis (e.g. Negri et al. 2004; Linderman et al. 2005), and observational field campaigns (e.g. Avissar et al. 2002). These studies reveal that deforestation results in higher surface albedo (Myhre and Myhre 2003; Hales et al. 2004) and lower surface roughness (Sen et al. 2004). This leads not only to a decrease in evapotranspiration and an increase of surface temperature locally, but can also impact global hydro-meteorology through teleconnections (e.g. Avissar and Werth 2005).

The Southeast Tibetan Plateau (SETP), sometimes also called Southwest China, refers to the geographic region that encompasses the Southeast Tibet Autonomous Region, Western Sichuan, Northern Yunnan, Southwest Gansu, and Southeast Qinghai. The elevation of this area ranges from 2000m to more than 7000m above sea level (a.s.l.). Major forest cover changes have occurred in this region during the second half of the twentieth century (Figure 3.1). Figure 3.1a shows the forest cover of the year 1950, which is obtained from the International Satellite Land Surface Climatology Project (ISLSCP) initiative II data collection (Klein Goldewijk, 2001). In 1950, the steep slopes of the SETP were mostly covered by coniferous forest, which contained China's largest forest resource (Studley 1999). However, most of the forest has been cleared by the year 1992/1993 as shown in Figure 3.1b derived from 1-km Advanced Very High Resolution Radiometer (AVHRR) data (available from U.S. Geological Survey 2001). Beginning in the 1950s and accelerating in the 1960s (Studley 1999; Houghton and Hackler 2003), deforestation reduced the forest area from about  $121 \times 10^6$  ha to  $24 \times 10^6$  ha (Fang et al. 2001). In the Tibet Autonomous Region (TAR) it reduced from 55% to 30% and in Sichuan from 30% to 6.5% (Studley 2001). The major factors responsible for forest loss in the SETP have been unsustainable logging practices (Studley 2001; Houghton and Hackler 2003), agricultural use and urbanization (Liu et al. 2005).

The forests of the SETP fulfill a crucial hydrological function both in and beyond China. One third of the world's population lives along the rivers that originate on the Tibetan Plateau (TP) and flow through the SETP, including the Huanghe, Yangtze, Mekong, and Salween. Deforestation in the SETP may impair forest functions of safeguarding watersheds and river flow (Houghton and Hackler, 2003). For example, deforestation in the upper reaches of the Yangtze basin in China led to a reduction of forest cover from 22% of total area in 1957 to only 10% in 1986. As a result, soil erosion from the upper reaches and silation in the middle and lower reaches has intensified. These effects might

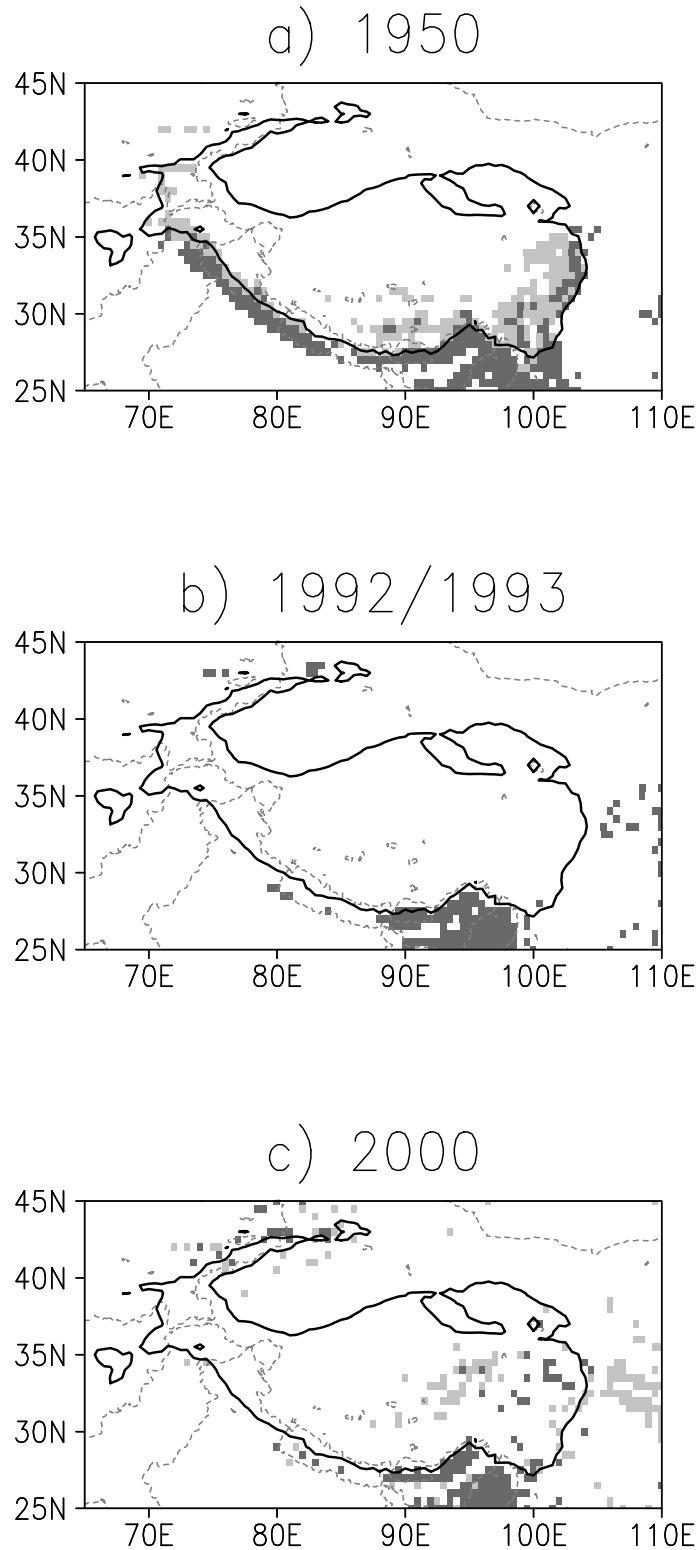


Figure 3.1. Forest cover on and adjacent to the Tibetan Plateau of a) 1950, b) 1992/1993, and c) 2000. Dataset information can be found in text. Contour line of 3000m a.s.l. shows the location of the Tibetan Plateau. Light grey stands for boreal coniferous forest, while dark grey for warm broadleaf forest.

have contributed to the most severe flood in Chinese history in the Yangtze valley in 1998, affecting 223 million people and causing more than US\$36 billion in economic loss (Zhang et al. 2000).

In 1998, the Chinese central government recognized the disastrous consequences of forest degradation resulting in the loss of biodiversity, unacceptable levels of soil erosion and catastrophic flooding. A new forest policy called the Natural Forest Conservation Program (NFCP) was implemented in 1998 (Zhang et al. 2000). Chinese national forest survey shows that after 1980 the forest cover in China has already increased by about  $20 \times 10^6$  ha as the result of plantations, although the natural forests continued to decline (Houghton and Hackler, 2003). Figure 3.1c shows the forest cover including natural forest as well as plantations over the TP region in the year 2000 taken from the Global Land Cover 2000 database (GLC2000 2003). Comparison with Figure 3.1b reveals two reforestation centres, one in the east of Sichuan along the Yangtze River valley, and another in the centre of the Tibet Autonomous Region (TAR). Reforestation of the eroded semi-desert landscape of the SETP might be extremely difficult, but still appears to have a huge potential (Miehe et al. 2003). Experimental evidence shows that the southern TAR can be reforested with indigenous tree species without irrigation if grazing is excluded (Miehe et al. 2003).

The effect of deforestation/reforestation around and on the SETP on local and/or regional and global climate, and how it interacts with different climate background conditions has not yet been studied. Despite high uncertainties existing in GCM or CGCM simulations of climate and circulation on the TP, they are useful tools, for example, to investigate the sensitivity of the TP's elevation on global climate (e.g. Broccoli and Manabe 1992; see Cui et al. 2005a (chapter 2) for a review). The present paper simulates the climate impact of deforestation on the TP during the second half of the twentieth century. How such impact differs with future climate background conditions will be presented in a companion paper (Cui et al. 2005b (chapter 4); referred to as Part II). Sharma et al. (2000) used a water balance and distributed deterministic modelling approach to analyze the hydrological sensitivity to different projected land-use scenarios in the Kosi Basin, located in the mountainous are of the central Himalayas. They found that runoff would decrease in the scenario of a maximum increase in forest areas below 4000m, while it would increase in the case of possible maximum conversion of forest into agricultural land under contemporary climate conditions. Cui et al. (2005a; chapter 2) first simulated the climate impact of anthropogenic land cover change on the TP with an Atmospheric General Circulation Model (AGCM). They found a warmer and drier climate on the TP due to anthropogenic land cover changes and a possible modification of the Asian monsoon intensity as well. However, deforestation was not included in their scenarios of land cover change. Following the study of

Cui et al. 2005a (chapter 2), the same AGCM is applied but with different land cover scenarios aiming to simulate the effects of the deforestation at the SETP on local and remote climate. The model and experiments will be introduced in section 3.2. In section 3.3, results will be presented. A conclusion and summary will be given in section 3.4.

## **3.2. Model and Experiments**

### **3.2.1 Model Introduction**

The most recent version of the Max Planck Institute for Meteorology atmospheric general circulation model ECHAM5 (Roeckner et al. 2003) is used in this study. The previous version ECHAM4 has been applied to study the sensitivity of the local and global climate to deforestation and reforestation in the Mediterranean region at T42 horizontal resolution (Duemenil Gates and Liess 2001). ECHAM5 has been used to simulate the effects of land cover change on the TP at T63 horizontal resolution (Cui et al. 2005a; chapter 2). The simulations in this study are also performed at T63 resolution, corresponding to a grid size of about  $1.875^\circ$ , approximately 150 km in longitude and 200 km in latitude in the TP region. For more details of ECHAM5, please see Cui et al. (2005a; chapter 2), Roeckner et al. (2003; 2004) and at: <http://www.mpimet.mpg.de/en/extra/models/echam/echam5.php>.

### **3.2.2 Experimental Setup**

A control experiment “C” to represent the current climate has been performed as control run in Cui et al. (2005a; chapter 2). It is integrated for 22 years driven with climatological global sea surface temperature (SST) and sea ice averaged over the period 1978-1994 used for the Atmospheric Model Intercomparison Project 2 (AMIP2; Gates et al. 1999) to eliminate additional inter-annual variability. The atmospheric variability represented in such integrations is generally less than that in simulations with inter-annually varying boundary conditions of SST and sea ice (Bengtsson et al., 1996). While this suppresses important interactions between deforestation and hydroclimatic processes, it considerably simplifies the detection of land cover teleconnections (Avisar and Werth, 2005). The last 10-year averages are analyzed here discarding the first 12 years needed for model spin-up.

An experiment, named “F”, has been conducted with the replacement of the current land surface (figure 2.2a in Cui et al. 2005a; chapter 2) in the SETP with forest as was found in 1950 (Figure 3.1a), leaving other parameters identical as in experiment C (forest cover applied shown in Figure 3.1b). The experiment C

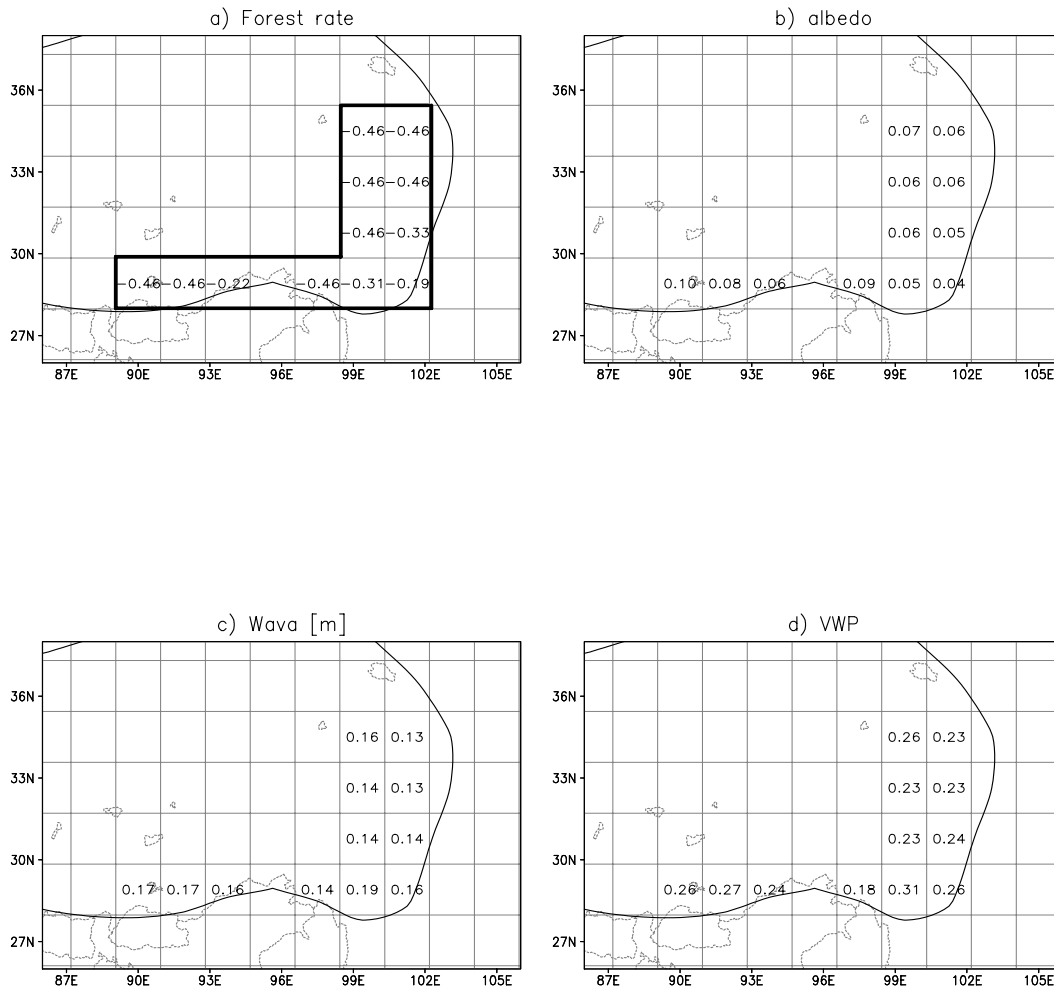


Figure 3.2. Differences of land surface parameters between forest and current scenario (current-forest) including a) forest coverage, b) background albedo, c) plant-available soil water holding capacity Wava, and d) volumetric wilting point (VWP). The black thick rectangle in a) stands for deforested area for later area average calculation. The solid black contour lines show the height of 3000m a.s.l.

is treated in the present paper as a ‘deforested’ scenario in which forest is cleared and replaced with grassland, cropland and built-up areas. Experiment F is integrated for 15 years starting from the equilibrium conditions of the control run with the average of the last 10 years analyzed. The forest cover changes in the SETP are only available at 0.5° resolution for the year of 1950 (shown in Figure 3.1a), while the surface parameters related to vegetation in ECHAM5 are archived from the 1km resolution AHVRR data (Hagemann 2002). Therefore, in scenario F, coniferous boreal forests are replaced in the SETP region at T63 resolution (Figure 3.2a). This approximation may not represent the reality of historic forest changes in this region (see the difference between Figure 3.1a and Figure 3.1b). It should, however, not hinder the ability of this study to

quantitatively investigate the influences of deforestation in this region. The surface ecosystem types and related surface parameters are prescribed in ECHAM5. They include background surface albedo, surface roughness length due to vegetation, fractional vegetation cover ( $C_v$ ) and leaf area index (LAI) for the growing and dormant season, forest coverage, plant-available and total soil water holding capacity (Table 1; Hagemann 2002). Several surface parameters varied as shown in Figure 3.2 for C and F scenarios. It includes a) decreasing forest area, b) increasing background surface albedo, c) generally increasing plant-available soil water holding capacity, and d) volumetric wilting point. In addition, decreasing surface roughness length due to vegetation ( $\sim 1\text{m}$ ; Table 1) is negligible compared to the surface roughness length due to orographic variations ( $\sim 20\text{m}$ ). A full annual cycle of fraction of vegetation ( $C_v$ ) and Leaf

**Table 1:** Surface parameters for major land cover types on the southeastern Tibetan Plateau. It includes background surface albedo  $\alpha$ , surface roughness length due to vegetation  $Z_{0,\text{veg}}$ , fractional vegetation cover  $C_v$ , leaf area index (LAI) for the growing (g) and dormancy season (d), forest ratio  $C_f$ , plant-available soil water holding capacity  $W_{\text{ava}}$ , and the volumetric wilting point (VMP). (from Hagemann, 2002).

Global Ecosystems Legend	Albedo $\alpha$	$Z_{0,\text{veg}}$ [m]	$C_{v,g}$	$C_{d,v,d}$	$\text{LAI}_g$	$\text{LAI}_d$	$C_f$	$W_{\text{ava}}$ [m]	VMP
Conifer Boreal Forest	0.13	1	0.52	0.52	6.	6.	0.46	0.14	0.33
Crops, Grass, Shrubs	0.19	0.1	0.65	0.33	2.7	0.4	0.	0.53	0.46
Urban, buildups	0.2	2.5	0.	0.	0.	0.	0.	0.	0.48

Area Index (LAI) are implemented in ECHAM5 as well, which is thought to improve the seasonality of surface evaporation calculated by the GCM (van den Hurk et al. 2003). Figure 3.3 shows the changes of LAI and fractional vegetation cover due to deforestation. LAI decreases in all four seasons since forest in the F scenario is cleared and replaced with grassland, cropland and built-up areas in the C scenario. LAI decreases dramatically in winter and spring when the grassland and cropland cannot survive due to low temperatures in this region. Correspondingly, the fractional vegetation cover also decreases dramatically in these two seasons, while it increases in summer and autumn.

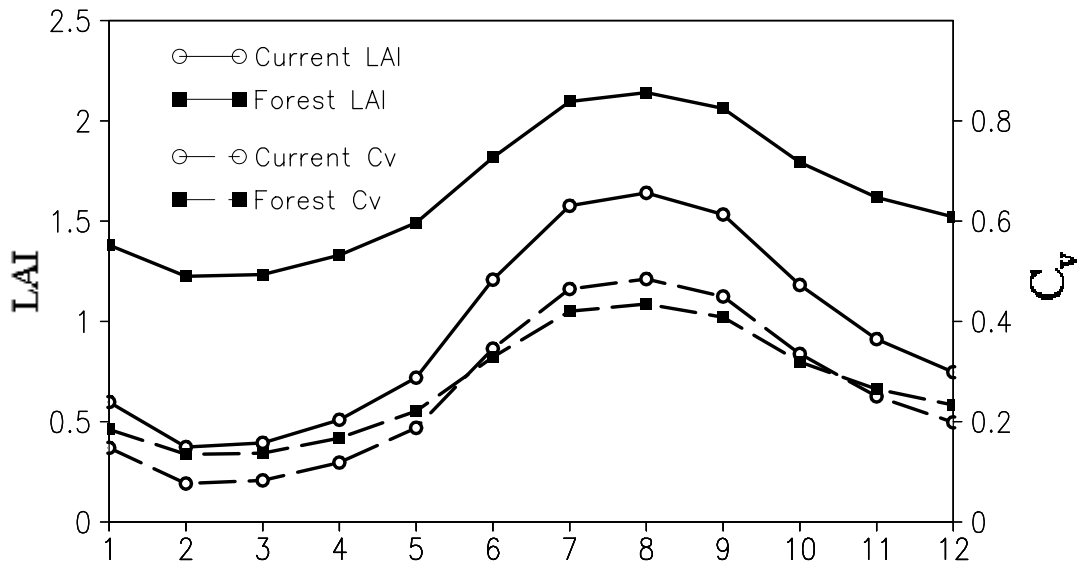


Figure 3.3. Seasonal variations of the area averaged of leaf area index (LAI; solid line) and vegetation fraction (Cv; dashed line) on the southeast Tibetan Plateau for current (circle) and forest (square) scenario.

The differences between the results from the scenarios F and C are assumed to represent the impact of deforestation at the SETP. The ‘Paired Difference Test’ (Von Storch and Zwiers 1999) t-test method is applied to test the statistical significance of the two non-independent scenarios. Physical insight is required to ascertain that the statistical significance is indeed of physical significance (von Storch and Zwiers, 1999). Statistical significance is determined using seasonal (December, January, February (DJF); March, April, May (MAM); June, July, August (JJA); September, October, November (SON)) or annual rather than monthly averages to include less of the year-to-year variability (Bonan, 1997). It may be argued that natural seasons might be a better choice to represent Southeast Asian climate, but for the sake of simplicity we have used boreal seasons. Each year of model output represents one seasonal or annual ‘sample’. The analyzed number of both experiments (each 10 years) means that there are only 9 degrees of freedom when testing for the difference between two means with the method applied here.

## **3.3 Results:**

### **3.3.1. Evaluation of the ECHAM5 Model**

ECHAM5 and its previous versions have been used extensively to produce climate scenarios under various forcing conditions, and its capacity to reproduce the current climate has been described in various publications (e.g., Roeckner et al 2003). ECHAM5 has been, and is participating in AMIP and AMIP 2 (Gates et al. 1999; see also <http://www-pcmdi.llnl.gov/amip>), and the Coupled Model Intercomparison Project (CMIP; Meehl et al. 2000; Covey et al. 2003; see also <http://www-pcmdi.llnl.gov/cmip>). Its capability to simulate the atmospheric circulation and the major weather systems in the Asian region has been evaluated by Cui et al. (2005a; chapter 2) by comparison with European Centre for Medium-Range Weather Forecasts (ECMWF) Reanalysis data (ERA40; Simmons and Gibson, 2000), National Centres for Environmental Prediction-National Centre for Atmospheric Research (NCAR-NCEP) Reanalysis data (Kistler et al. 2001; Kanamitsu et al. 2002), Climate Research Unit data (CRU; Mitchell and Jones 2005), and other datasets. It has been shown that ECHAM5 produces reasonably well the seasonal shifts of the monsoon rainfall belt as well as near surface temperature. The global circulation in the lower and upper troposphere, as a key parameter to investigate the remote impact of the deforestation, will be discussed briefly below.

Figure 3.4 compares global mean DJF circulation from observations and ECHAM5 simulation C at 200 and 850 hPa, respectively. The observations are 20-year averages from the NCEP-NCAR reanalysis (1979-80 through 1999-2000). The distributions show the boreal winter patterns associated with the classical Walker and Hadley circulations. The Walker circulation is dominated by a low-latitude region of negative (divergent) and positive (convergent) velocity potential. ECHAM5 simulates well the centres of low-level convergence and high-level divergence just west of the date line and over northern South America, which are characterized by strong upward velocities at 500 hPa representing the well known centres of organized deep convection (Mestas-Nuñez and Enfield 2001). Subsidence regions of opposite polarity are seen in the eastern “cold-ocean” regions of the Pacific and Atlantic oceans. The meridional Hadley circulations are evident in the northern winter hemisphere, with strong northward outflow from the 200 hPa divergent centres toward convergent zonal ridges of the velocity potential in the 20°-30° N band over Afro-Asia, the North Pacific, and the North Atlantic. Similar banded structures are nearly absent in the southern (summer) hemisphere. In general, ECHAM5 represents well the circulations with slightly different amplitudes in some locations.

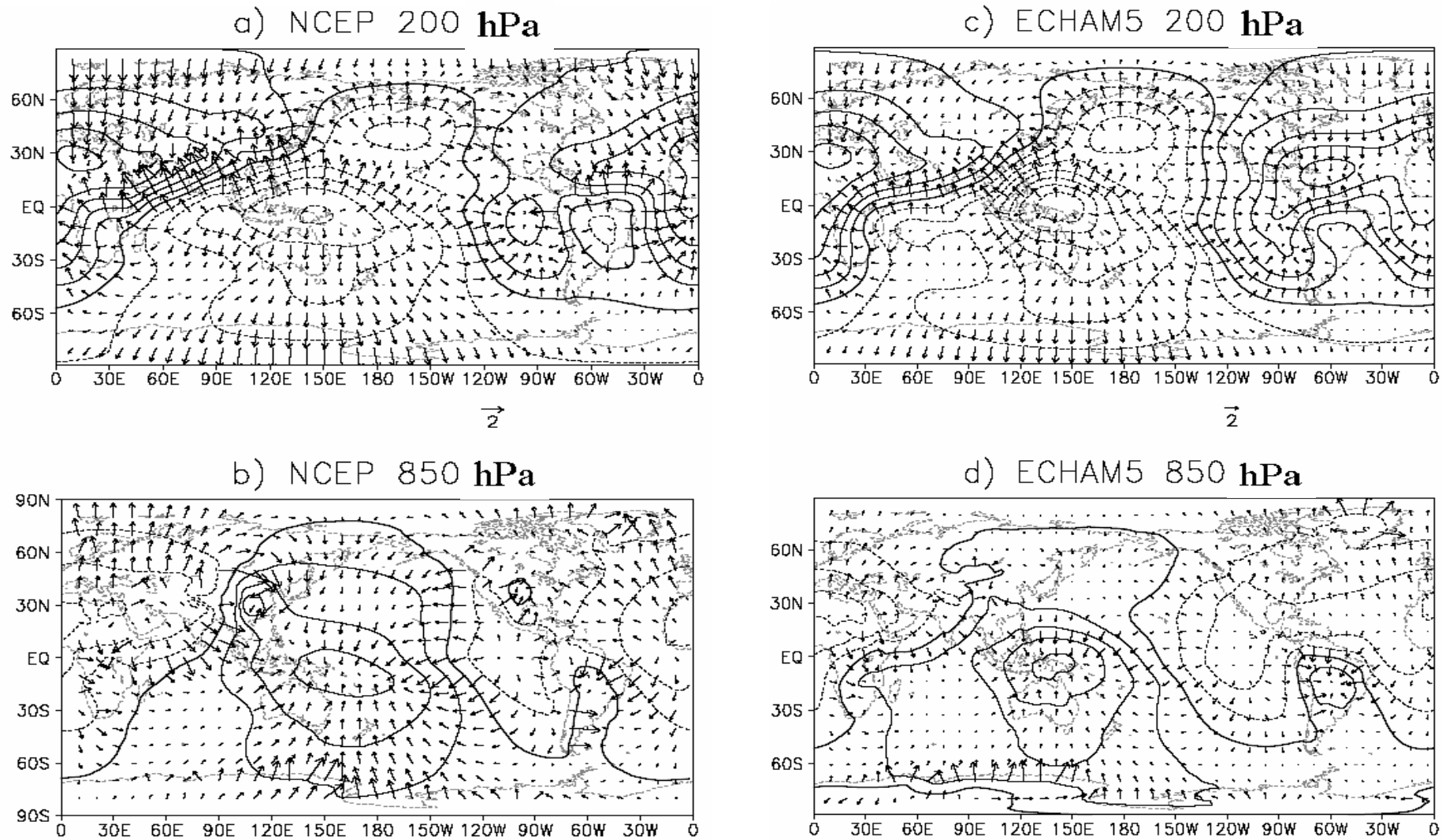


Figure 3.4. Comparison of DJF atmospheric circulation (velocity potential and divergent winds) between NCEP analysis and ECHAM5 current scenario in the upper (a, c) and lower (b, d) troposphere. The contour intervals for velocity potential are  $2 \times 10^6 \text{ m}^2 \text{ s}^{-1}$ .

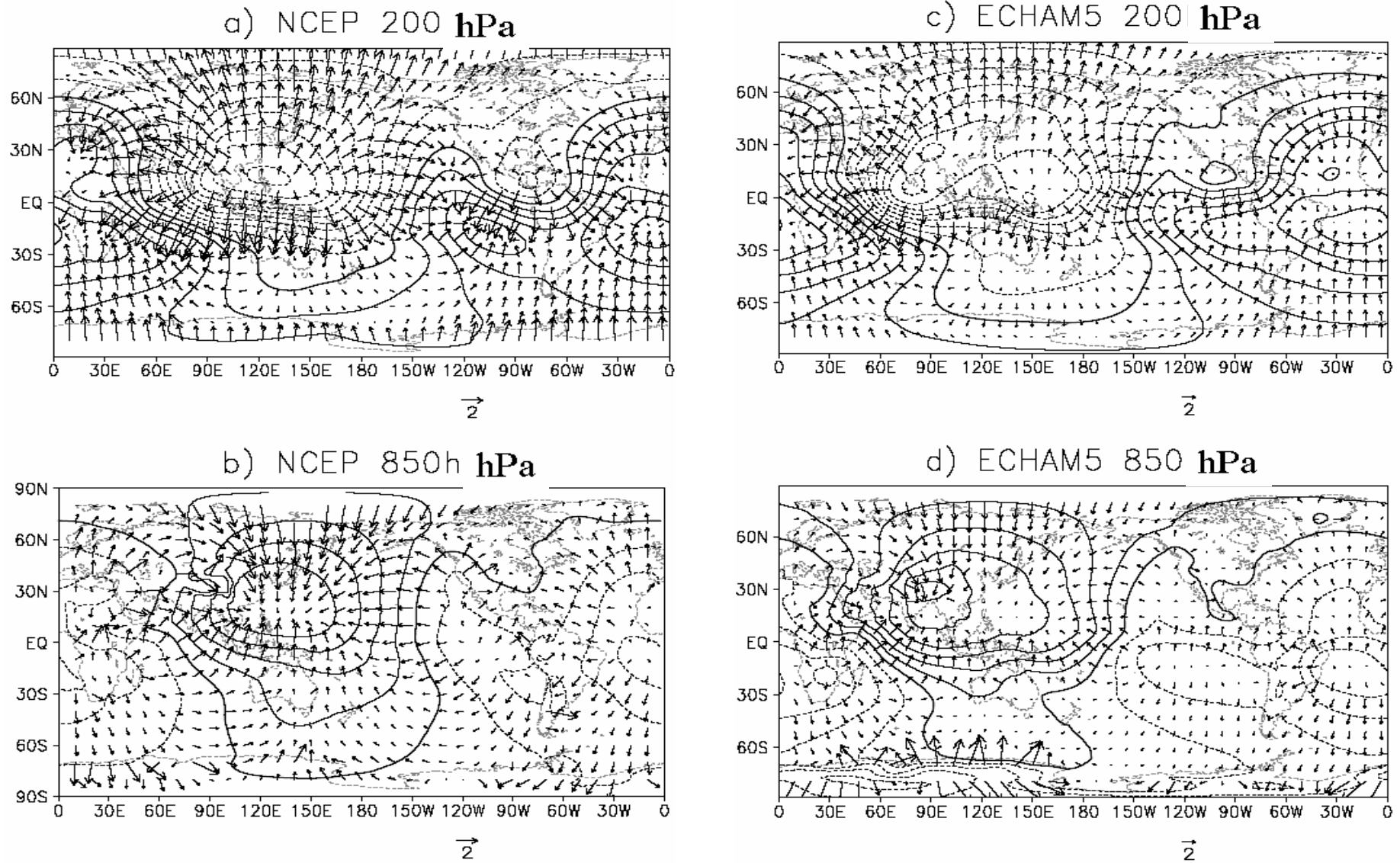


Figure 3.5. Same as Figure 3.4, but for JJA summer season.

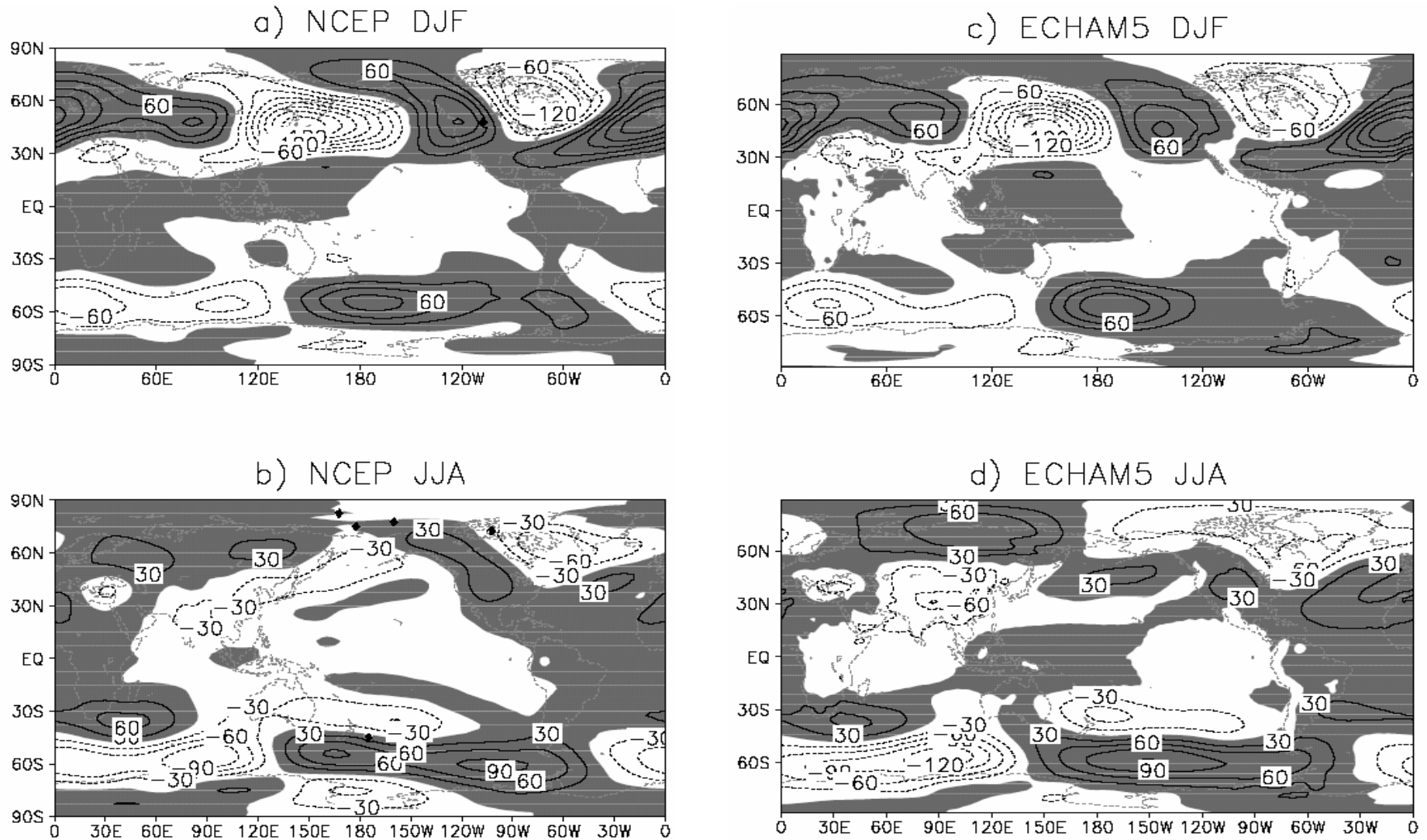


Figure 3.6. Comparison of 500-hPa geopotential height difference between NCEP analysis and ECHAM5 current scenario in a, c) DJF and b, d) JJA, respectively. The positive areas are shaded.

Figure 3.5 shows the global circulation comparisons for JJA, the boreal summer season. The overhead sun migrates to the northern Hemisphere in the boreal summer and so do the diabatic heating centres and corresponding centres of divergent circulations. The divergent circulation of a monsoon system is driven by the east-west differential heating in such a way that diabatic heating (cooling) centres coincide with the upper-level divergent (convergent) centre of the monsoon circulation (Chen 2003). In comparison with observations, ECHAM5 represents a broader but weaker upper-level divergent centre over the western tropical Pacific. The divergent circulation at the Gulf of Mexico is also underestimated. The convergent circulation simulated by the model is generally weaker than observed. The convergent circulation at the lower troposphere moves its centre from the western tropical Pacific in winter northward to subtropical areas. It provides the dynamic process transferring moisture and hot air masses from tropical areas northward. ECHAM5 captures this northward shift of the convergent circulation centre. However, it simulates a divergent centre on the TP region which does not exist in the reanalysis data. In addition, ECHAM5 also produces a stronger divergent circulation over South Africa and the South Atlantic Ocean. The lower-level divergent circulation over the eastern Pacific simulated by ECHAM5 is also located more to the southwest than in the observation. Overall, the characteristics of divergent/convergent circulation produced by ECHAM5 generally agree with the reanalysis data, but with biases in some regions which are larger during summer than winter.

Figure 3.6 compares the seasonal mean 500 hPa geopotential height anomalies from the zonal mean between the analysis data and ECHAM5 scenario C. In winter, ECHAM5 represents well the stationary planetary waves. It shows the two extreme troughs in the Northern Hemisphere. One is located over North America and the other one over East Asia. The East Asia trough, centred at 140° E, 50° N and extending to the Indian continent, is the dominant weather system for the Asian region (Webster et al. 1998). In summer, the East Asia trough is strongly weakened and moves towards the southwest. ECHAM5 represents well the weakening and moving but with slightly larger amplitude over the TP. The trough over North America is weaker in summer than in winter in both the analysis data and the model simulation. The model reasonably simulates the large-scale features in the Southern Hemisphere both in winter and summer. Together with the comparison of divergent circulation at 200 and 850 hPa, it can be concluded that ECHAM5 simulates reasonably well the large-scale atmospheric circulation in the troposphere in both winter and summer. This provides the basis for the later analysis of the results of the sensitivity study and the hypothesis of an underlying mechanism.

### **3.3.2. Impact of vegetation change on climate**

#### **a) Local and Regional Impacts**

To reveal the local impact of deforestation on the SETP climate, Figure 3.7 shows the changes of surface parameters in the deforested area indicated in Figure 3.2a. Due to deforestation (scenario C minus scenario F), the surface albedo values increased, particularly during the winter because grassland/cropland dies during that time (Figure 3.7a). Negative radiative forcing of deforestation (e.g. Myhre and Myhre 2003) is only found during April and May in our experiment. The net surface solar radiation remains unchanged during summer and even increases during February, March, September, October, and also during November and December with smaller amplitude. Total cloud cover decreases during spring and winter (Figure 3.7c), which might relate to the changes of mesoscale circulation created by deforestation, which critically modulates the radiative exchanges (Chagnon et al. 2004). The radiative forcing is not linear with surface albedo changes and is dependent on the snow distribution (Myhre and Myhre 2003). The radiative forcings of deforestation observed here should be treated cautiously due to the coarse resolution applied in the experiment and should be investigated in the future using a higher resolution GCM or a regional model. The latent heat fluxes in the experimental area generally decreased due to the decreased transpiration from the leaves of vegetation (Figure 3.7d). The near surface air temperature remains almost unchanged with slight cooling in winter, which may imply that the energy budget is only slightly changed (Figure 3.7e). However, the changes of latent heat flux might exert strong influences on the horizontal and convective circulations of the atmosphere, and consequently, change the distribution of precipitation. The mean precipitation in the area increases in the summer half year from April to August but decreases in the winter half year except September and October (Figure 3.7f) due to deforestation. Together with decreased evaporation (Figure 3.7d), the surface runoff increases significantly, influencing the discharge of the rivers originating from the TP. Such changes of river discharge may contribute to the increasing frequency of flooding downstream (e.g. Zhang et al. 2000). In summary, the local surface climate becomes wetter in summer and drier and colder in winter due to deforestation. The summer trends found here agree with the observed trends (Niu et al., 2004) and tree ring records for the period of 1961-1990 (Braeuning and Mantwill, 2004). In total, the precipitation in the deforested area increases (+30.5 mm/year) while surface evaporation gets weaker (-47.9 mm/year), thus leading to an increase of surface runoff of 95 mm per year, an amount of  $4.5 \times 10^8 \text{ m}^3$  for the whole TP. Surface temperature changes slightly at a rate of  $-0.11^\circ \text{C}$  per day. However, it should be noted that the averages over the whole deforested area of the SETP may have missed some detail of regional features.

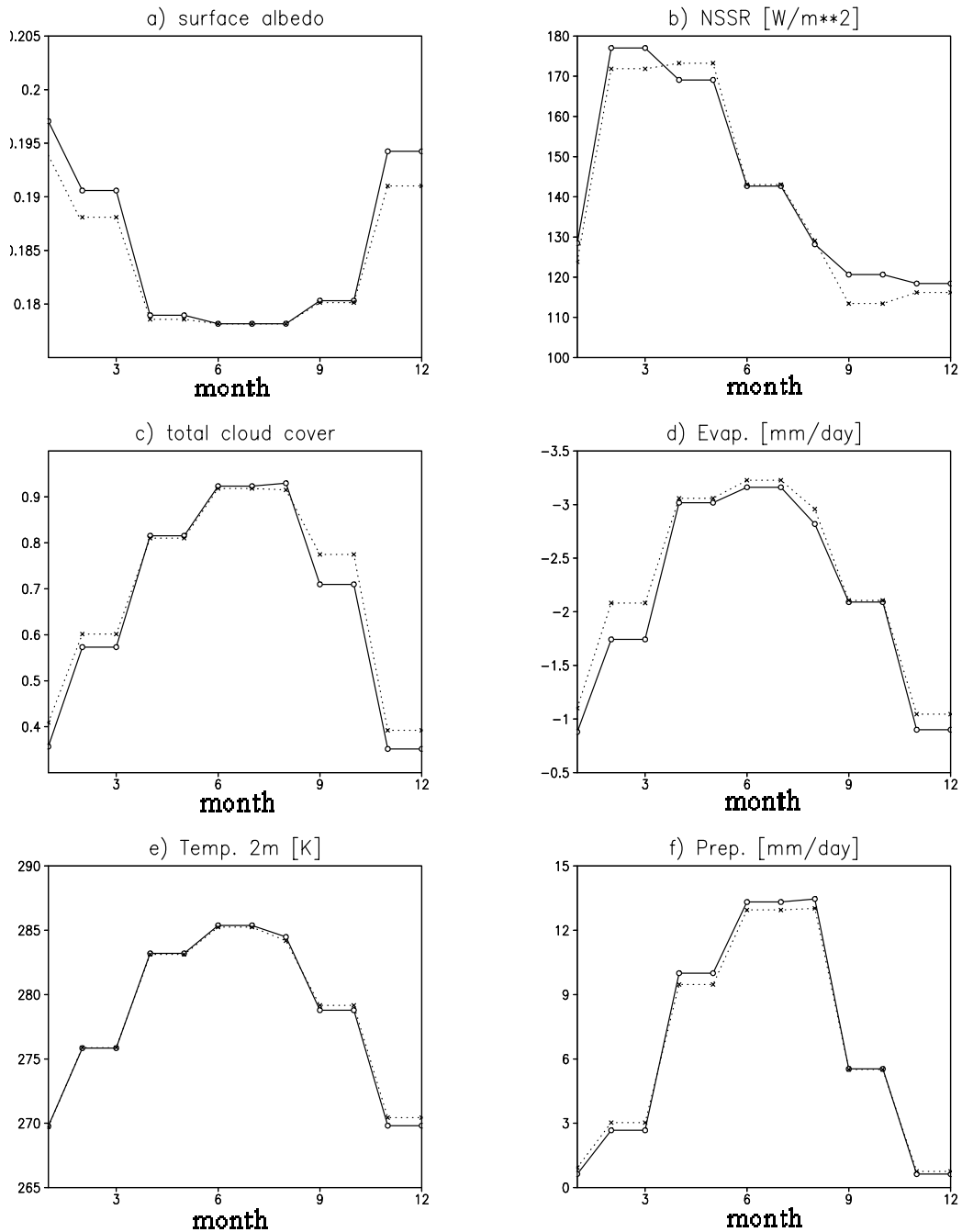


Figure 3.7. Annual cycle of 10 year mean surface parameters from the current (solid) and forest (dotted) scenarios conducted by ECHAM5, for a) surface albedo, b) net surface solar radiation (NSSR), c) total cloud cover fraction, d) surface evaporation, e) 2m air temperature, f) daily precipitation.

The TP plays an important role in forming and inducing variations of regional weather and climate in East and South Asia, as well as of the Northern Hemisphere atmospheric circulation in general (e.g. Ye and Gao 1979). Anthropogenic land cover changes over the TP intensify the Indian monsoon and weaken the East China monsoon, while leading to warmer and drier climate at the TP (Cui et al. 2005a; chapter 2). The regional impact of deforestation on the Asian climate system will be addressed in more detail in this section. The analyses are conducted on a four-season basis to capture the seasonal variations.

Figure 3.8 shows the spatial distribution of differences of seasonal mean near surface temperature between scenario C and F. In winter, a zonal band of cooling stretches in the midlatitudes from the Ural Mountains towards Japan with amplitudes well over 1° C. Significant warming is found over East Siberia. The TP cools slightly, however at marginal significance, while West India, the Southwest China, the tropical Indian ocean and the Southern tip of the Malaysian peninsula warm significantly despite of the fixed SSTs. In spring not much significant anomalies occur. Some warming tendency in midlatitude Central Siberia and Northeast India is seen as well as cooling over South China. Summer shows mainly significant warming over West Siberia and contrasting anomalies between the western (cold) and eastern (warm) TP. Fall exhibits strong significant warming over easternmost Siberia, cooling centered over Northeast China and Southeast Siberia and the eastern TP as well as warming over India, the Caucasus region and southern SE Asia (Malaysia, Indonesia).

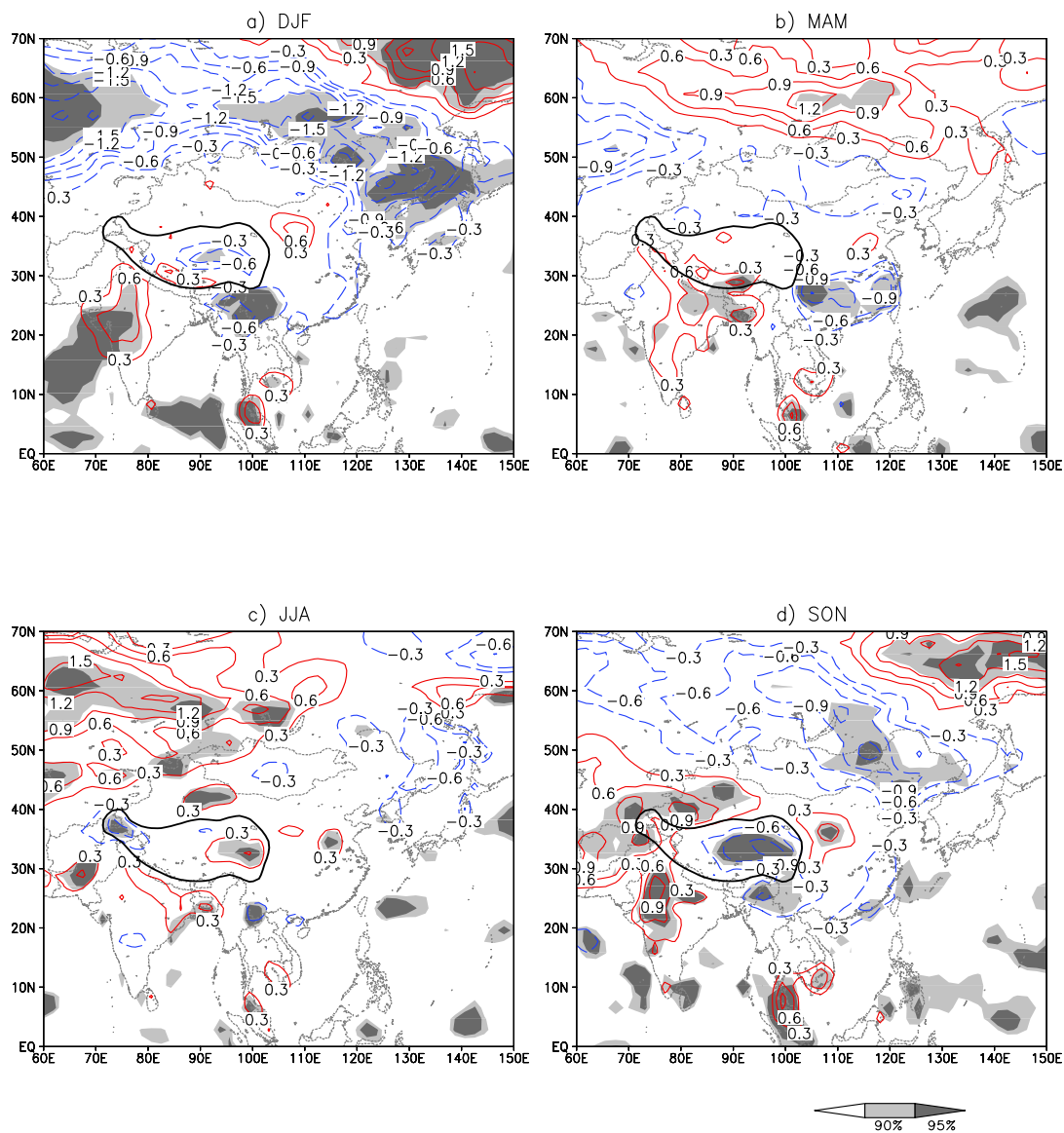


Figure 3.8. Difference of 10-year mean 2m temperature between current and forest scenarios (current minus forest) in a) DJF, b) MAM, c) JJA, and d) SON seasons. Statistical significance of 90% and 95% is shaded. Black thick contour shows the location of the Tibetan Plateau.

The Asian region is characterized by its monsoonal climate. Figure 3.9 shows the rainfall and moisture flux in spring and summer and their changes due to deforestation at the SETP. Most of the annual rainfall occurs in summer and is mainly related to the moisture transported from tropical or ocean regions (Figure 3.9a, b; for a review see Webster et al. 1998). The mesoscale atmospheric circulation changes created by deforestation in the SETP modulate the moisture transport as well. In spring, the anticyclonic circulation in the western Tropical Pacific is weakened in East China (Figure 3.9c), leading to less moisture transported in central China along the Yangtze River while more moisture restricted in south China. This can be clearly seen from the significant changes in rainfall in the corresponding areas from Figure 9e. Interestingly, a ‘wet-dry’ oscillation extends to south Siberia through north China. In summer, the increasing of moisture flux convergence on the TP indicates that more moisture is transported into this area from south and east (Figure 3.9d). Around the TP humidity becomes less except in the northern part. Correspondingly, statistically significant increases of rainfall exist on the TP and its southern tip. Rainfall decreases in India and East China. The drying along the Yangtze River is statistically significant. The rainfall changes found here are different from the so-called “northern drought with southern flooding” trends of summer rainfall in China during the last half century (Xu 2001).

### **b) Global Perspective**

Zhang et al. (1996b) discussed the influence of tropical deforestation on the large-scale climate system. It was concluded that the modification of the model surface parameters simulating tropical deforestation produced significant modifications in both the Hadley and Walker circulations. A mechanism for the propagation of disturbances arising from tropical deforestation to middle and high latitudes was proposed, based on the mechanisms of Rossby wave propagation. Mabuchi et al. (2005a; b) also suggested a similar mechanism of climate impact of vegetation changes in the Asian tropical region. To reveal the global impact of deforestation over the SETP, Figure 3.10 shows the changes of atmospheric circulation in the upper and lower troposphere for summer and winter. Note that, because of the smaller contour intervals and vector scales used for the anomaly maps, these anomalies do not change or reverse the average situation in Figure 3.4 and Figure 3.5, but rather represent a significant weakening or strengthening of it.

In winter (Figure 3.10a; b), the high level divergent circulation is strengthened in the western North Pacific and South America, while weakening can be seen from South Asia to the western South Pacific. The convergent circulations in the upper troposphere are strengthened in the warm pool in west Pacific, while they decrease elsewhere. The changes are weakly statistically significant. Correspondingly, in the lower troposphere, the divergent circulation is strengthened over the eastern tropical Pacific and weakened elsewhere. The convergent circulations are generally weakened. In summer, a planetary wave number 2 anomaly is found in variations of the divergent circulations of the upper troposphere. The divergent circulation is strengthened in Southeast Asia

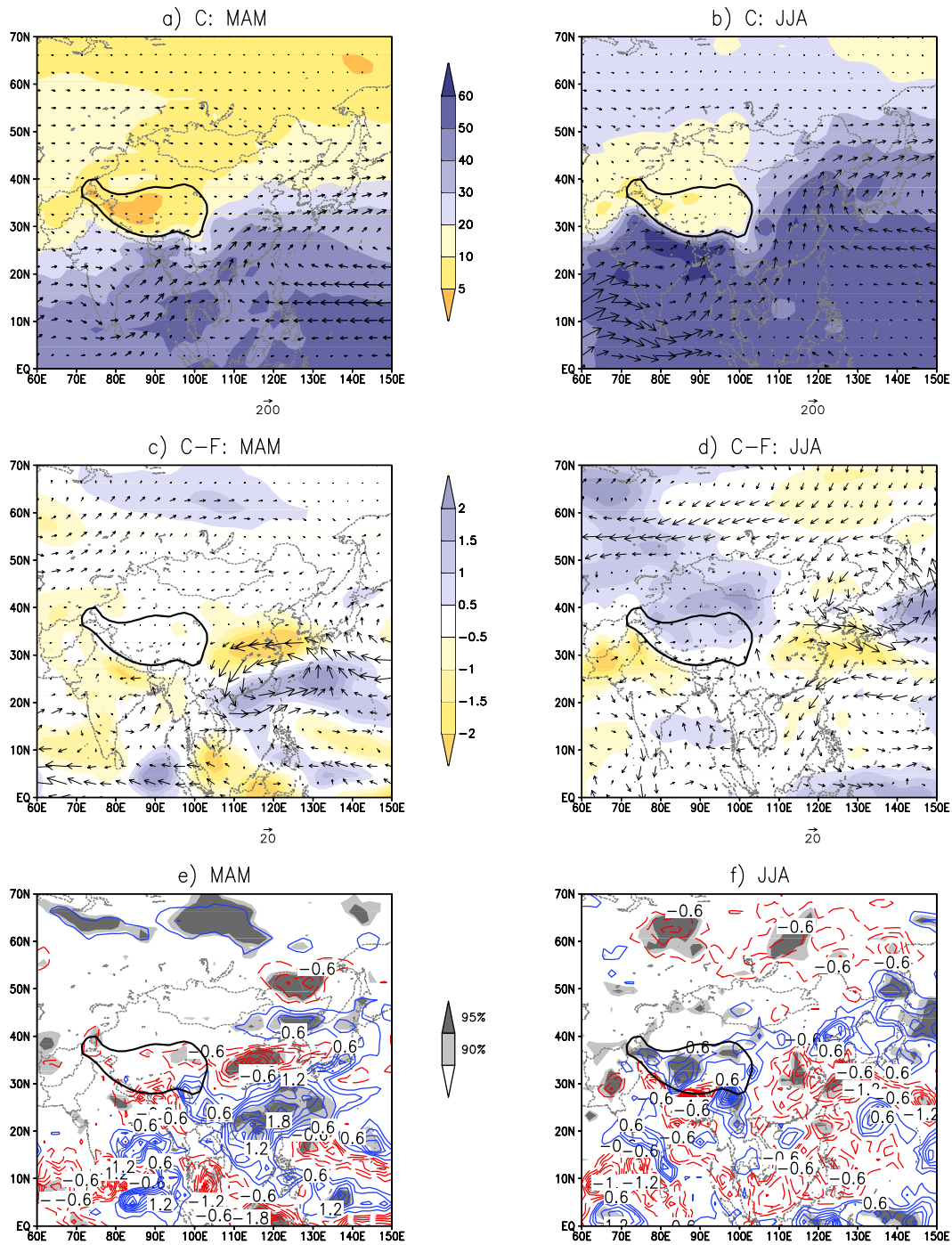


Figure 3.9. Moisture flux of the whole atmosphere (vector;  $[\text{kg}\times\text{m}/\text{s}]$ ) and moisture convergence (shaded;  $[\text{kg}/\text{s}]$ ) from ECHAM5 current simulation (C) during a) MAM and b) JJA, and the differences of current minus forest scenario during c) MAM and d) JJA. Daily precipitation changes (contour;  $[\text{mm}/\text{day}]$ ) are shown in e) for MAM and f) for JJA, respectively, and statistically significant changes at the 90% and 95% levels are shaded in e) and f).

warm pool in the western Pacific, and eastern North America. The convergent circulation is strengthened over the eastern Pacific, Africa, and the western Atlantic. The areas of changes do not surmount the 90% statistical significance level. Correspondingly, in the lower troposphere, the convergent circulation is strengthened over the western tropical Pacific, while the divergent circulation is strengthened in the eastern Pacific and Africa. The divergent circulation over South America is weakened. Different from the circulation changes in winter, the divergent/convergent circulations are generally intensified in summer.

The strengthening of the convergent circulation in the lower atmospheric level over the western tropical Pacific and north China will induce a strengthening of the monsoonal winds over these regions. There is a weakening area over south China, which will induce a weakening of monsoonal winds over this region as well. The circulation changes are associated with the summer rainfall increases over the TP and Japan and decreases over south China (Figure 3.9f). These changes in the atmospheric circulation might induce changes of global patterns of surface temperature and precipitation as well.

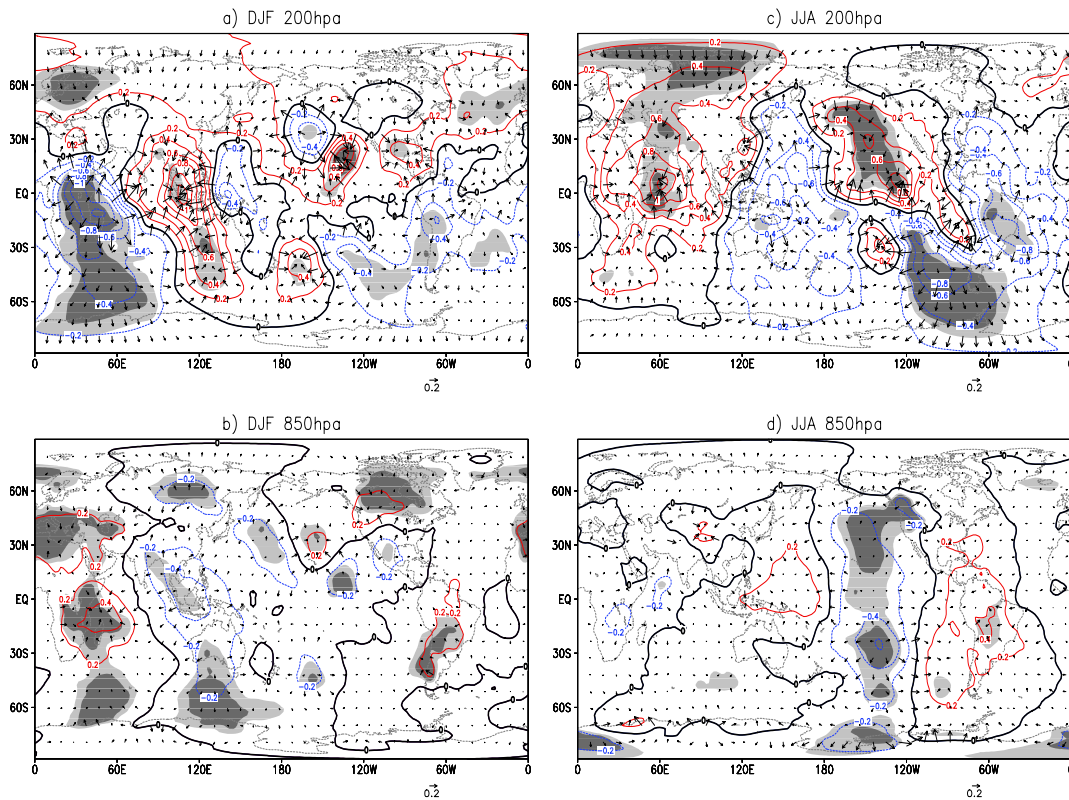


Figure 3.10. Differences of atmospheric circulation between current and forest scenarios (current minus forest) in the upper (a, c) and lower (b, d) troposphere in DJF (a, b) and JJA (c, d). The contour intervals for the velocity potential are  $0.2 \times 10^6 \text{ m}^2 \text{ s}^{-1}$ .

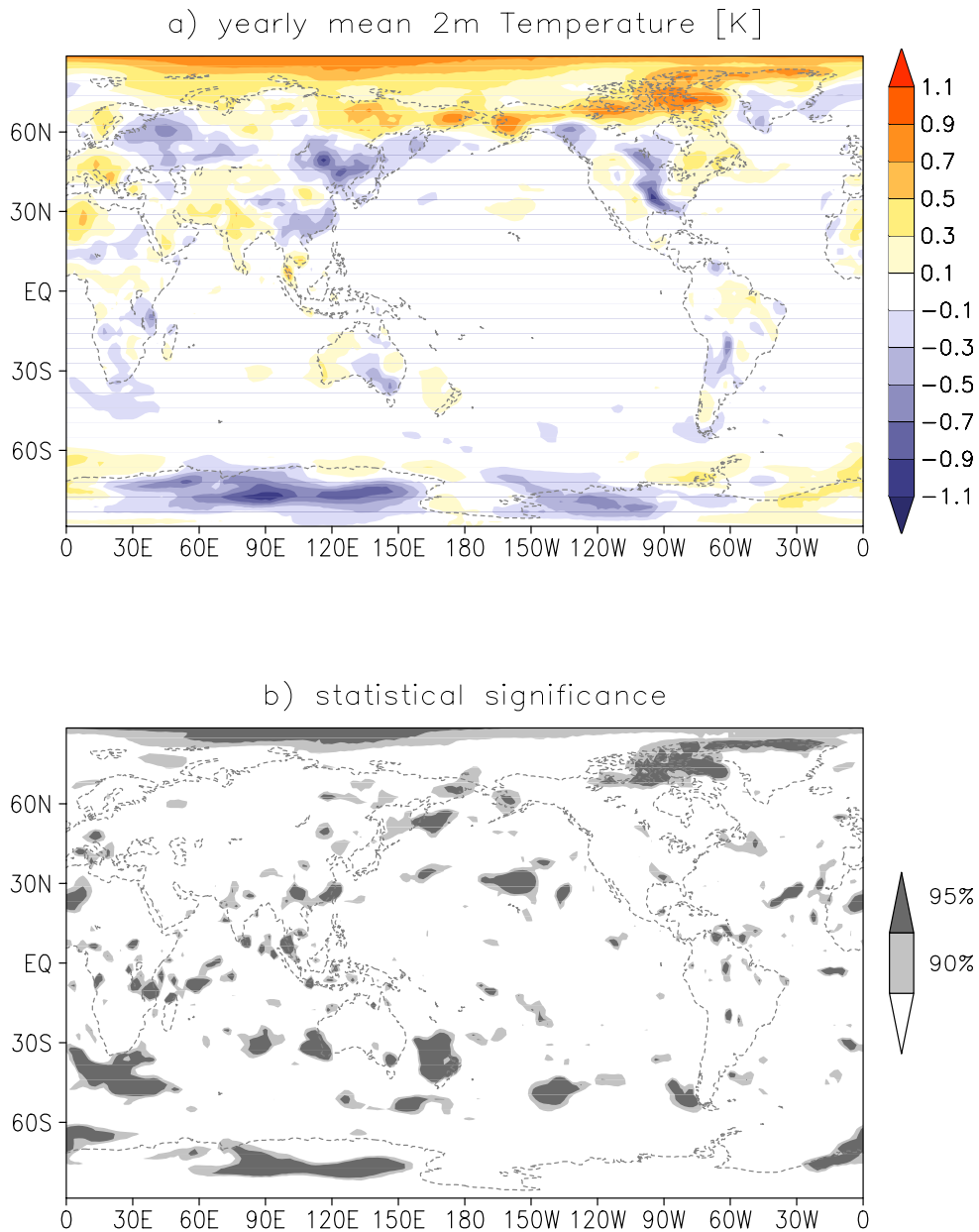


Figure 3.11. Difference of 10-year mean of yearly 2m temperature between current and forest scenarios (current minus forest). Absolute values (a) and statistically significant changes (b) are shaded.

Figure 3.11 shows the yearly mean 2m temperature changes between the scenarios C and F and its statistical significance. There are quite large changes in polar regions with general cooling over Antarctica and warming over the Arctic, but these will not be addressed in the present paper due to problems with parameterization and numerical methods in high latitudes (Randall et al. 1998). The area averages discussed only include areas between 70° N and 70° S. Only a few significant anomalies remain. There is some warming in southern Europe and North Africa, India and tropical southeastern Asia as well as a cooling

tendency over northeastern and South China. Figure 3.12 shows the changes of yearly mean precipitation due to deforestation. Since precipitation is highly related to the local and regional processes, these anomalies are very scattered, and remote impacts should be treated cautiously. More scenario experiments are needed to investigate such remote impacts, and will be presented in a future paper. Therefore, only several regions of precipitation changes are mentioned here. Most important seem to be the significant anomalies over the maritime continent straddling the equator with positive anomalies to the north and negative to the south. The remote precipitation changes due to deforestation of the SETP are related to the circulation changes presented in Figure 3.10.

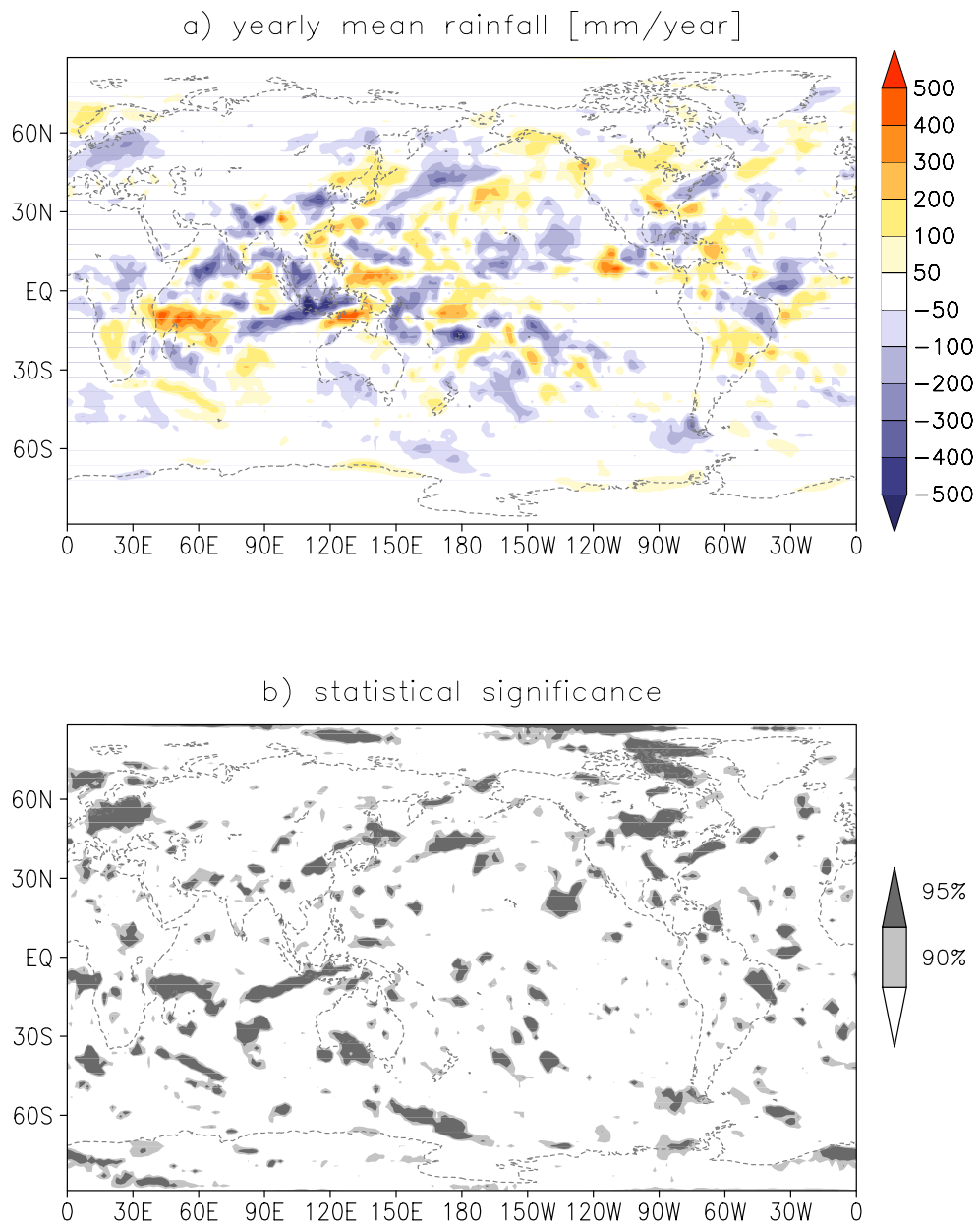


Figure 3.12. Same as Figure 3.11, but for annual mean precipitation.

Mabuchi et al. (2005b) suggest that DJF height anomalies at the 500 hPa level due to deforestation in Asian tropical regions were similar to those of an ENSO event. To reveal whether our experiment also presents a similar pattern or not, Figure 3.13 shows the geopotential height anomalies in DJF and JJA at 500 hPa level due to deforestation at the SETP. In winter over the Northern Hemisphere, areas of negative difference are found from central Eurasia to North America, and areas of positive anomalies exist over western Europe, the North Pacific, and eastern Canada. An ENSO-like height anomaly in DJF at 500 hPa level is not found in our experiment. This response might be model dependent and, therefore, needs to be addressed in the future with more model experiments. Over the Southern Hemisphere, a planetary wave number 4 pattern is found at mid-latitudes. Statistically significant areas of positive differences exist at 100° E, 180°, 70° W, and 0°. In summer (Figure 3.13b), the geopotential height anomalies are different from those in winter. The planetary wave pattern in the Southern Hemisphere disappears and is replaced by a belt of negative differences. Interestingly a tropical belt with a slightly enhanced geopotential height of 500 hPa is statistically significant round the globe. In the Northern Hemisphere, statistically significant areas of positive differences exist over Siberia, the midlatitude Pacific, eastern North America, and the Labrador Sea. Statistically significant areas of negative geopotential difference exist over the Bering Sea.

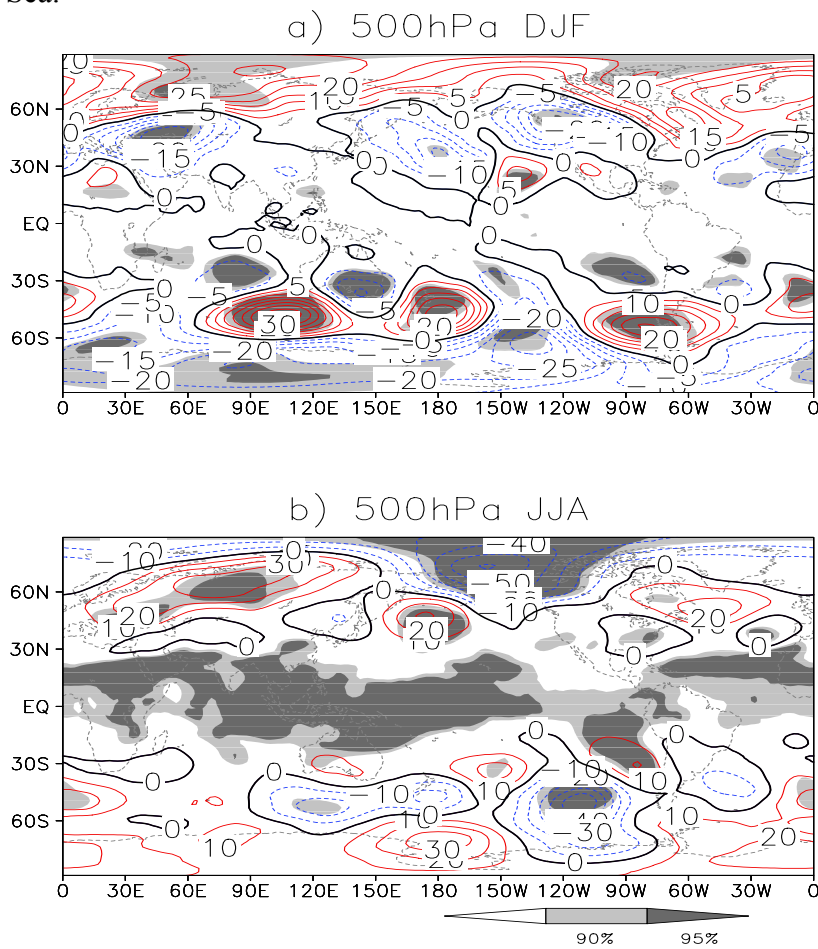


Figure 3.13. Difference of 500-hpa geopotential heights [unit: gpm] between current and forest scenarios (current minus forest) a) for DJF and b) for JJA. Statistically significant changes at the 90% and 95% levels are shaded.

## **4. Conclusions**

Numerical experiments have been conducted with a global atmospheric climate model at 1.875° resolution to investigate the climatic impacts of deforestation in the southeastern Tibetan Plateau, which mainly happened during the second half of the 20<sup>th</sup> century. By comparison of the scenarios of C and F, it can be concluded that: 1) Deforestation on the SETP induces decreased transpiration and increased precipitation locally. Deforested areas get wetter and might provide more runoff into the rivers originating from the TP. 2) The TP, as a whole, gets warmer in summer but colder in autumn and winter as well as wetter in summer. 3) The deforestation on the SETP has regional impact on the Asian climate. The Indian continent becomes warmer throughout the year. South China gets cooler in spring. Precipitation downstream of the SETP is increased during spring and decreased during summer. 4) The remote impacts of deforestation on the SETP are induced by modification of the atmospheric circulation.

The results are drawn from only one scenario conducted by one model. More scenarios and possibly other models should be used in the future to support the conclusions drawn here. It was considered that influences of vegetation changes in the Asian tropical region were more complicated than those in the Amazon region (Mabuchi et al. 2005a; b). Hales et al. (2004) found that land cover changes involve surface conductance and albedo effects as well and concluded that surface conductance in wetter, more heavily vegetated regions gives way to stronger influences of albedo than in more arid, less vegetated regions. In this study, a cooling due to increasing surface albedo of deforestation was not found. The surface temperature does not change much indicating that the energy budget does not change much. However, the albedo effect and surface conductance are integrated together in our experiment. Therefore, a further study is needed to investigate this issue.

It is also worth to mention that, in this study, we examined a simplification case scenario for deforestation/reforestation in which the grassland/cropland at the SETP is replaced by boreal conifer forest in the model experiment. Different deforestation scenarios might be used in the future to project the climate changes in these regions. Meanwhile more observational studies in this region are needed to provide more realistic surface parameters, e.g. for surface albedo, roughness length, surface temperature, precipitation, and soil properties, to be used in the model studies or to evaluate the model performances.

In the present paper, the impact of deforestation in the SETP on current climate was discussed as Part I. In Part II (Cui et al. 2005b; chapter 4) the analysis deals with the interactions of such deforestation effects and an atmosphere with doubled CO<sub>2</sub> concentration.

## References:

- Avissar, R., P. L. S. Dias, M. A. F. S. Dias, and C. A. Nobre, 2002: The large-scale biosphere-atmosphere experiment in Amazonia (LBA): Insights and future research needs. *J. Geophys. Res.*, **107**, 8086, doi:10.1029/2002JD002704.
- Avissar, R., and D. Werth, 2005: Global hydroclimatological teleconnections resulting from tropical deforestation. *J. Hydrometeorology*, **6**, 134-145.
- Bonan, G. B., 1997: Effects of land use on the climate of the United States. *Climatic Change*, **37**, 449-486.
- Braeuning, A., and B. Mantwill, 2004: Summer temperature and summer monsoon history on the Tibetan Plateau during the last 400 years recorded by tree rings. *Geophys. Res. Lett.*, **31**, L24205, doi:10.1029/2004GL020793.
- Broccoli, A.J., and S. Manabe, 1992: The effect of orography on middle latitude northern hemisphere dry climates, *J. Climate*, **5**, 1181-1201.
- Chagnon, F. J. F., R. L. Bras, and J. Wang, 2004: Climatic shift in patterns of shallow clouds over the Amazon. *Geophys. Res. Lett.*, **31**, L24212. doi:10.1029/2004GL02118.
- Charney, J.G., 1975. Dynamics of deserts and droughts in the Sahel. *Q. J. R. Meteor. Soc.*, **101**, 193-202.
- Chen, T. C., 2003: Maintenance of summer monsoon circulations: A planetary-scale perspective. *J. Climate*, **16**, 2022-2037.
- Covey, C., K. M. AchutaRao, U. Cubasch, P. Jones, S. J. Lambert, M. E. Mann, T. J. Philips, and K. E. Taylor, 2003: An overview of results from the Coupled Model Intercomparison Project (CMIP). *Glob. Planet. Change*, **37**, 103-133.
- Cui, X. F., H.-F. Graf, B. Langmann, W. Chen, and R. H. Huang, 2005a: Climate impacts of anthropogenic land use changes on the Tibetan Plateau. *Glob. Planet. Change*, in press.
- Cui, X. F., H.-F. Graf, B. Langmann, W. Chen, and R. H. Huang, 2005b: Impacts of deforestation/reforestation at the southeast Tibetan Plateau. Part II: on future warming climate. *J. Climate*, Submitted.
- Duemenil Gates, L. D., and S. Liess, 2001: Impacts of deforestation and afforestation in the Mediterranean region as simulated by the MPI atmospheric GCM. *Glob. Planet. Change*, **30**, 309-328.
- Fang, J., A. Chen, C. Peng, S. Zhao, and L. Ci, 2001: Changes in forest biomass carbon storage in China between 1949 and 1998. *Science*, **292**, 2320-2322.
- FAO 2001: *State of the world's forestry 2001*. FAO, available at <http://www.fao.org/forestry/site/11747/en>
- Frauenfeld, O.W., T. Zhang, and M. C. Serreze, 2005: Climate change and variability using European Centre for Medium-Range Weather Forecasts reanalysis (ERA40) temperatures on the Tibetan Plateau. *J. Geophys. Res.*, **110**, D02101, doi: 10.1029/2004JD005230.
- Ganzeveld, L., and J. Lelieveld, 2004: Impact of Amazonian deforestation on atmospheric chemistry. *Geophys. Res. Lett.*, **31**, L06105, doi:10.1029/2003GL019205.
- Gates, W. L., J. S. Boyle, C. Covey, C. G. Dease, C. M. Doutriaux, R. S. Drach, M. Fiorino, P. J. Gleckler, J. J. Hnilo, S. M. Marlais, T. J. Philips, G. L. Potter, B. D. Santer, K. R. Sperber, K. E. Taylor, and D. N. Williams, 1999: An overview of the results of the Atmospheric Model Intercomparison Project (AMIP). *Bull. Am. Meteorol. Soc.*, **80**, 29-55.

- GLC2000, 2003: European Commission, Joint Research Centre, available at: <http://www.gvm.jrc.it/glc2000>
- Hales, K., J. D. Neelin, and N. Zeng, 2004: Sensitivity of tropical land climate to leaf area index: Role of surface conductance versus albedo. *J. Climate*, **17**, 1459-1473.
- Hagemann, S., 2002: *An improved land surface dataset for global and regional climate models*. Report No. 336, Max-Planck-Institut fuer Meteorologie, Hamburg, pp. 10. available at: <http://www.mpimet.mpg.de>
- Henderson-Sellers, A., and V. Gornitz, 1984: Possible climatic impacts of land cover transformation, with particular emphasis on tropical deforestation. *Climatic Change*, **6**, 231-258.
- Houghton, J. T., Y. Ding, D. J. Griggs, M. Noguer, P. J. van der Linden, X. Dai, K. Maskell, and C. A. Johnson, Eds., 2001: *Climate Change 2001: The Scientific Basis*. Cambridge University Press, 881 pp.
- Houghton, R. A., and J. L. Hackler, 2003: Sources and sinks of carbon from land-use change in China. *Global Biogeochemical Cycles*, **17(2)**, 1034, doi:10.1029/2002GB001970.
- Kalnay, E., and M. Cai, 2003: Impact of urbanization and land-use change on climate, *Nature*, **423(6939)**, 528-531.
- Kanamitsu, M., W. Ebisuzaki, J. Woolen, J. Potter, and M. Fiorino, 2002: NCEP/DOE AMIP-II Reanalysis (R-2), *Bull. Am. Meteor. Soc.*, **83**, 1631-1643.
- Kistler, R., E. Kalnay, W. Collins, S. Saha, G. White, J. Woollen, M. Chelliah, W. Ebisuzaki, M. Kanamitsu, V. Kousky, H. van den Dool, R. Jenne, and M. Fiorino, 2001: The NCEP-NCAR 50-year reanalysis: Monthly means CD-ROM and documentation. *Bull. Amer. Meteor. Soc.*, **82**, 247-267.
- Klein Goldewijk, K., 2001: Estimating global land use change over the past 300 years: The HYDE database. *Global Biogeochemical Cycles*, **15(2)**, 417-433.
- Linderman, M., P. Rowhani, D. Benz, S. Serneels, and E. F. Lambin, 2005: Land-cover change and vegetation dynamics across Africa. *J. Geophys. Res.*, **110**, D12104, doi:10.1029/2004JD005521.
- Liu, J., Tian, H., Liu, M., Zhuang, D., Melillo, J.M., Zhang, Z., 2005: China's changing landscape during the 1990s: large-scale land transformation estimated with satellite data. *Geophys. Res. Lett.*, **32**, L02405, doi:10.1029/2004GL021649.
- Mabuchi, K., Y. Sato, and H. Kida, 2005a: Climatic impact of vegetation change in the Asian tropical region. Part I: Case of the Northern Hemisphere summer. *J. Climate*, **18**, 410-428.
- Mabuchi, K., Y. Sato, and H. Kida, 2005b: Climatic impact of vegetation change in the Asian tropical region. Part II: Case of the Northern Hemisphere winter and impact on the extratropical circulation. *J. Climate*, **18**, 429-446.
- Meehl, G. A., G. J. Boer, C. Covey, M. Latif, and R. J. Stouffer, 2000: The Coupled Model Intercomparison Project (CMIP), *Bull. Am. Meteor. Soc.*, **81**, 313-318.
- Mestas-Nuñez, A. M., and D. B. Enfield, 2001: Eastern equatorial Pacific SST variability: ENSO and non-ENSO components and their climatic associations. *J. Climate*, **14**, 391-402.
- Miehe, G., S. Miehe, K. Koch, and M. Will, 2003: Sacred forests in Tibet. *Mountain Research and Development*, **23(4)**, 324-328.

- Mitchell, T. D., and P. D. Jones, 2005: An improved method of constructing a database of monthly climate observations and associated high-resolution grids. *Int. J. Climatol.*, **25**, 693-712.
- Myhre, G., and A. Myhre, 2003: Uncertainties in radiative forcing due to surface albedo changes caused by land-use changes. *J. Climate*, **16**, 1511-1524.
- Negri, A. J., R. F. Adler, L. Xu, and J. Surratt, 2004: The impact of Amazonian deforestation on dry season rainfall. *J. Climate*, **17**, 1306-1319.
- Niu, T., Chen, L., Zhou, Z., 2004. The characteristics of climate change over the Tibetan Plateau in the last 40 years and the detection of the climate jumps. *Advances in Atmospheric Sciences*, **21(2)**, 193-203.
- Randall, D., Curry, J., Battisti, D., Flato, G., Grumbine, R., Hakkinen, S., Martinson, D., Preller, R., Walsh, J., Weatherly, J., 1998. Status of and outlook for large-scale modelling of atmosphere-ice-ocean interactions in the Arctic. *Bull. Amer. Meteor. Soc.*, **79(2)**, 197-219.
- Roeckner, E., G. Bauml, L. Bonaventura, R. Brokopf, M. Esch, M. Giorgetta, S. Hagemann, I. Kirchner, L. Kornblueh, E. Manzini, A. Rhodin, U. Schlese, U. Schulzweida, and A. Tompkins, 2003: *The atmospheric general circulation model ECHAM5. Part I: Model description*. Report No. 349, Max-Planck-Institut fuer Meteorologie, Hamburg, pp. 5-6. available at <http://www.mpimet.mpg.de>
- Roeckner, E., R. Brokopf, M. Esch, M. Giorgetta, S. Hagemann, L. Kornblueh, E. Manzini, U. Schlese, and U. Schulzweida, 2004: The atmospheric general circulation model ECHAM5. Part II: Sensitivity of simulated climate to horizontal and vertical resolution. Report No. 354, Max-Planck-Institut fuer Meteorologie, Hamburg, pp 18-20. available at <http://www.mpimet.mpg.de>
- Roy, S. B., and R. Avissar, 2002: Impact of land use/land cover change on regional hydrology in Amazonia. *J. Geophys. Res.*, **107**, 8037, doi:10.1029/2000JD000266.
- Sen, O. L., Y. Wang, and B. Wang, 2004: Impact of Indochina deforestation on the East Asian summer monsoon. *J. Climate*, **17**, 1366-1380.
- Sharma, K.P., C. J. Vorosmarty, and B. Moore III, 2000: Sensitivity of the Himalayan hydrology to land-use and climate changes. *Climatic Change*, **47**, 117-139.
- Shukla, J., C. Nobre, P. J. Sellers, 1990: Amazon deforestation and climate change. *Science*, **247**, 1322-1325.
- Simmons, A.J., and J. K. Gibson, 2000: *The ERA40 Project Plan. ERA40 Project Report Series No.1*, ECMWF, Reading, UK, pp. 63.
- Snyder, P. K., J. A. Foley, M. H. Hitchmann, and C. Delire, 2004: Analyzing the effects of complete tropical forest removal on the regional climate using a detailed three-dimensional energy budget: An application to Africa. *J. Geophys. Res.*, **109**, D21102, doi:10.1029/2003JD004462.
- Studley, J., 1999: Forests and environmental degradation in SW China. *International Forestry Review*, **1(4)**, 260-265. available from: [http://www.geocities.com/john\\_f\\_studley/](http://www.geocities.com/john_f_studley/)
- Suh, M. S., and D. K. Lee, 2004: Impacts of land use/cover changes on surface climate over east Asia for extreme climate cases using RegCM2. *J. Geophys. Res.*, **109**, D02108, doi:10.1029/2003JD003681.
- U. S. Geological Survey, 2001: *Global land cover characteristics data base version 2.0*. available from: [http://edcdaac.usgs.gov/glcc/globdoc2\\_0.html](http://edcdaac.usgs.gov/glcc/globdoc2_0.html).

- van den Hurk, B. J. J. M., P. Viterbo, and S. O. Los, 2003: Impact of leaf area index seasonality on the annual land surface evaporation in a global circulation model. *J. Geophys. Res.*, **108(D6)**, 4191, doi: 10.1029/2002JD002846.
- von Storch, H., and F. W. Zwiers, 1999: *Statistical Analysis in Climate Research*, Cambridge University Press. p113.
- Webster, P. J., V. O. Magaña, T. N. Palmer, J. Shukla, R. A. Tomas, M. Yanai, and T. Yasunari, 1998: Monsoons: Processes, predictability, and the prospects for prediction. *J. Geophys. Res.*, **103(C7)**, 14451-14510.
- Werth, D., and R. Avissar, 2002: The local and global effects of Amazon deforestation. *J. Geophys. Res.*, **107(D20)**, 8087, doi: 10.129/2001JD000717.
- Xu, Q., 2001: Abrupt change of the mid-summer climate in central east China by the influence of atmospheric pollution. *Atmospheric Environment*, **35**, 5029-5040.
- Xue, Y., H. H. Juang, W. P. Li, S. Prince, R. DeFries, Y. Jiao, and R. Vasic, 2004: Role of land surface processes in monsoon development: East Asia and West Africa. *J. Geophys. Res.*, **109**, D03105, doi:10.1029/2003JD003556.
- Ye, D. and Y. Gao, 1979: *The meteorology of the Qinghai-Xizang (Tibet) Plateau*, Sciences Press, Beijing, pp. 278 (in Chinese).
- Zhang, H., A. Henderson-Sellers, and K. McGuffie, 1996a: Impacts of tropical deforestation. Part I: Process analysis of local climatic change. *J. Climate*, **9**, 1497-1517.
- Zhang, H., K. McGuffie, and A. Henderson-Sellers, 1996b: Impacts of tropical deforestation. Part II: The role of large-scale dynamics. *J. Climate*, **9**, 2498-2521.
- Zhang, P., Shao, G., Zhao, G., Master, D.C. Le, Parker, G.R., Dunning, J.B. Jr., Li, Q., 2000: China's forest policy for the 21st century. *Science*, **288**, 2135-2136 (in policy forum).



## **Chapter IV:**

# **Deforestation/Reforestation at the Southeast Tibetan Plateau**

## **Part II: Compounding Effects with Warming Climate**

### **Abstract**

Results are reported from a series of numerical experiments conducted with an atmospheric general circulation model regarding the impact of deforestation on the southeast Tibetan Plateau and its interactions with a possible warmer climate. Differences of doubled CO<sub>2</sub> concentration and forest replacement at warmer climate show that impacts of deforestation are strongly influenced by a warmer climate. This holds not only for the atmospheric circulation but also for surface climate, e.g. temperature and precipitation. The differences between the joint effects of deforestation on the southeastern Tibetan Plateau and doubled CO<sub>2</sub> concentration and the sum of the single disturbances indicate regionally and seasonally varying non-linearity. Annual mean surface temperature shows such non-linearity particularly over regions where the warming signal is strong in the 2×CO<sub>2</sub> climate.

Key Words: Deforestation, Tibetan Plateau, Doubled CO<sub>2</sub> concentration, Global warming

### **4.1. Introduction**

Between one third and one half of the land surface has been directly transformed by human activities (Vitousek et al. 1997). Besides the biogeophysical effect (Brovkin et al. 2004), such as changing surface roughness, transpiration, and albedo, land cover changes also impact on atmospheric composition and climate via biogeochemical feedbacks (Stich et al. 2005), like CO<sub>2</sub> emissions into the atmosphere (Houghton 2003). Reforestation has been proposed to help mitigate climate change. However, using the Hadley Centre General Circulation Model (GCM), Betts (2000) shows how reforestation in the temperate and boreal zones can also lead to a net warming, with the biogeophysical (snow-albedo) feedback exceeding biogeochemical effects, thereby accelerating rather than mitigating climate change. In contrast,

large-scale tropical deforestation leads to net warming as the biogeochemical effect associated with increases in atmospheric CO<sub>2</sub> concentrations is larger than the biogeophysical effects (Claussen et al. 2001). Unfortunately, an evaluation of the overall net result remains open, since the effects are too small to discern them from natural variability (Stich et al. 2005).

Land use change has modified the greenhouse warming signal and hence detection of the impacts of both effects is very difficult (Pielke et al. 1998). Non-linearity in the responses of the disturbances (tropical deforestation and doubled CO<sub>2</sub> concentration) shown by Zhang et al. (2001) further complicates this situation. Chen et al. (2001) stated that the observed precipitation trends in the Amazonia seem to proceed in a direction opposite to the predictions of numerical models only considering biogeophysical impacts of deforestation. Results from the only two GCM simulations that consider both greenhouse gas increases (doubled CO<sub>2</sub> concentration) and Amazonian deforestation (Costa and Foley 2000; Zhang et al. 2001) suggest that the combined effects of greenhouse gases and deforestation may be somewhat more coherent with the observed isotope-derived trends described by Henderson-Sellers et al. (2002) than with deforestation alone (Henderson-Sellers and Pitman 2002). Zhang et al. (2001) find that the reduction in precipitation and evaporation in the wet season is much smaller in the combined experiment even though their annual totals are rather similar. Costa and Foley (2000), who incorporate plant physiology, found that annual mean precipitation and evaporation changes are much smaller for the combined impact case than for deforestation alone.

Cui et al. (2005a; chapter 2) showed that the anthropogenic land cover changes on the Tibetan Plateau (TP) have an impact on regional and, to a weaker degree, on global climate. Cui et al. (2005b; chapter 3; referred to as Part I) simulate the effect of deforestation of the Southeast TP (SETP) under current climate conditions. Deforestation effects might vary under different climate background conditions, like inter-decadal shifts of large-scale circulation patterns (Chen et al. 2001) or global warming (Henderson-Sellers et al. 2002). Zhang et al. (2001) concluded from their model simulation that annually averaged climatic changes due to deforestation over tropical rainforest regions in doubled CO<sub>2</sub> retain similar characteristics as those in which deforestation is imposed in the present-day climate. They proposed that the similarity between their pair of deforestation experiments could be due to the fact that the global warming signal in this model, as in others, is weak in the tropics. Climate in high altitudes, like the TP, is more vulnerable to global warming (see Beniston 2003 for a review). Zhang et al. (2001) also found that the cooling in extratropics due to tropical deforestation is intensified under the warming climate, although without large influence in the tropics. Therefore, it is interesting to investigate climate change of the TP region and to see how the impact of deforestation at SETP may differ in greenhouse gas warmed climate. A “worst scenario” of joint

doubled CO<sub>2</sub> concentration and deforestation of the SETP is proposed in this study. We investigate the following problems: 1) How does the deforestation impact on regional and global climate under future warming climate? 2) How does this impact differ from the current climate condition? 3) Are the two processes (doubled CO<sub>2</sub> concentration and deforestation at SETP) interacting linearly? The paper is organized as follows: Section 4.2 introduces the model and experiments carried out. In section 4.3, a climate scenario with doubled CO<sub>2</sub> concentration simulated by ECHAM5 is presented. Section 4.4 presents the deforestation impact under the greenhouse-warmed climate and compares the results with those under present-day climate. Linearity of deforestation at SETP and doubled CO<sub>2</sub> concentration will be discussed in section 4.5. A summary is given in section 4.6.

## **4.2. Model and Experimental Setup**

In this study, a series of experiments is conducted with the atmospheric general circulation model ECAHAM5 (Roeckner et al. 2003; 2004) developed at Max Planck Institute for Meteorology. ECHAM5 has been and is participating the Atmospheric Model Intercomparison Project (AMIP; Gates et al. 1999; see also <http://www-pcmdi.llnl.gov/amip>), the Coupled Model Intercomparison Project (CMIP; Meehl et al. 2000; Covey et al. 2003; see also <http://www-pcmdi.llnl.gov/cmip>), and IPCC Assessment Report series (e.g. Houghton et al. 1996). Brief description can be found in Cui 2005a (chapter 2) and Part I (chapter 3) and more details can be found from the website: [www.mpimet.mpg.de/en/models/echam/echam5.php](http://www.mpimet.mpg.de/en/models/echam/echam5.php). Four experiments are analyzed in this study: 1) A 22-year control experiment (C) with current land cover is characterized by a uniform CO<sub>2</sub> mixing ratio of 330 ppmv. The last 10 years are analyzed; 2) A 15-year forest experiment (F) with forest replaced on SETP in equilibrated C experiment, the last 10-year averages are assumed to represent the effect of deforestation at SETP by comparison with experiment C. 3) A 22-year doubled-CO<sub>2</sub> concentration simulation (2C) with the CO<sub>2</sub> concentration instantaneously increased from 330 ppmv to 660 ppmv globally. Here also the last 10 years are analyzed. The assumed future climate is characterized by a doubled CO<sub>2</sub> mixing ratio and the other factors kept identical as in C. 4) A 15-year forest experiment in a doubled atmospheric CO<sub>2</sub> concentration environment (2CF) in which the same forest cover was replaced as in experiment F and again, the last 10-year averages are analyzed.

All the experiments are conducted with T63 resolution and driven with the climatological SST and sea ice conditions averaged over the AMIP2 period of 1978 to 1994 (Gates et al. 1999). The simulation of global future warming is often conducted with global coupled ocean-atmosphere general circulation models (coupled GCMs) that include interactive submodels of the oceans and sea ice in addition to an atmospheric component (Covey et al. 2004). However,

some studies show that the differences between the simulations of atmospheric GCMs with observed Sea Surface Temperature (SST) and sea ice and coupled GCMs are remarkably small (Boville and Hurrell 1998; Covey et al. 2004). For global sensitivity measures, the atmospheric model treats the relevant global feedbacks, while the ocean plays a secondary role (Meehl et al. 2004b). However, ocean anomalies can be important for regional climate changes. For example, Findell and Delworth (2005) found that atmospheric circulation changes driven from tropical SST changes may play key role in future regional hydrologic changes in a world with elevated levels of atmospheric greenhouse gases. Therefore, prescribed ocean forcing applied in the present study might exclude the interactive responses of the ocean component and might suppress important interactions between deforestation and hydroclimatic processes. It, however, considerably simplifies the detection of land-cover change teleconnections (Avissar and Werth 2005).

The control experiment C and the forest experiment F were analyzed extensively in Part I. Therefore, in this paper, the joint effects of deforestation at SETP and doubled CO<sub>2</sub> concentration will be addressed mainly by investigating the following major issues: First, the differences between the 2CF experiment and the 2C experiment describe the impact of deforestation in a greenhouse-warmed climate. Second, comparing the impacts of deforestation at SETP under greenhouse-warmed climate with those of deforestation under present-day climate allows studying the question of whether the climatic impacts due to deforestation are enhanced or dampened by greenhouse warming. Third, comparing results of model-simulated impacts of deforestation with the model-simulated climate change due to the enhanced CO<sub>2</sub> concentration allows us to assess how land use change may alter our prediction of future climate.

### **4.3. Doubled CO<sub>2</sub> Warming Climate**

To estimate the influence of tropical deforestation on a greenhouse-warmed climate, it is necessary first to analyze how the climate is affected by doubling the atmospheric CO<sub>2</sub> concentration. Some characteristics of the simulation results, mainly the annual mean precipitation and surface temperature, are presented below. As always, it is difficult to determine whether or not a model is “good enough” to be trusted when used to study climate in the distant past or to make predictions of the future (Covey et al. 2003). The doubled CO<sub>2</sub> concentration scenario is by no means regarded as future climate prediction but one worst scenario to provide a possible different warming climatic background. Therefore, we do not aim to evaluate the model performance, but we provide an image of the possible climate changes induced by doubled CO<sub>2</sub> concentration. The differences found with other model simulations in the literature (e.g. Houghton et al. 1996) will not influence the core of this paper to study the compounding effects and interactions of deforestation at SETP and greenhouse

warming.

Figure 4.1 shows the changes of annual mean near surface air temperature due to doubled atmospheric CO<sub>2</sub> concentration. Note that the 2×CO<sub>2</sub> climate provides a global scale statistically significant warmer atmosphere than the current climate. In response to a doubling of CO<sub>2</sub> the globally averaged surface air temperature simulated by the model increases by 0.22K, mainly occurring over continental regions in the middle and high latitudes. This warming pattern agrees with the IPCC Second Assessment (Houghton et al. 1996) but with smaller amplitude (e.g. 2.9K from Findell and Delworth 2005). The global warming amplitude is restricted by the prescribed SST and sea ice as applied in the present experiment. However, some regions show strong signals like Siberia with 2.5K and North America with 2K. The temperature increases by 0.5K at the southeastern Tibetan Plateau and 0.6K over the whole Tibetan Plateau.

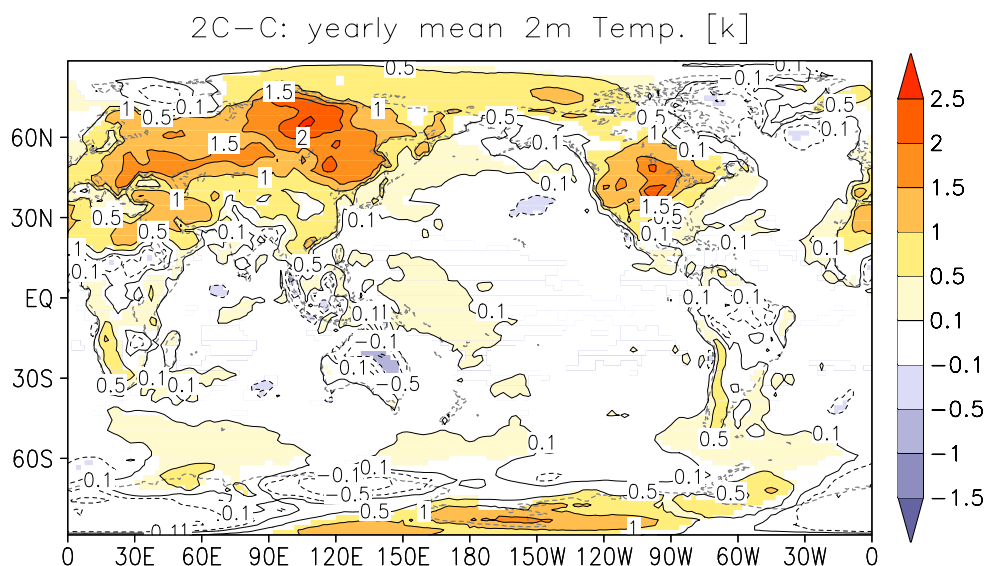


Figure 4.1. Difference of 10-year mean of yearly 2m temperature between doubled CO<sub>2</sub> and current scenarios (2C minus C). Areas are shaded where statistical significant levels higher than 90% statistical significant level.

As stated in the IPCC Second Assessment (Houghton et al. 1996), increasing atmospheric CO<sub>2</sub> concentration leads to changes in global atmospheric circulation and global water and energy cycles. However, because of poor signal-to-noise ratios and model uncertainty, anthropogenic rainfall changes cannot presently be detected even on a global scale (The International Ad Hoc Detection and Attribution Group 2005). An increase of atmospheric CO<sub>2</sub> is likely to lead to increased summertime drying and wintertime wetting of soils in mid-latitude continental regions, particularly in North America and Asia (e.g. Manabe and Wetherald 1987) and might lead to a weaker monsoon (Kimoto 2005) by the so-called “thermodynamic mechanism” (Findell and Delworth

2005). Figure 4.2 shows the annual mean precipitation changes due to doubled CO<sub>2</sub> concentration simulated by our model. Large changes are found over the maritime continent straddling the equator, despite the prescribed ocean conditions applied in our experiment. But, only several small areas are statistically significant. This might indicate the complexity of precipitation processes and uncertainty in our model. Globally mean precipitation decreases 25 mm per year due to doubled CO<sub>2</sub> concentration. Precipitation over SETP increases by 127 mm per year. Over the whole TP the increase is smaller with 78mm.

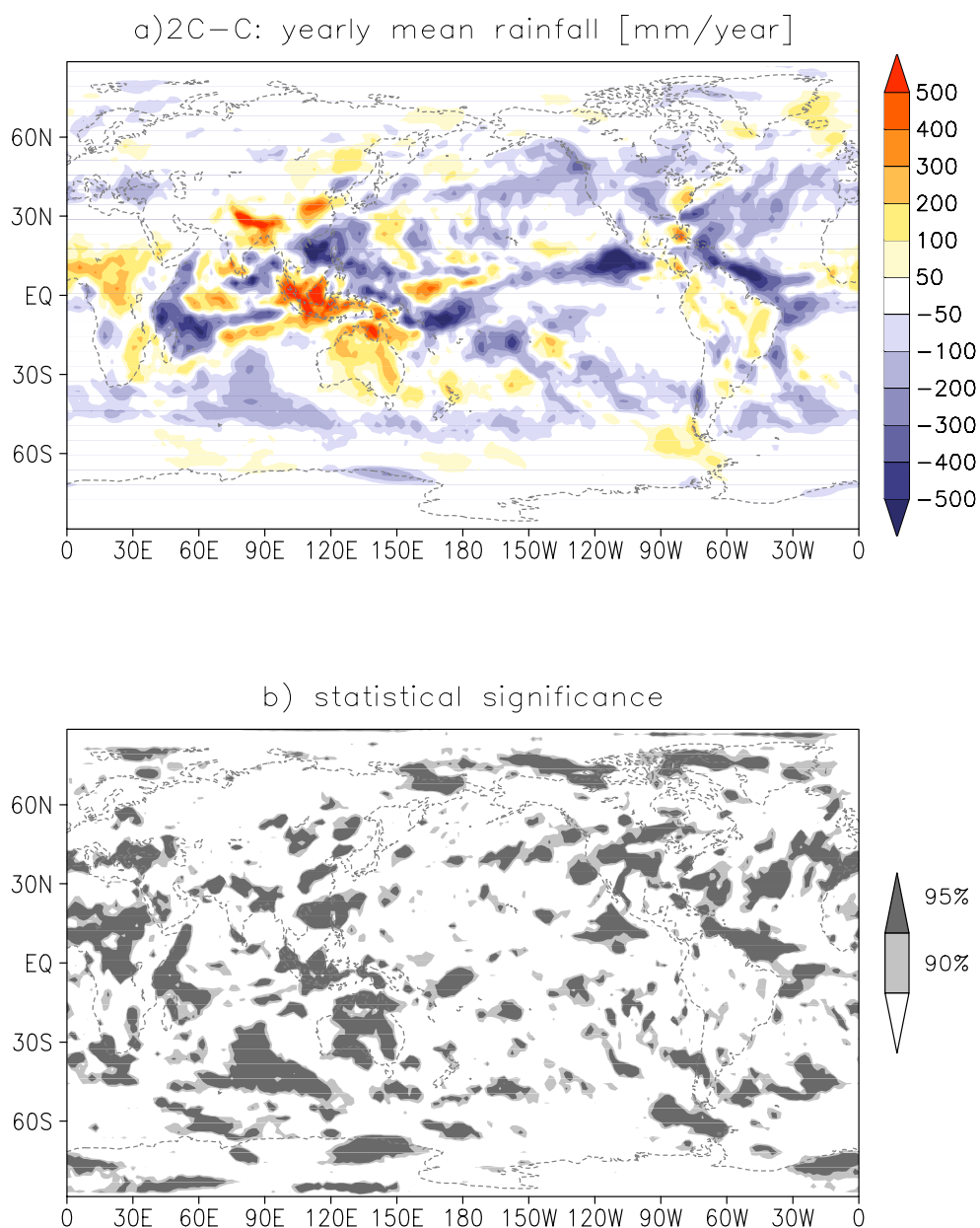


Figure 4.2. Difference of 10-year mean of yearly rainfall between doubled CO<sub>2</sub> and current scenarios (2C minus C). a) absolute values and b) statistical

significance are shaded respectively.

## **4.4. Impacts of Deforestation in a Greenhouse-Warmed Climate**

Differences between the joint 2CF experiment and the doubled CO<sub>2</sub> experiment 2C are analyzed to show how the climate is affected by deforestation at SETP under greenhouse-warmed climate condition and whether it is similar as the effect under present-day climate condition shown in Part I (chapter 3). Therefore, a comparison of the effect induced by deforestation at warmed-climate and present-day climate condition will be discussed in particular to reveal whether the impact of deforestation is affected by the climate of doubled CO<sub>2</sub> concentration.

Changes of atmospheric circulation are potentially important for hydrological changes; therefore they are analyzed first. Figure 4.3 shows the atmospheric circulation changes due to deforestation at SETP under doubled CO<sub>2</sub> concentration at higher and lower troposphere. In winter, the divergent circulation in the upper troposphere over the Indian Ocean and south Asia is statistically significantly strengthened and correspondingly is the lower troposphere convergent circulation in this area. East to the strengthening region, a weakening area exists over the Pacific Ocean both in upper and lower troposphere. However, west to it, the convergent circulation in the upper troposphere is strengthened over Europe and the Atlantic Ocean and correspondingly also is the divergent circulation in the lower troposphere. The maximum changing areas are statistically significant. Compared to the changes of deforestation at present-day climate presented in Part I (chapter 3), the atmospheric circulation is modulated and a stronger meridional circulation is present in the warming climate. In summer, the changes of divergent circulation are similar with that of present-day climate. In the upper troposphere, divergent circulation is strengthened over the western tropical Pacific and southeast Pacific and convergent circulation is strengthened in North America. They are both statistically significant. The amplitude of intensification over the western tropical Pacific is larger in a warming climate than under present-day climate conditions. In the lower troposphere, the convergent circulation over the western Pacific and Asia is strengthened, it shows larger amplitude and covers a larger region than that under present-day climate. Although these features are not all statistically significant, this might lead to monsoon changes in the Asian region, which will be discussed later.

2C-2CF: seasonal circulation

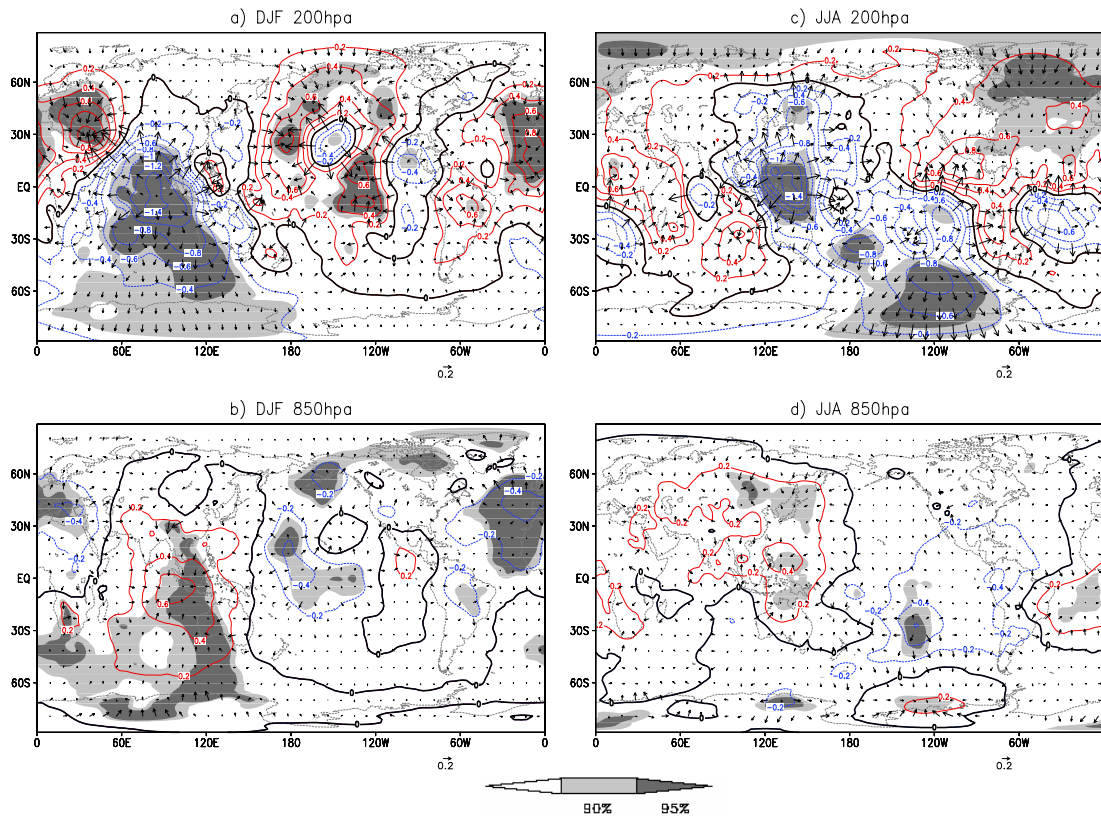


Figure 4.3. Differences of atmospheric circulation due to forest replacement under doubled CO<sub>2</sub> concentration at higher (a, c) and lower (b, d) troposphere in DJF (a, b) and JJA (c, d). The contour intervals for velocity potential are  $0.2 \times 10^6 \text{ m}^2 \text{ s}^{-1}$ .

To provide a clearer image of the changes of atmospheric circulation due to deforestation under warming climate, geopotential height changes at 500hPa are shown in Figure 4.4. It shows the responses of 500hPa geopotential heights due to deforestation at SETP. In winter, these are different even in sign over some regions under the greenhouse-warmed and present-day climate conditions while similar in summer. A statistically significant planetary scale “positive-negative” pattern is found in the Northern Hemisphere as the effect of deforestation under warmer climate, which is not visible under present-day climate (Figure 3.13a in Part I; chapter 3). The increasing geopotential height over Siberia weakens the East Asia trough influencing the Asian climate in winter. Differences in some areas are also found in the Southern Hemisphere during winter and summer. In summary, the model results indicate that the effect induced by deforestation at SETP is influenced by global warming in terms of atmospheric circulation, leading to changes in water and energy cycles.

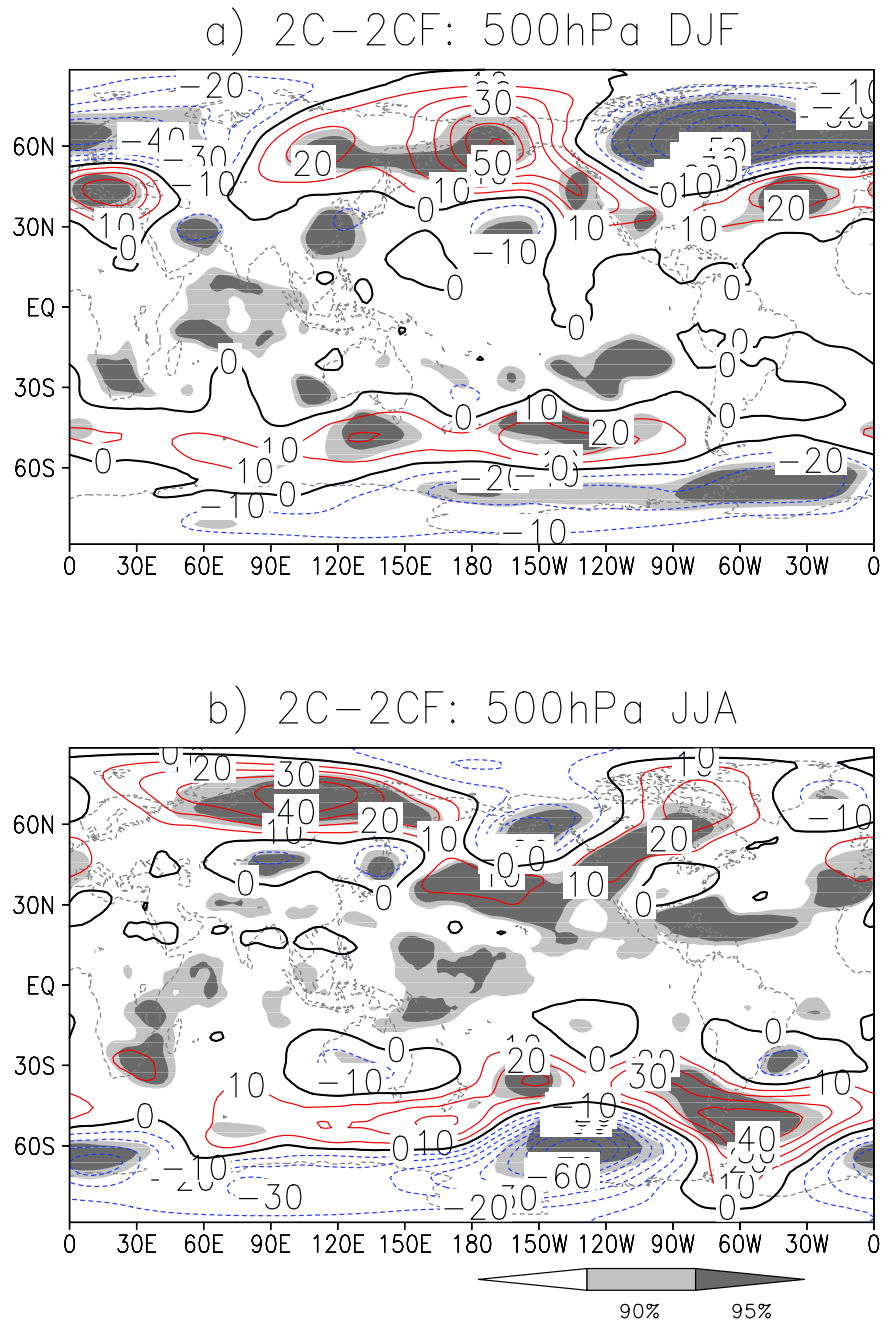


Figure 4.4. Difference of 500-hPa geopotential height due to forest replacement under doubled CO<sub>2</sub> concentration a) DJF and b) JJA. Statistical significances of 90% and 95% are shaded.

To reveal the global scale surface climate responses to deforestation at SETP under greenhouse warmed climate, Figure 4.5 and 4.6 are shown for surface atmospheric temperature and annual mean precipitation, respectively. Annual mean temperature increases statistically significantly over Siberia and Europe by more than 1K. The western United States and parts of Africa also get slightly warmer. Statistically significant changes occur in Antarctica, however, they will not be discussed here due to known polar problems in the numerical simulations. Statistically significant cooling is simulated in Canada and Iceland. The cooling amplitude reaches more than 1K. A slight cooling can be found in tropical continental regions, however barely statistically significant. Few common statistically significant changes can be found in comparison with the changes of deforestation under present-day climate shown in Figure 3.11 in Part I (chapter 3). However, it can be easily found that the warming regions in Figure 4.5 are associated with the larger warming areas in Figure 4.1, while the cooling areas are associated with smaller warming or cooling areas in Figure 4.1. This may suggest that the effect of deforestation at SETP is modulated by the warming climate over regions where strong warming signals exist, even though the global averaged warming is moderate compared to other model simulations (Houghton et al. 1996) due to prescribed current SST applied in this experiment. The annual mean precipitation changes under greenhouse-warming climate

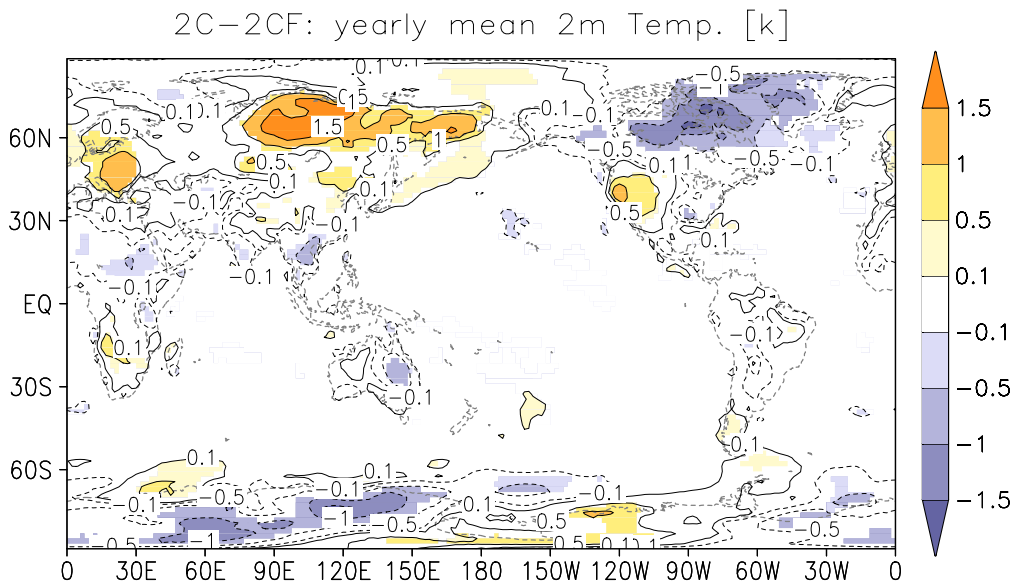


Figure 4.5. Same as Figure 4.1, but for the differences due to forest replacement under doubled CO<sub>2</sub> concentration (2C-2CF).

precipitation changes due to deforestation under greenhouse-warming climate are mainly located over the tropical maritime continent (Figure 4.6) with barely statistical significance. However, it is not similar either with the changes due to deforestation under present-day climate (Figure 3.12 in Part I; chapter 3) or with the changes of doubled CO<sub>2</sub> concentration (Figure 4.2). Therefore, hydrological impacts of deforestation at SETP should be taken with caution and need to be investigated in future studies.

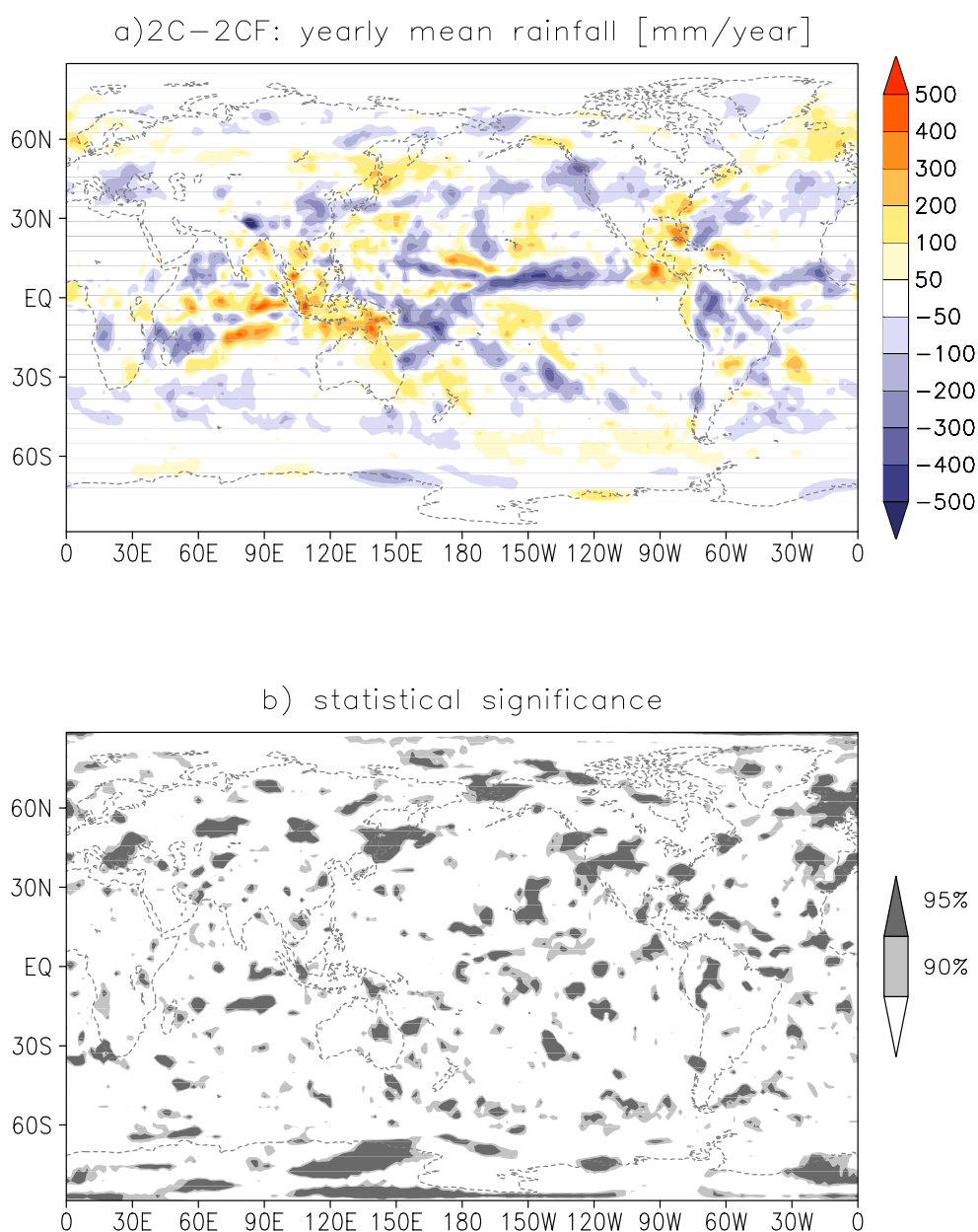


Figure 4.6. Same as Figure 4.2, but for the differences due to forest replacement

under doubled CO<sub>2</sub> concentration (2C minus 2CF).

Overall, our model results indicate that the local climate impacts due to deforestation at SETP under warmer climate conditions are different from those induced in present-day climate. The yearly mean temperature increases by 0.28K averaged over SETP, which presents the deforested area, under greenhouse-warmed climate condition while it decreases by -0.11K under present-day climate (see Table 4.1). This disagrees with the similarity of local temperature changes of tropical deforestation under warmed-climate and present-day climate from Zhang et al. (2001), possibly because of the strong warming signal in the extra-tropics, where the SETP locates. Annual mean precipitation decreases by -73.86 mm over SETP under warmer climate while it increases by 30.53 mm under present-day climate. The whole Tibetan Plateau gets warmer (0.24K) and drier (-35.24mm) due to deforestation at SETP under warmer climate than that under present-day climate (-0.08K and -10.48mm, respectively). Northern and Southern Hemisphere and globally averaged mean temperature and precipitation are given in Table 4.1. The globally averaged signals simulated by the model are very small. But the global mean eliminates regional signals which vary largely as shown in Figure 4.5 and Figure 4.6. Therefore, we conclude that the model simulates strong influence of global warming on the deforestation at SETP. How far the warming climate modulates the deforestation at SETP and the interactions between the two disturbances will be discussed in the next section.

## **4.5. Joint Impacts of Deforestation and Doubled CO<sub>2</sub> Concentration**

Zhang et al. (2001) suggest that their model tends to perform non-linearly in its responses to tropical deforestation and doubled CO<sub>2</sub> concentration, when analyzing the changes of surface and atmosphere energy budgets. The main scientific question to be answered in this section is whether the deforestation at SETP and doubled CO<sub>2</sub> concentration are linear in our model simulations. The joint effects of greenhouse-warming and deforestation at SETP should have little difference from the sum of the effects of the two disturbances happening alone, if they are more linear than non-linear. Therefore, we compare the sum of the effects due to doubled CO<sub>2</sub> concentration (2C-C) and deforestation under warmer climate conditions (2C-2CF) and the joint effects of the two disturbance both happening (2C-F). The ‘non-linearity’ differences (Zhang et al. 2001) from such comparisons ((2C-C)+(2C-2CF)-(2C-F); referred as DIFF hereafter) should be small where the two processes (doubled CO<sub>2</sub> concentration and deforestation at SETP) interact more linearly.

Figure 4.7 shows atmospheric circulations of DIFF in the upper and lower troposphere in winter and summer. It clearly demonstrates that the models

degree of linearity to these two processes (doubled CO<sub>2</sub> concentration and deforestation at SETP) is variable seasonally and regionally. Large values of difference present high non-linearity while smaller values mean linearity. The model reacts more nonlinearly in winter than in summer. The amplitudes of DIFF are comparable with that of deforestation under warmer climate or present-day climate conditions. The pattern is closer to the deforestation at warmer climate conditions. Similar characteristics can be found at 500hPa geopotential heights of DIFF shown in Figure 4.8. The pattern and magnitude of the differences are very close to that shown in Figure 4.4. As discussed above, large differences between the effects under warmer climate and present-day climate conditions present intensive influences of warming climate on effects induced by deforestation. The nonlinearity differences are closer to the difference of deforestation under warmer climate than to that under present-day climate, indicating that a warming climate intensifies influences of deforestation over areas of non-linearity. Overall, the atmospheric circulation results suggest that the model tends to perform more non-linearly than linearly in its response to the two imposed disturbances. Note that such large-scale changes cannot be directly linked to changes of surface climate (e.g. precipitation and temperature) over specific regions which are determined by complex interactions between atmospheric dynamics and physics calculated by the model (Zhang et al. 2001).

DIFF: seasonal circulation

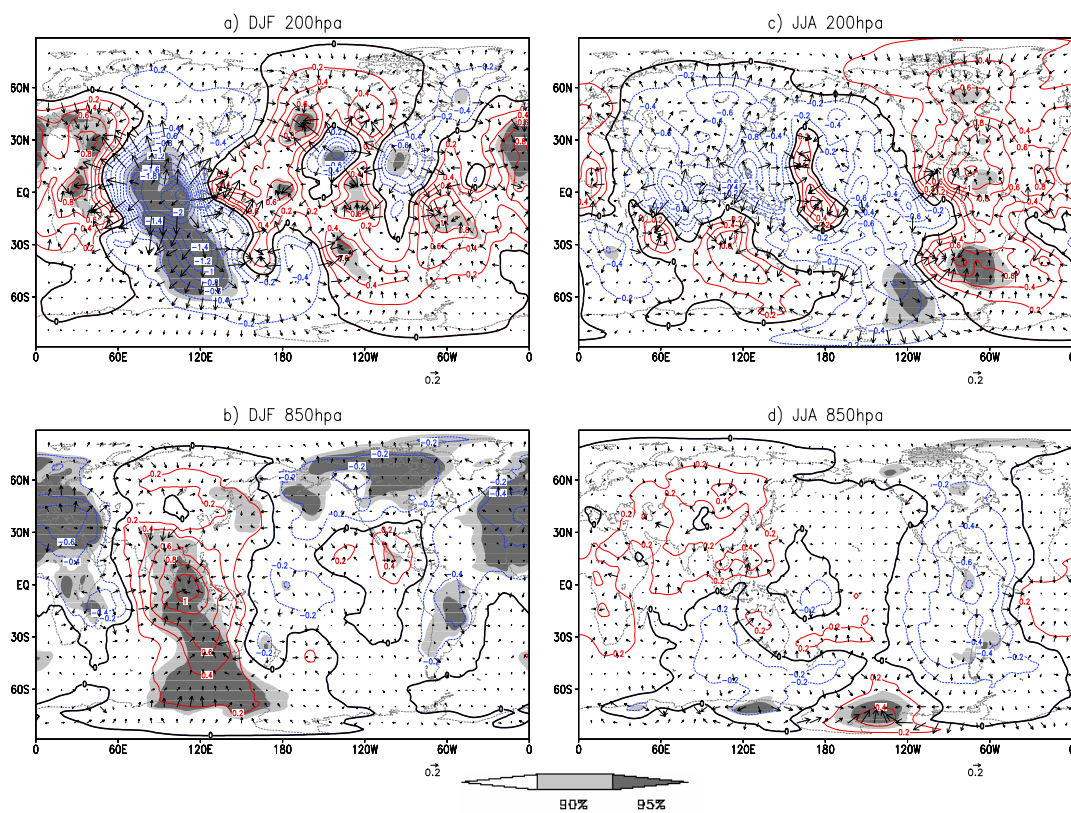


Figure 4.7. Same as Figure 4.3, but for differences between the joint effects of deforestation and warming of doubled CO<sub>2</sub> concentration and the sum of the effect of the two disturbances alone (see text for detail).

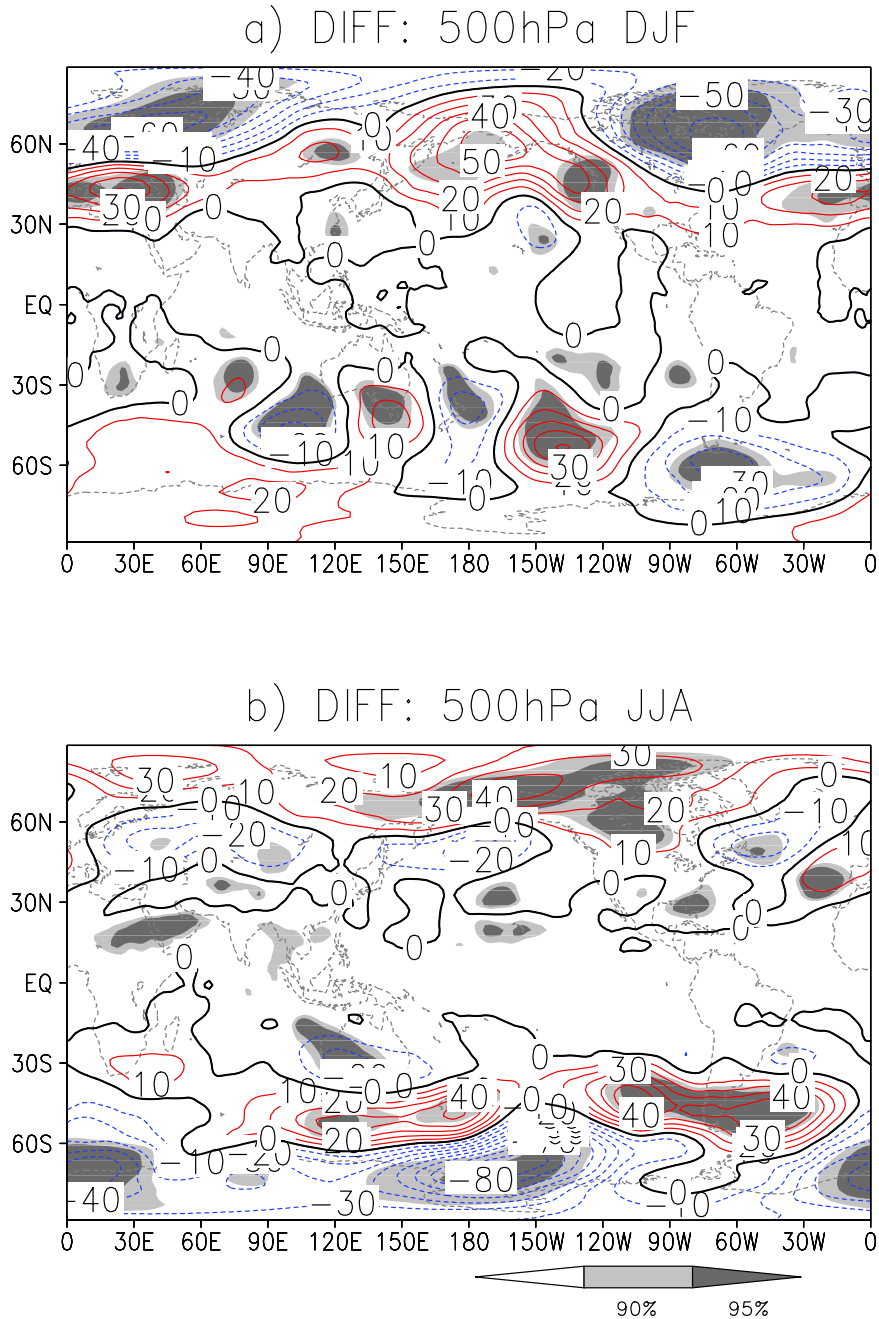


Figure 4.8. Same as Figure 4.4, but for differences between the joint effects of deforestation and warming of doubled  $\text{CO}_2$  concentration and the sum of the effect of the two disturbances alone (see text for detail).

Surface temperature of DIFF, shown in Figure 4.9, clearly demonstrates some statistically significant non-linear difference. Siberia and North Asia show positive differences of over 1K. Europe, South Africa, and the Western United States also show slightly positive differences. A large statistically significant negative difference area exists over Canada. Slightly negative difference can also be found in the tropical continental areas with partly statistical significance. Smaller differences of surface temperature indicate more linearity of the two disturbances, while the larger differences at higher latitude indicate more non-linearity. Note that the patterns of differences are associated with that of deforestation at SETP under warm climate conditions (Figure 4.5). The impacts of deforestation on surface temperature are modulated strongly by doubled CO<sub>2</sub> concentration over regions where the two disturbances interact more nonlinearly than linearly. It indicates that changes of the surface energy budget are complicated by the interactions between processes induced by deforestation and processes changed by the doubled-CO<sub>2</sub> concentration in the atmosphere (Zhang et al. 2001).

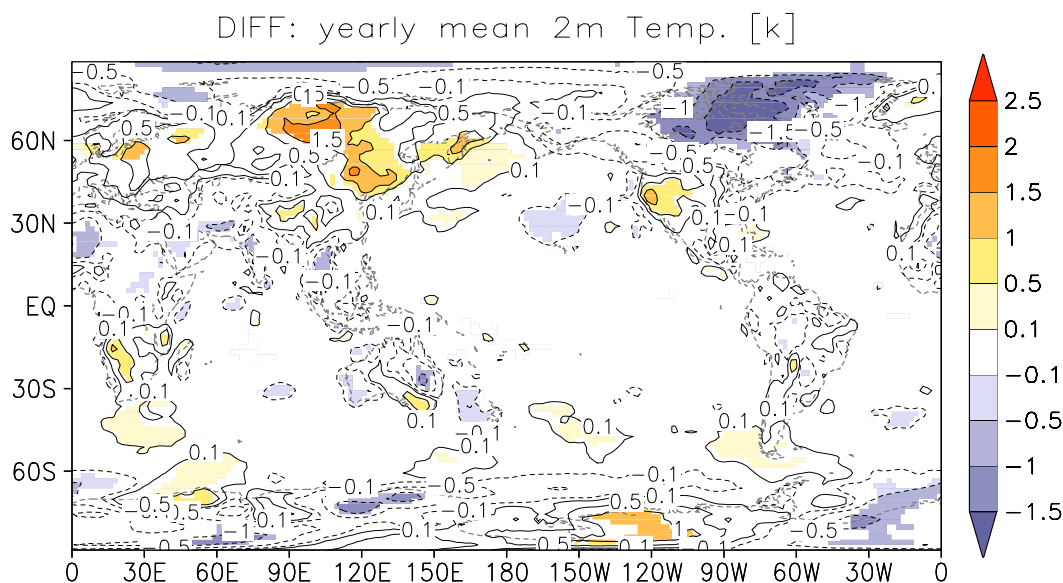


Figure 4.9. Same as Figure 4.1, but for differences between the joint effects of deforestation and warming of doubled CO<sub>2</sub> concentration and the sum of the effect of the two disturbances alone (see text for detail).

Figure 4.10 shows the annual mean precipitation of DIFF. It demonstrates large differences over the maritime continent. Statistically significance barely exists in the tropical regions where the largest differences are located. The differences of precipitation, opposite to surface temperature, are not similar with either difference induced by deforestation under warmer climate conditions or under present-day climate conditions. Highly regional variability with little statistical significance might indicate that the water cycle becomes more complicated due to the nonlinear interaction of the deforestation at SETP and doubled CO<sub>2</sub> concentration found in atmospheric circulation and surface temperature.

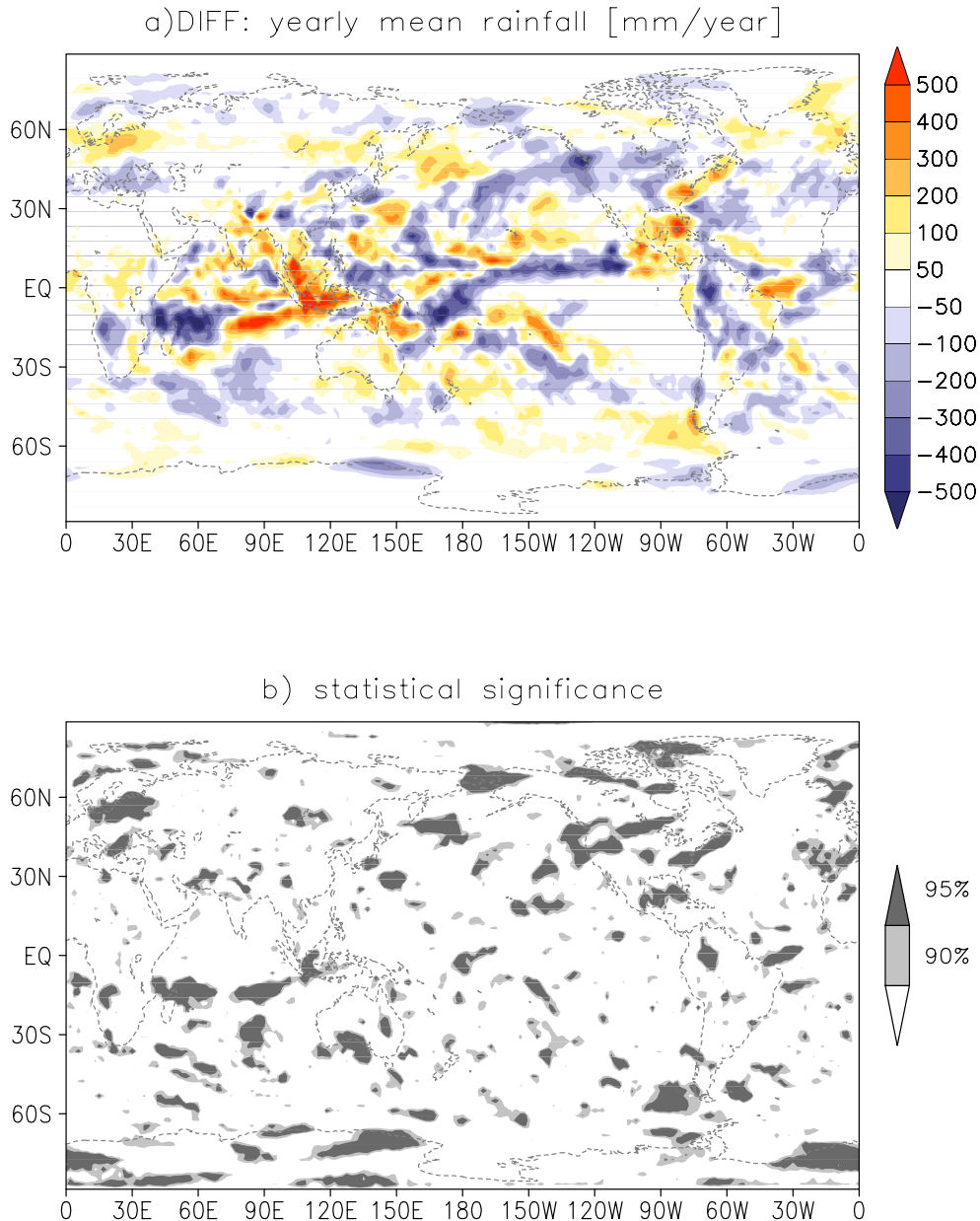


Figure 4.10. Same as Figure 4.2, but for differences between the joint effects of deforestation and warming of doubled CO<sub>2</sub> concentration and the sum of the effect of the two disturbances alone (see text for detail).

## **4.6. Conclusions**

Numerical simulations are conducted with an atmospheric general circulation model to investigate the compounding effects of deforestation at the southeast Tibetan Plateau and doubled CO<sub>2</sub> concentration. First, the impacts due to deforestation over the southeastern Tibetan Plateau under warmer climate and present-day climate conditions are compared. The impacts of deforestation at SETP under warmer climate are found different from that under present-day climate conditions, indicating modification by the greenhouse-warmed climate. The impacts of deforestation under warm climate are modulated locally at SETP and elsewhere in terms of surface temperature and precipitation and associated atmospheric circulation. Surface temperature is modulated strongly over regions where the stronger warming signals are.

Secondly, the linearity of deforestation at SETP and doubled CO<sub>2</sub> concentration are analyzed by comparison of the joint effects of the two disturbances and the sum of the two disturbances imposed alone. It is found that our model tends to response to the two processes more non-linearly than linearly. The comparison of annual mean surface temperature indicates that the two processes interact more non-linear than linear over regions where the warming signals are strong in the greenhouse-warmed climate, which are associated with the areas where effects of deforestation at SETP are modulated strongly.

However, the results concluded here are based on simulations conducted with only one atmospheric GCM. Other models might conclude different results. Therefore, an ensemble experiments like AMIP (Gates et al. 1999) or CMIP (Meehl et al. 2000) with more models are highly recommended for future studies. It is also worth mentioning that the experiments in the present study are conducted with an AGCM driven with the climatological SST and sea ice, not with a coupled GCM. This set-up was aiming at simpler detections of the interactions of deforestation and hydroclimatic processes. Experiments conducted with coupled GCMs including interactive ocean are highly recommended to test the hypothesis drawn in the present study. High uncertainty of precipitation found in our model simulations intimates further investigation of this issue in the future. Assessment of hydrological effects of future different land use policy, like reforestation, is highly needed by the local or regional community and government. It will be interesting to investigate the effects of deforestation/reforestation at SETP with a configuration of regional climate models driven by more realistic future warming scenarios produced by coupled GCMs, like the new IPCC scenarios.

Table 4.1: Area averages of near surface temperature  $T_s$  [unit: K] and annual precipitation [unit: mm/year] from different scenarios and differences between them. Areas includes the deforested region southeast Tibetan Plateau (SETP) shown in Figure 4.2a, the Tibetan Plateau (TP), Northern Hemisphere (NH) averaged from equator to 70N, Southern Hemisphere (SH) averaged from equator to 70S, and global averages from 70S to 70N, respectively. Scenarios include ECHAM5 current scenario (C), forest replacement experiment (F), Doubled CO<sub>2</sub> concentration warming scenario (2C), and forest replacement under doubled CO<sub>2</sub> concentration (2CF). Differences of C-F present deforestation on current climate and 2C-2CF shows the deforestation impact on warming climate, while 2C-C presents the warming difference due to doubled CO<sub>2</sub> concentration globally and 2C-F indicates the joint effects of deforestation at SETP and doubled CO<sub>2</sub> concentration.

<i>Precipitation P [mm/year]</i>								
	<b>C</b>	<b>2C</b>	<b>F</b>	<b>2CF</b>	<b>C-F</b>	<b>2C-C</b>	<b>2C-2CF</b>	<b>2C-F</b>
<b>SETP</b>	2383.23	2511.51	2353.7	2585.37	30.53	127.28	-73.86	157.81
<b>TP</b>	1116.31	1194.42	1126.79	1229.66	-10.48	78.11	-35.24	67.63
<b>NH</b>	1135.7	1104.87	1137.67	1107.91	-1.97	-30.83	-3.04	-32.8
<b>SH</b>	1089.27	1070.44	1088.71	1068.11	0.56	-18.83	2.33	-18.27
<b>Globe</b>	1112.49	1087.65	1113.19	1088.01	-0.7	-24.84	-0.36	-25.54
<i>Near surface temperature <math>T_s</math> [K]</i>								
	<b>C</b>	<b>2C</b>	<b>F</b>	<b>2CF</b>	<b>C-F</b>	<b>2C-C</b>	<b>2C-2CF</b>	<b>2C-F</b>
<b>SETP</b>	278.356	278.881	278.465	278.606	-0.11	0.53	0.28	0.42
<b>TP</b>	271.697	272.286	271.775	272.043	-0.08	0.59	0.24	0.51
<b>NH</b>	290.113	290.488	290.091	290.441	0.02	0.38	0.05	0.4
<b>SH</b>	289.587	289.654	289.585	289.652	0	0.07	0	0.07
<b>Globe</b>	289.85	290.072	289.833	290.047	0.02	0.22	0.03	0.24

References:

- Avissar, R., and D. Werth, 2005: Global hydroclimatological teleconnections resulting from tropical deforestation. *J. Hydrometeorology*, **6**, 134-145.
- Beniston, M., 2003: Climatic change in mountain regions: A review of possible impacts. *Climatic Change*, **59**, 5-31.
- Betts, R. A., 2002: Offset of the potential carbon sink from boreal forestation by decreases in surface albedo, *Nature*, **408**, 187-190.
- Boville, B. A., and J. W. Hurrell, 1998: A comparison of the atmospheric circulations simulated by the CCM3 and CSM1. *J. Climate*, **11**, 1327-1341.
- Brovkin, V., S. Sitch, W. von Bloh, M. Claussen, E. Bauer, and W. Cramer, 2004: Role of land cover changes for atmospheric CO<sub>2</sub> increases and climate change during the last 150 years, *Global Change Biol.*, **10**, 1-14.
- Chen, T.C., J. H. Yoon, K. J. St. Croix, and E. S. Takle, 2001: Suppressing impacts of the Amazonian deforestation by global circulation changes. *Bull. Amer. Meteor. Soc.*, **82**, 2209-2216.
- Claussen, M., V. Brovkin, and A. Ganopolski, 2001: Biogeophysical versus biogeochemical feedbacks of large-scale land cover change, *Geophys. Res. Lett.*, **28(6)**, 1011-1014.
- Costa, M. H., and J. A. Foley, 2000: combined effects of deforestation and double atmospheric CO<sub>2</sub> concentrations on the climate of Amazonia. *J. Climate*, **13**, 18-34.
- Covey, C., K. M. AchutaRao, U. Cubasch, P. Jones, S. J. Lambert, M. E. Mann, T. J. Philips, and K. E. Taylor, 2003: An overview of results from the Coupled Model Intercomparison Project (CMIP). *Glob. Planet. Change*, **37**, 103-133.
- Covey, C., K. M. AchutaRao, P. J. Gleckler, T. J. Philips, K. E. Taylor, and M. F. Wehner, 2004: Coupled ocean-atmosphere climate simulations compared with simulations using prescribed sea surface temperature: effect of a "perfect ocean". *Global Planet. Change*, **41**, 1-41.
- Cui, X. F., H.-F. Graf, B. Langmann, W. Chen, and R. H. Huang, 2005a: Climate impacts of anthropogenic land use changes on the Tibetan Plateau. *Global Planet. Change*, in press.
- Cui, X. F., H.-F. Graf, B. Langmann, W. Chen, and R. H. Huang, 2005b: Deforestation/reforestation at the southeast Tibetan Plateau. Part I: Impacts on current climate. *J. Climate*, Submitted.
- Findell, K. L., and T. L. Delworth, 2005: A modeling study of dynamic and thermodynamic mechanisms for summer drying in response to global warming. *Geophys. Res. Lett.*, **32**, L16702, doi:10.1029/2005GL023414.
- Gates, W.L., Boyle, J.S., Covey, C., Dease, C.G., Doutriaux, C.M., Drach, R.S., Fiorino, M., Gleckler, P.J., Hnilo, J.J., Marlais, S.M., Philips, T.J., Potter, G.L., Santer, B.D., Sperber, K.R., Taylor, K.E., Williams, D.N., 1999. An overview of the results of the Atmospheric Model Intercomparison Project (AMIP). *Bull. Am. Meteorol. Soc.*, **80**, 29-55.
- Henderson-Sellers, A. K., K. McGuffie, and H. Zhang, 2002: Stable isotopes as validation tools for global climate model predictions of the impact of Amazonian deforestation. *J. Climate*, **15**, 2664-2667.
- Henderson-Sellers, A. K., and A. J. Pitman, 2002: Comments on "Suppressing impacts of the Amazonian deforestation by global circulation changes". *Bull. Amer. Meteor. Soc.*, **83**, 1657-1661.
- Houghton, J. T., L. G. Meria Filho, B. A. Callender, H. Harris, A. Kattenberg, and K. Maskell (eds.), 1996: *The Science of Climate Change*, Cambridge University Press, Cambridge, U. K., p. 572.

- Houghton, J. T., Y. Ding, D. J. Griggs, M. Noguera, P. J. van der Linden, X. Dai, K. Maskell, and C. A. Johnson, Eds., 2001: *Climate Change 2001: The Scientific Basis*. Cambridge University Press, 881 pp.
- Houghton, R. A., and J. L. Hackler, 2003: Sources and sinks of carbon from land-use change in China. *Global Biogeochemical Cycles*, **17(2)**, 1034, doi:10.1029/2002GB001970.
- Kimoto, M., 2005: Simulated change of the east Asian circulation under global warming scenario. *Geophys. Res. Lett.*, **32**, L16701, doi:10.1029/2005GL023383.
- Matthews, H. D., A. J. Weaver, M. Eby, and K. J. Meissner, 2003: Radiative forcing of climate by historical land cover change, *Geophys. Res. Lett.*, **30(2)**, 1055, doi:10.1029/2002GL016098.
- Matthews, H. D., A. J. Weaver, K. J. Meissner, N. P. Gillett, and M. Eby, 2004: Natural and anthropogenic climate change: Incorporating historical land cover, vegetation dynamics and the global carbon cycle, *Clim. Dyn.*, **22**, 461-479, doi:10.1007/s00382-004-0392-2.
- Meehl, G. A., G. J. Boer, C. Covey, M. Latif, and R. J. Stouffer, 2000: The Coupled Model Intercomparison Project (CMIP), *Bull. Am. Meteorol. Soc.*, **81**, 313-318.
- Meehl, G. A., W. M. Washington, J. M. Arblaster, and A. Hu, 2004: Factors affecting climate sensitivity in global coupled models. *J. Climate*, **17**, 1584-1596.
- Meehl, G. A., W. M. Washington, T. M. L. Wigley, J. M. Arblaster, and A. Dai, 2003: Solar and greenhouse gas forcing and climate response in the twentieth century. *J. Climate*, **16**, 426-444.
- Pielke, R. A., R. Avissor, M. Raupach, H. Dolman, X. Zeng, and S. Denning, 1998: Interactions between the atmosphere and terrestrial ecosystems: Influence on weather and climate, *Global Change Biol.*, **4**, 461-475.
- Roeckner, E., G. Bauml, L. Bonaventura, R. Brokopf, M. Esch, M. Giorgetta, S. Hagemann, I. Kirchner, L. Kornbluh, E. Manzini, A. Rhodin, U. Schlese, U. Schulzweida, and A. Tompkins, 2003: The atmospheric general circulation model ECHAM5. Part I: Model description. *Report No. 349, Max-Planck-Institut fuer Meteorologie*, Hamburg, pp. 5-6.
- Roeckner, E., R. Brokopf, M. Esch, M. Giorgetta, S. Hagemann, L. Kornbluh, E. Manzini, U. Schlese, and U. Schulzweida, 2004: The atmospheric general circulation model ECHAM5. Part II: Sensitivity of simulated climate to horizontal and vertical resolution. *Report No. 354, Max-Planck-Institut fuer Meteorologie*, Hamburg, pp 18-20.
- Stich, S., V. Brovkin, W. von Bloh, D. Van Vuuren, B. Eickhout, and A. Ganopolski, 2005: Impacts of future land cover changes on atmospheric CO<sub>2</sub> and climate. *Global Biogeochemical Cycles*, **19**, GB2013, doi:10.1029/2004GB002311.
- The International Ad Hoc Detection and Attribution Group, 2005: Detecting and attributing external influences on the climate system: A review of recent advances. *J. Climate*, **18**, 1291-1314.
- Vitousek, P. M., H. A. Mooney, L. Lubchenco, and J. M. Melillo, 1997: Human domination of Earth's ecosystems, *Science*, **277**, 494-499.
- Zhang, H., Hender-Sellers, and K. McGuffie, 2001: The compounding effects of tropical deforestation and greenhouse warming on climate. *Climatic Change*, **49**, 309-338.

## **Chapter V:**

# **Application of the Regional Climate Model REMO over the Tibetan Plateau**

### **Abstract**

The regional climate model REMO is applied over the Tibetan Plateau and a “double-nesting” technique is implemented to solve the downscaling problems at lateral boundaries. Summer 1998 is simulated driven by “perfect boundary” and model results are evaluated with reanalysis and observation data. REMO can represent reasonably the large-scale circulation and provide more realistic regional characteristics and surface climate than the driving data due to the better topographical representation. The comparisons with observation from two stations reveal that REMO can produce major precipitation events at daily scale and simulate the spatial differences. It is also found that REMO can reproduce well the monsoonal rainfall period.

Key words: Regional Climate Model REMO; Tibetan Plateau; nesting; Precipitation.

### **5.1. Introduction**

The climate over the Tibetan Plateau (hereafter referred to as TP) displays a pronounced variability of temporal and spatial scales due to its complex mountainous terrain, high elevation, and huge size (e.g. Ye and Gao 1979). The seasonal variability on the TP is characterized clearly by a rainy and a dry period, governed strongly by the monsoonal circulation called the Tibetan Plateau monsoon (Tang et al. 1998). Large differences are also found between daytime and nighttime precipitation: daytime precipitation appears along major mountains, and nighttime precipitation along major river basins (Ueno 1998). Effects of surface heating or local topographical circulation have been emphasized as direct factors initiating the development of disturbances causing precipitation on the plateau (Ueno et al. 2001). Much rainfall is brought both by convection during the daytime and by stratiform precipitation during the evening and night (Shimizu 2001). Ueno et al. (2001) characterize the TP as a weak and frequent precipitation area. Quantitative estimation of spatial distribution of precipitation is one of the important aspects for estimating latent

heating (Xu and Haginoya 2001), understanding the water cycle processes over this unique highland, and evaluating water resources for major rivers that originate from the plateau, including the Huang He River, the Changjiang River and the Mekong River.

However, one of the main problems in understanding consistent plateau-wide precipitation analyses is the inadequate number of surface observation points in such remote areas, especially those in the western plateau and mountainous regions (Ueno 1998; Zhou et al. 2000). In addition, there are high uncertainties within the current observational data (Ueno and Ohata 1996). The difficulties are also due to the considerable problems in representing complex terrain in current general circulation climate models (GCMs). As is stated in Houghton et al. (2001), the reliability of GCM prediction is still low on a regional scale owing partly to simplified land surface processes in complex topographic areas, especially over the TP. The topographic and altitudinal effects on climate over mountainous regions are lost due to the smoothing effect. Therefore, regional climate models (RCM) have become a powerful tool for downscaling the climate information originating from GCMs to the regional scale.

One of the significant advancements in the last decade has been the application of RCMs to study the East Asian monsoon system (Leung et al. 2003). It is clearly shown that the spatial patterns produced by the RCMs are in better agreement with observations because of the better representation of high-resolution topographical forcings and improved land/sea contrasts (Houghton et al. 2001). It is difficult to apply RCMs on the TP due to its variable topography terrain and huge size. To the author's knowledge, there are no RCMs applied to study the climate over the whole Tibetan Plateau with high resolution so far. The TP is always tried to be excluded in the Asian monsoon model simulations at the western lateral boundary (e.g. Fu et al. 2005) or is exclusively analyzed (e.g. Cui 2005; Kang et al. 2005). In this paper, the regional climate model REMO is applied and evaluated over the Tibetan Plateau. A double-nesting technique is implemented.

A model application in a new target region should be accompanied by evaluation with observational data as well as sensitivity experiments (e.g. Giorgi and Mearns 1999; Leung et al. 1999). Therefore, simulation of summer 1998 driven by "perfect boundaries" is chosen as a case study here. This is characterized as a period when the strong 1997/8 El Nino was decaying and La Nina was developing (e.g., Anyamba et al. 2002). In the summer 1998, cloudy and rainy weather was dominant over most of eastern Asia. The amount of precipitation along the Yangtze River valley, which runs along 30°N was about 2 times the normal summer monsoon precipitation. A record-breaking flood occurred over the Yangtze River and adjacent river valleys in China, and lasted for three months (June, July and August; JJA). This basin-wide flood was the

second largest on record, comparable to that occurred in 1954 (Chinese National Climate Center 1998). During May to September 1998, GAME/Tibet performed intensive field observations on the TP under the framework of the World Climate Research Programme (WCRP)/Global Energy and Water Cycle Experiment (GEWEX) Asian Monsoon Experiment (GAME; more information available at <http://monsoon.t.u-tokyo.ac.jp/tibet.html>). The measurements offer the possibility to evaluate the performance of climate or land surface models over the TP. Therefore, REMO is configured over the Tibetan Plateau for summer 1998 and we aim to answer: 1) How realistic can the model represent the large-scale characteristics and seasonal mean climate? 2) Can the model reproduce the monsoon temporal evolution on the Tibetan Plateau? To achieve these goals, section 5.2 will briefly introduce the regional climate model REMO and the experiments carried out. Validation datasets will be listed in section 5.3. In section 5.4, model simulation results are analyzed and compared with observation data. A summary is given in section 5.5.

## **5.2. Model and Experimental Setup**

### **5.2.1 Model**

The regional climate model REMO developed at the Max Planck Institute for Meteorology in Hamburg (Jacob and Podzun 1997) originates from the former operational numerical weather prediction model Europa Modell (EM) of the German Weather Service (DWD). It has been applied in several regions of the Earth: Europe, Arctic, Antarctic, Siberia, Indonesia, India, Brazil, Peru, Africa, North America, Baltic Sea, North Sea, North Atlantic, Pacific, and East Asia (e.g. Jacob 2001; Cui 2005). Horizontal resolutions between  $1/10^\circ$  and  $1^\circ$  are currently used for simulations covering time scales from days to decades. Besides the physics parameterizations of DWD (Majewski 1991), new physical parameterizations were implemented based on parameterizations of the ECHAM-4 general circulation model (Roeckner et al. 1996). The approach with the same physical parameterizations of RCM and GCM may be preferable to maximize consistency between RCM and GCM results. To prepare for the future ECHAM/REMO application in the Asian region, REMO version 5.0 with the ECHAM-4 physics parameterizations are applied and evaluated in this study.

The prognostic variables of the model are surface pressure, horizontal wind components, temperature, water vapor and cloud water. The finite difference equations are solved on an Arakawa-C grid with 20 vertical levels within a terrain-following hybrid coordinate system ( $\sigma$ -coordinates near the surface transforming gradually into pressure coordinates). In REMO, a rotated spherical coordinate system is employed. Leap-frog time stepping with semi-implicit

correction and Asselin-filter is used. The turbulent fluxes in the surface layer are calculated from Monin-Obukhov similarity theory. A 1.5-order closure scheme is applied to compute the turbulent transfer within and above the atmospheric boundary layer. It is based on a formulation by Brinkop and Roeckner (1996), in which the eddy diffusivity is expressed in terms of the turbulent kinetic energy. Radiation is calculated with a two-stream approximation which divides the spectrum into two short-wave and six long-wave bands. In the parameterization of clouds and precipitation it is distinguished between grid scale (Roeckner et al. 1996) and convective (Tiedtke 1989) clouds and precipitation. For more details, please refer to: <http://ww.mpimet.mpg.de/en/depts/dep1/reg/index.php>.

### 5.2.2 Experiments

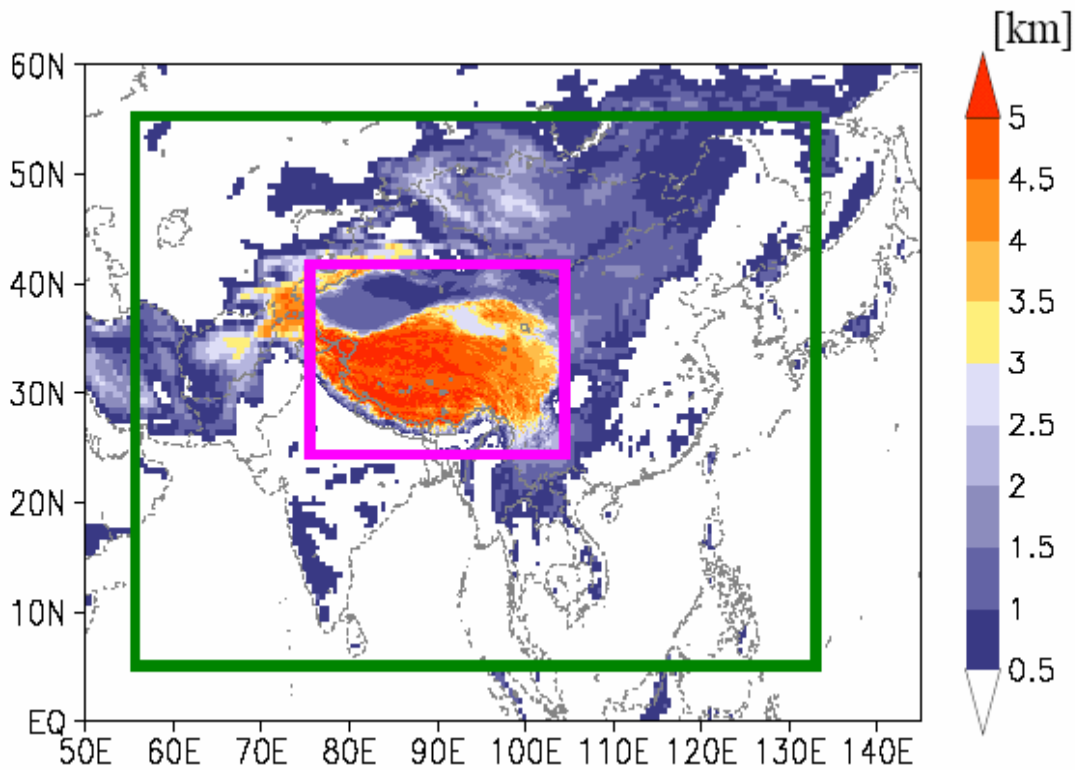


Figure 5.1. Geographical map of the Tibetan Plateau. Topography higher than 500m is shaded. The green rectangle represents the domain of REMO1/2, the purple one for that of REMO1/6.

The integration of REMO is conducted from April 01 to October 31 in 1998. Such short simulations can also identify major systematic RCM biases if the simulation results show derivations from observations significantly greater than the observed natural variability (Christensen et al. 1997). The simulation strategy is divided into two steps, the so-called double-nesting procedure. First, REMO is applied in the ‘forecast mode’ with 0.5° horizontal resolution (about 55km) over a large domain (5.5°N-55.5°N, 60.5°E-132.5°E; shown in Figure 5.1;

referred to as REMO1/2 hereafter). ‘Forecast mode’ means that results of consecutive short-range forecasts are used to cover a certain period of time (30 hours used here). REMO is initialized and linearly interpolated at the lateral boundary 6-hourly with data from the European Centre for Medium-Range Weather Forecasts (ECMWF) reanalysis (ERA-40; Simmons and Gibson 2000), which are regarded as “perfect” boundaries. Secondly, REMO is applied in the ‘climate mode’ with 1/6° horizontal resolution (about 18km) over a smaller domain (25°N-43°N, 75°E-107°E; referred to as REMO1/6 hereafter; see also Figure 5.1) driven by the output from REMO1/2. Contrary to the forecast mode, climate mode’ simulation is only nudged by large-scale data at the lateral boundary during the whole integration (Jacob and Podzun 1997). The first month is eliminated from the analysis to account for a ‘spin-up’ period of the simulation. Using this double-nesting procedure, we expect to downscale the large-scale driving signals from ERA40 to the Asian region in the first step and then develop the mesoscale phenomena through a more detailed land surface representation by the model dynamical processes in the second step. By doing so, we aim to bridge the resolution gap between reanalysis data and the high resolution model REMO1/6 and decrease the influence of the biases from reanalysis data to the interest area, the TP.

The choice of an appropriate domain is not trivial since the size of the domain and the location of the lateral boundaries obviously affect how uncertainties in the large-scale analysis propagate within the model domain. The domain of the regional model should be large enough to allow full development of meso-scale systems and include relevant regional forcing. Additionally, the resolution of regional model has to be high enough to adequately capture the scale and effects of such local forcing as topography and land-surface processes (Giorgi and Mearns 1999). Cui (2005) concluded that REMO1/2 can reasonably downscale the large-scale atmospheric circulation and provide realistic surface climate by comparison with observation data. He also found that the 50-km resolution is insufficient to fully capture the orographical precipitation on the TP. By comparison of the results from REMO1/2 and REMO1/6 and observational data, it is aimed to illuminate some aspects of the domain and resolution choices over the TP.

### **5.3. Validation datasets**

A serious problem in GCM and RCM evaluation is the lack of good quality high-resolution observation data. Over the TP, observations are extremely sparse and biased as aforementioned. In addition, only little work has been carried out on how to use point measurements to evaluate the grid-box mean values from a climate model, especially when using sparse station networks or stations in complex topography terrain (e.g., Osborn and Humle 1997). Traditionally, temperature and precipitation - the most important parameters of the climate

system - are used as basic quantities to classify climate. Therefore, surface temperature and precipitation data from observations, and atmospheric circulation from reanalysis datasets are used to evaluate the model performance and are listed below:

### **5.3.1 ERA 40 reanalysis data**

The ERA model is based on a spectral formulation of the grid. Due to the truncation at wavenumber 106 its resolution (1.125°) is much coarser than the resolution of REMO. This leads to considerable differences in the representation of orography, which is important for the TP region. Due to the relatively large elevation discrepancy between the REMO and ERA orography, a comparison of surface variables like 2-m temperature or precipitation, or a comparison at the lower model vertical level might reveal large biases. However it is still meaningful. The comparison with the driving data indicates the differences of the model derived from the driving large-scale signals. By comparison with other reliable observation datasets, the biases transported from the lateral boundaries and the mesoscale phenomena within the model interior produced by the model's physical and dynamical parameterizations and processes can be addressed.

### **5.3.2 GAME reanalysis and observation station data**

The GAME project was the first simultaneous intensive observation effort to understand the water and energy cycles of the Asian monsoon system over the Asian continent. One of its important fundamental purposes was to obtain a high quality four-dimensional data assimilation analysis for energy and water cycle processes of the Asian summer monsoon. The reanalysis product from this project is called the GAME reanalysis dataset (hereafter referred to as GAME), which covers April to October 1998 with horizontal resolution of 0.5 degree for the Asian and Pacific region (30° E-180°, 80° N-30° S). This dataset has the advantage of including the GAME special observation off-line radio-sonde dataset. GAME is used in its current newest version 1.5 and is available at: [http://gain-hub.mri-jma.go.jp/GAME\\_reanal.html](http://gain-hub.mri-jma.go.jp/GAME_reanal.html). Two stations with observed daily precipitation obtained by GAME-Tibet are also used and the details of data from the GAME-Tibet project can be found at: <http://monsoon.t.u-tokyo.ac.jp/iop/index.html>

### **5.3.3 CRU data**

Climatic Research Unit data (known as CRU; New et al. 2002) includes monthly mean surface temperature and precipitation with 0.5 degree resolution from 1900 to 2000, which is constructed based on global stations over land areas. The data information is available at <http://www.cru.uea.ac.uk/>.

### **5.3.4 New Gauge-based Precipitation**

A special gauge-based daily precipitation dataset over East Asia developed by Xie et al. (2004) is employed in this study (hereafter, named as XIE) as well. The dataset covers a 26-year period from 1978 to 2003 with a 0.5° degree resolution. The dataset combines observations of daily precipitation from over 3000 stations over the target domain of this dataset (5°N-60°N, 65°E-145°E) (Xie et al. 2004). In addition to the evaluation of the model performances, the difference between CRU and XIE may indicate the biases of observations over TP due to different numbers of stations used in the two datasets.

## **5.4. Results**

The comparison of numerical model results and observation data is the most important part of model validation (e.g. Christensen et al. 1996). The model behavior, with realistic forcing, should be as close as possible to the real atmosphere and experiments driven by analyses of observations can reveal systematic model biases primarily due to the internal model dynamics and physics. Analysis and comparison of the simulated surface parameters and associated circulation are presented in this section. Precipitation and temperature were chosen as the major parameters to reveal the performance of the REMO model in East Asia, since they are highly affected by regional features of the lower boundary conditions and are sensitive to the physics parameterizations. Cui (2005) concluded that REMO1/2 shows reasonable agreement with ERA40, GAME, and XIE for the whole REMO1/2 domain. Therefore, in the present study, we focus on the REMO1/6 domain with all datasets for comparison.

Extreme events like floods or droughts are always produced by anomalous intensity and/or anomalous length of the monsoonal rainfall, which, in turn, is produced by abnormalities in the planetary circulation systems (Liu et al. 1996). For example, during the summer of 1998, the low-pressure center over the Bay of Bengal was stronger and located more eastward than normal. It is quite unlikely that a model could reproduce the regional features of floods or droughts and, at the same time would not be able to reproduce a reasonable simulation of the anomalous patterns of the associated circulations. Therefore, we will first evaluate the circulation, expressed by atmospheric geopotential height together with wind vectors.

Figure 5.2 shows the summer (JJA) mean atmospheric circulations at 200 and 500 hPa from ERA40, REMO1/2, REMO1/6, and GAME, respectively. The atmospheric circulations represented by REMO1/2 and REMO1/6 are very similar in the geopotential heights and wind distributions from the upper to the lower troposphere and agree well with the patterns in ERA40 with a little higher

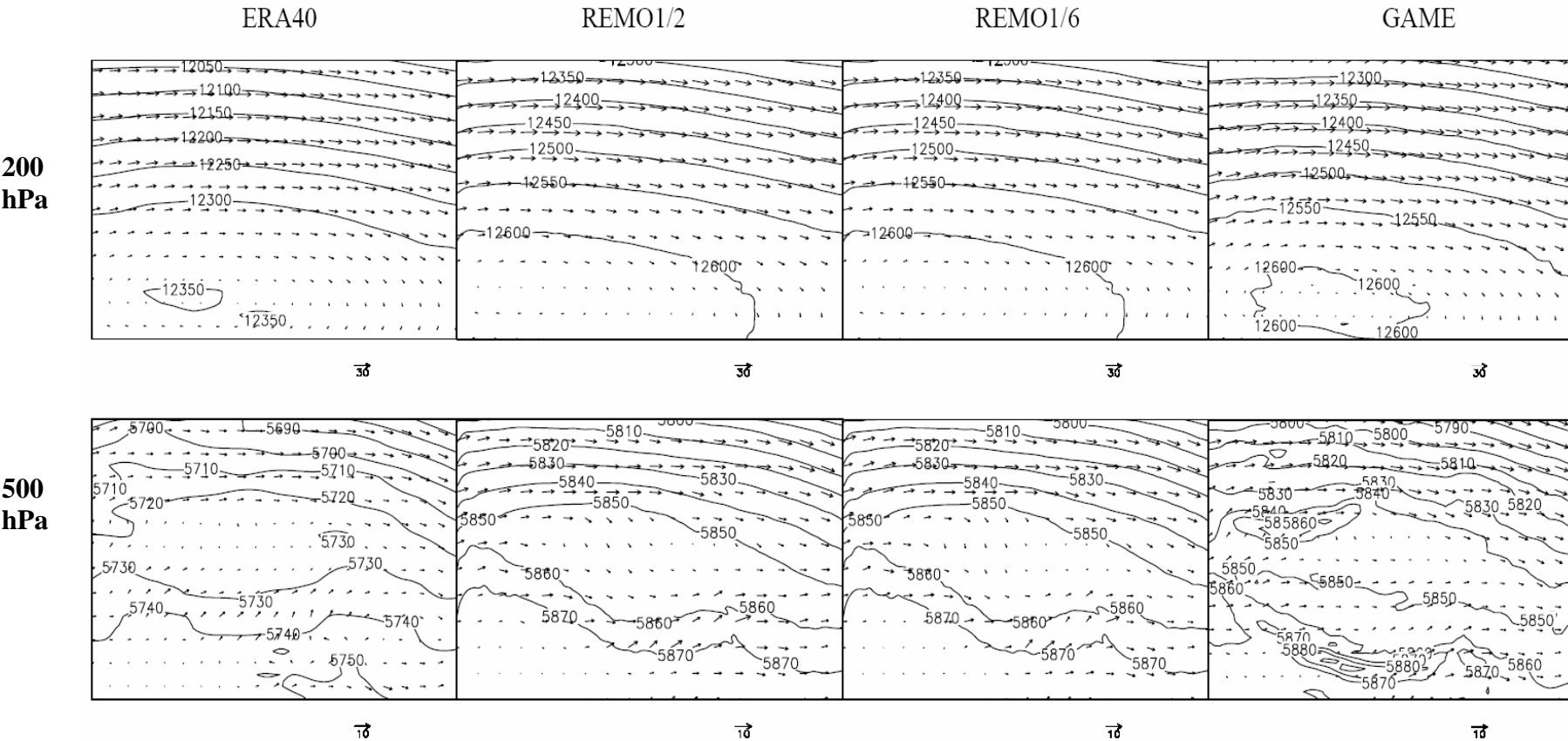


Figure 5.2. Comparison of summer (JJA) atmospheric circulation at a) 200hPa and b) 500hPa from ERA40, REMO1/2 and REMO1/6 simulations, and GAME reanalysis data (from left to right) in 1998, respectively. The area covers REMO1/6 domain (25°N-43°N, 75°E-107°E).

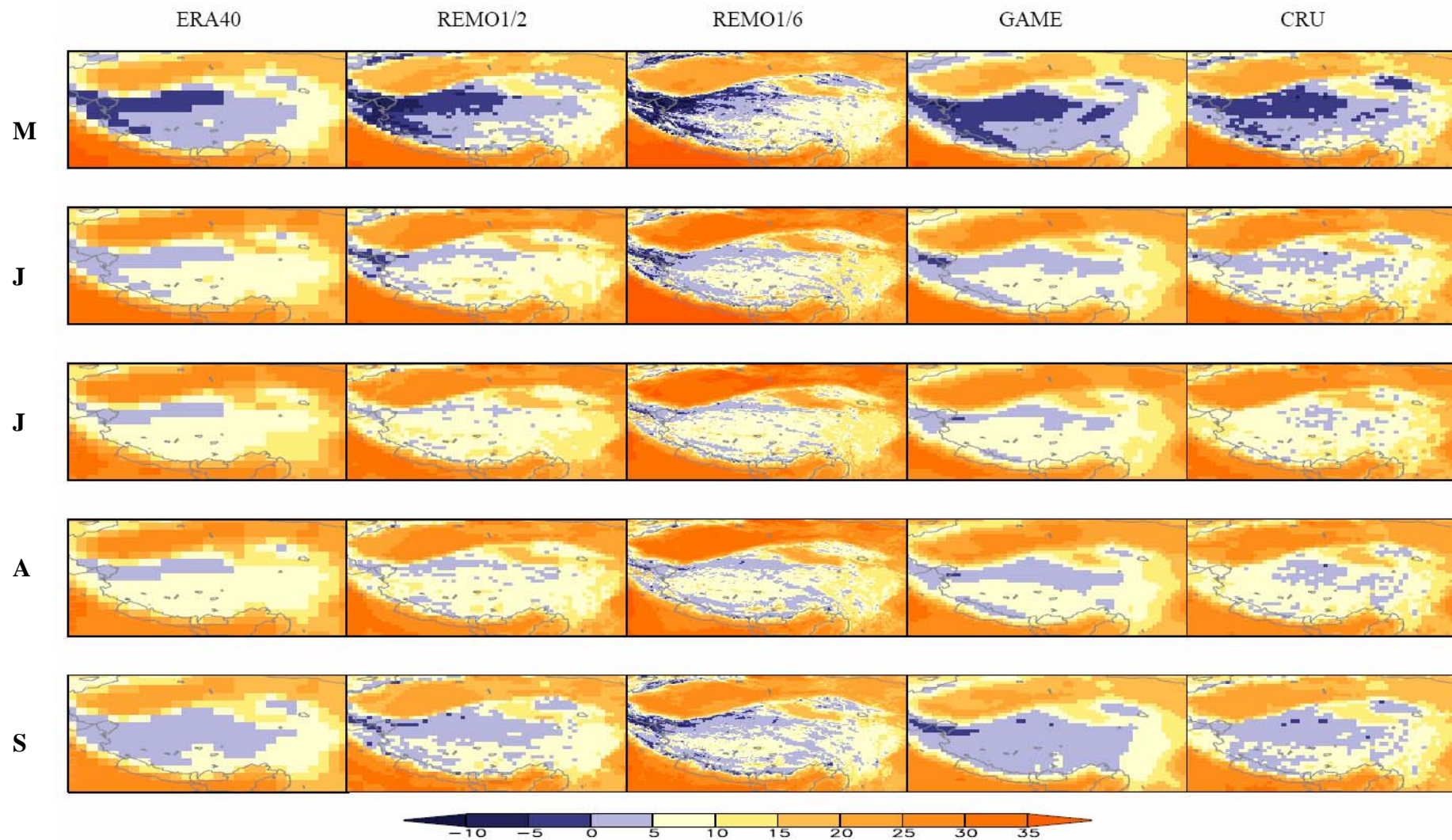


Figure 5.3. Comparison of monthly mean near surface atmospheric temperature [unit: K] during May to September in 1998 (top to bottom) from ERA40, REMO1/2 and REMO1/6 simulations, GAME, and CRU observations. The area covers REMO1/6 domain (25°N-43°N, 75°E-107°E)

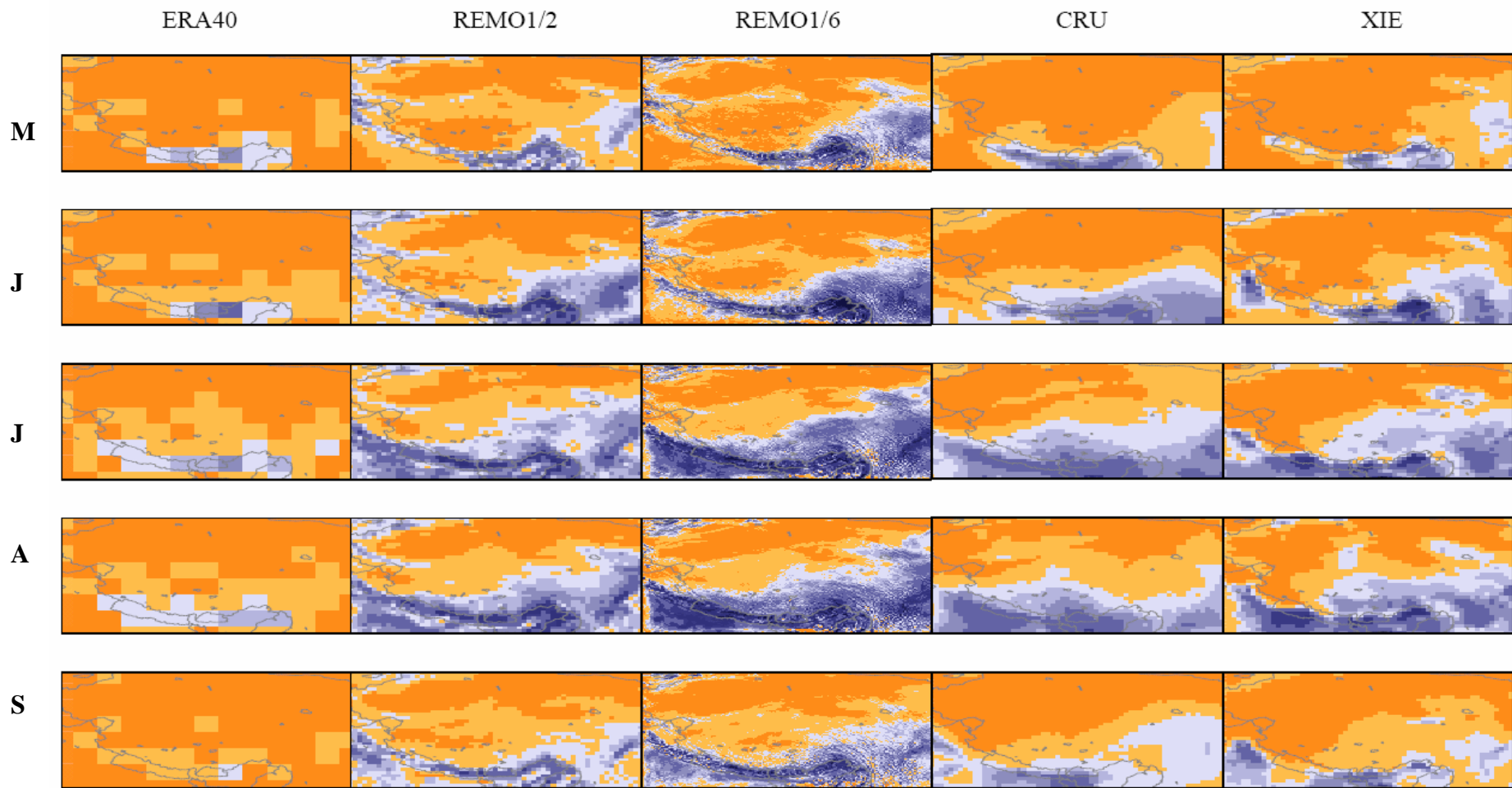


Fig  
REMO1/2 and REMO1/6 simulations, CRU and XIE observations.

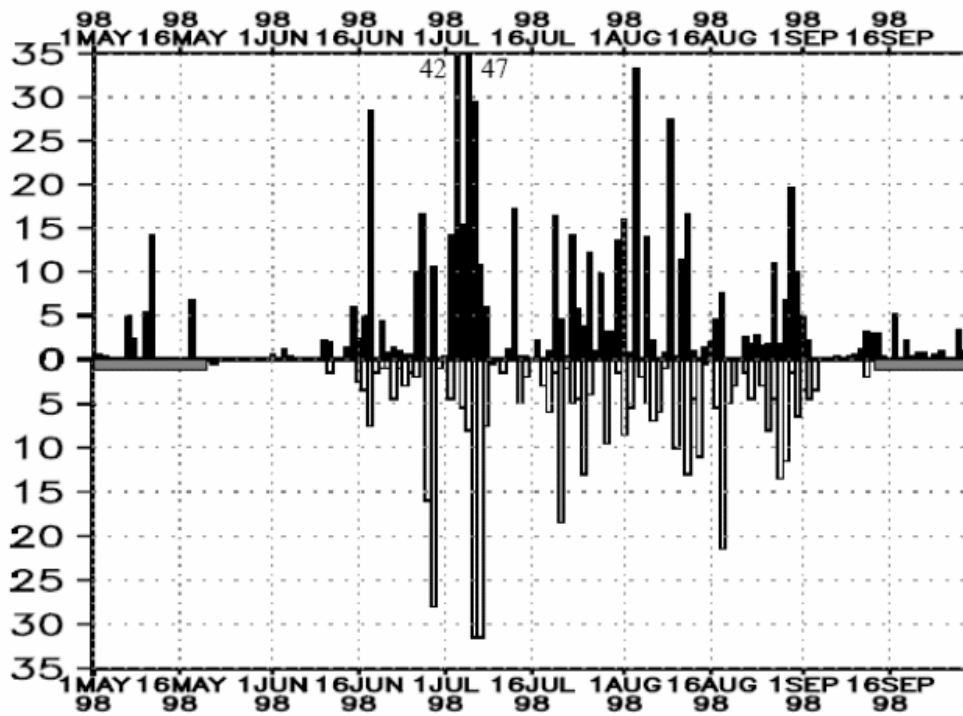
magnitude of geopotential heights in the middle and upper troposphere. The magnitude of geopotential heights are similar between model simulations and GAME data. This might imply the mismatch of magnitudes between ERA40 driving data and model simulations resulting from different topography due to different horizontal resolutions. In summary, REMO simulates reasonably the atmospheric circulations over the TP at seasonal scale. This provides a dynamical basis for representing the weather and climate systems induced by the circulations.

Figure 5.3 presents the temporal evolutions (May to September) of near surface atmospheric temperature at 2m height. As expected, this near surface temperature is significantly affected by the terrain structure. All the observations and model simulations demonstrate that the Tibetan Plateau is a relatively cold center with around 0°C in summer. REMO1/6 and REMO1/6 represent reasonably the patterns and spatial distributions of near surface temperature compared to the observations and REMO1/6 shows more details of temperature gradients over the mountainous areas in the western TP due to its higher resolution. However, here we only show the monthly mean values, the diurnal cycle of temperature simulated by REMO1/6 is too strong and this needs to be addressed in future studies.

Figure 5.4 presents the spatial distribution of accumulated monthly precipitation from May to September in 1998 from REMO simulations and observations. As discussed in section 5.3, the XIE dataset is most reliable due to the large number of stations included, whereas ERA40 due to coarse resolution has less reliability. Monthly precipitation simulated by REMO departs from the driving data ERA40 and agrees more with the observations. Better representation of topography might contribute to this performance. REMO represents well the summer monsoonal rainfall over the Tibetan Plateau, especially at the southeast and west margin of the TP. REMO1/6 shows more detailed local information with larger amplitudes than REMO1/2 and station observations. Precipitation varies highly at temporally and spatially and extrapolation from station observations to a spatial distribution remains high uncertain. It is necessary to evaluate the model performance with station observations and at higher temporal scale.

Daily precipitation comparisons at station MS3543 (31.58°, 91.9°) and D66 (35.52°, 93.78°) between REMO1/6 at one matching grid point are shown in Figure 5. Station MS3543 is located at a flat grassland area near Naqu in the south of TP. Station D66 is located in a flat grassland along the Tuotuohe river valley in the north of the TP. REMO reproduces the main precipitation cases at the two stations with somewhat larger amplitude. However, it should be kept in mind that the comparisons are made between an area average and a point observation and the observations might be biased on the TP (Ueno and Ohata 1996). REMO1/6 simulates the different precipitation characteristics at the two stations. The total amount of observed rainfall during June to August at D66 is 101 mm (143mm, simulated by REMO1/6), at MS3543 is 366mm (574mm, simulated by REMO1/6). Only two stations are shown in this thesis and more cases should be used in the future to capture regional characteristics.

a) MS3543



b) D66

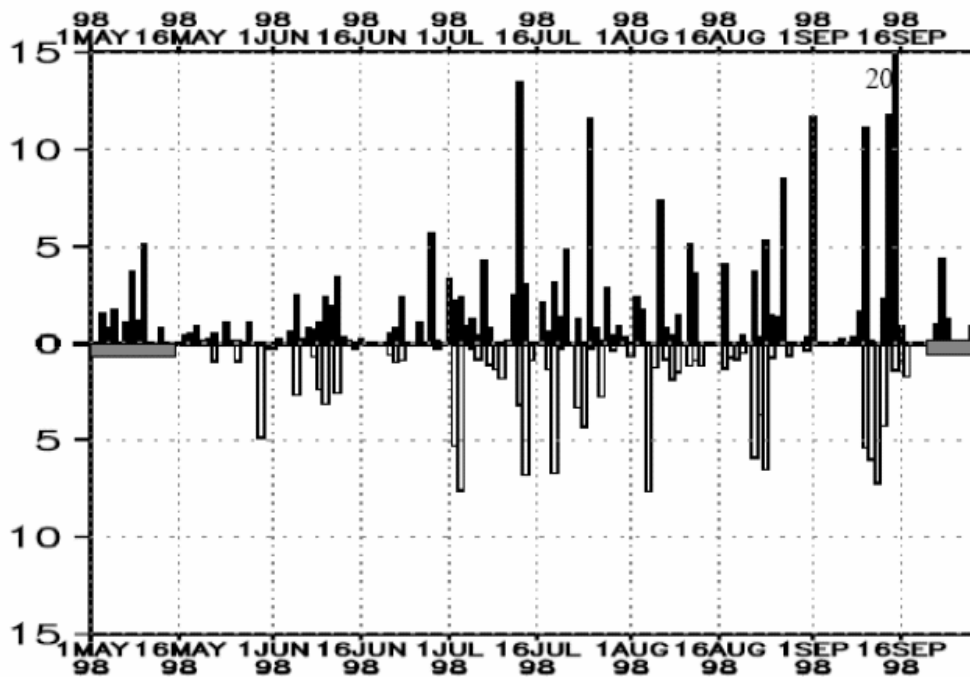


Figure 5.5. Comparison of daily mean precipitation [unit: mm/day] between REMO1/6 simulation results at one grid point (upward bold bar) and station observation (downward bar) at station a) MS3543 and b) D66, respectively. Grey shaded horizontal bars represent period without available observations.

The precipitation over Tibet shows the characteristics of a rainy monsoon season and a dry season (c.f. Ye and Gao 1979; Ueno et al. 2001). Figure 6 illustrates the longitude-time section of daily precipitation averaged at 30°N-32°N and latitude-time section averaged at 90°E-92°E from REMO1/6 and XIE. It shows that REMO1/6 reasonably represents the monsoonal period by continuous and heavy precipitation starting from late June to early September in 1998. The monsoon onset date is important to explore the precipitation processes over the monsoonal region and is also a key measure for model performance. By examining daily radar reflectivity, Yamada et al. (1999) conclude the monsoonal onset date over the TP in 1998 is about 13 June. REMO1/6 reveals that there is rainfall in the central TP since middle of June. However, monsoon onset is a complicated process and should be addressed extensively in future.

## **5.5 Conclusions and Discussions**

A regional climate model REMO is applied over the Tibetan Plateau with a “double-nesting” technique. By simulating the period of summer 1998 and evaluating with reanalysis and observation data, our model results demonstrate that REMO reasonably represents the large-scale circulation and, due to better orography representation, provide more realistic geopotential values than the driving data ERA40. REMO also simulates well the surface climate at a monthly time scale and provides more local scale variability at the higher horizontal resolution of 18km. By comparison with two station observations, REMO produces major precipitation events at daily scale and simulates the spatial differences. It also found that REMO can reproduce well the monsoonal rainfall period. However, it seems to overestimate precipitation by 20-40% than station observations, which might be the biases in observations, e.g., wind effects.

Several guidelines can be implied from this study for future application of regional climate models over the Tibetan Plateau or other mountainous areas. Firstly, the experiment points to an important forcing of topography. In higher resolution the model performs better, especially concerning the precipitation, due to more realistic terrain representation. The description of the hydrologic cycle generally improves with increasing resolution due to the better topographical representation (Christensen et al. 1996). For example, only at a very high resolution the mountain chains in Norway and Sweden become sufficiently well resolved to yield a realistic simulation of the surface hydrology (Christensen et al. 1996). High resolution topographical modification of the regional precipitation change signal in nested RCM simulations has also been documented in other studies (e.g., Kato et al. 1999). However, process parameterizations at higher resolution suitable for the TP need to be developed and validated for improved model simulation results. Furthermore, more reliable observations are urgently needed to evaluate such processes accurately.

Secondly, given observed large-scale forcing fields such as ERA40, REMO shows similar circulation and a more reasonable representation of surface climate, especially of precipitation. Thus, a prerequisite for RCM nested in GCM simulations is that the large-scale climatology of the driving GCM must be realistic over the region of interest. However, current GCMs are biased over the Asian monsoon region (Cui 2005). Therefore, as Seth and Giorgi (1998) suggested, in this case, larger domains, in which the model solution is more free responding to variations of internal parameters, is likely to be preferable. Considering the limitation of computational resources and request for higher resolution and larger domain, the “double-nesting” technique implemented in this study provides a good solution. However, more studies are needed in the future to find the optimal nesting solution, such as buffer size, domain size, and nudging time interval of the second inner model. It should be noted that our simulation integration time covers only one summer, which cannot fully reveal the model performance. For example, the soil temperature values derived from ERA40 can lead to an unrealistically cold initialization of the model’s deep soil, which needs about 5 years to come to equilibrium (Jacob 2001). Hence, longer integration samples may be required to confidently assess the mesoscale response of REMO over the TP before nesting it into GCMs.

Thirdly, many studies suggested that regional climate simulations could be very sensitive to the physical parameterizations used. RCM physics configurations are either derived from a pre-existing (and well tested) limited area model system with modification suitable for climate application (e.g., Giorgi and Mearns 1999) or are implemented directly from a GCM (Jacob and Podzun 1997). In the first approach, each set of parameterizations is developed and optimized for a respective model resolution. However, differences between nested regional model and driving GCM model results are difficult to interpret, as these will result not only from changes in resolution. The different model physical schemes may result in inconsistencies near the boundaries. The second approach maximizes compatibility between the regional and global models. However, physical schemes developed for coarse resolution GCMs may not be adequate for the high resolutions used in nested regional models and at least, may require recalibration. Overall, both strategies have shown performance of similar quality and neither one may be preferable (Giorgi and Mearns 1999). Overall, REMO is shown to be an appropriate tool for further climate nesting studies over the Tibetan Plateau. However, the work shown here is just a starting point for such studies.

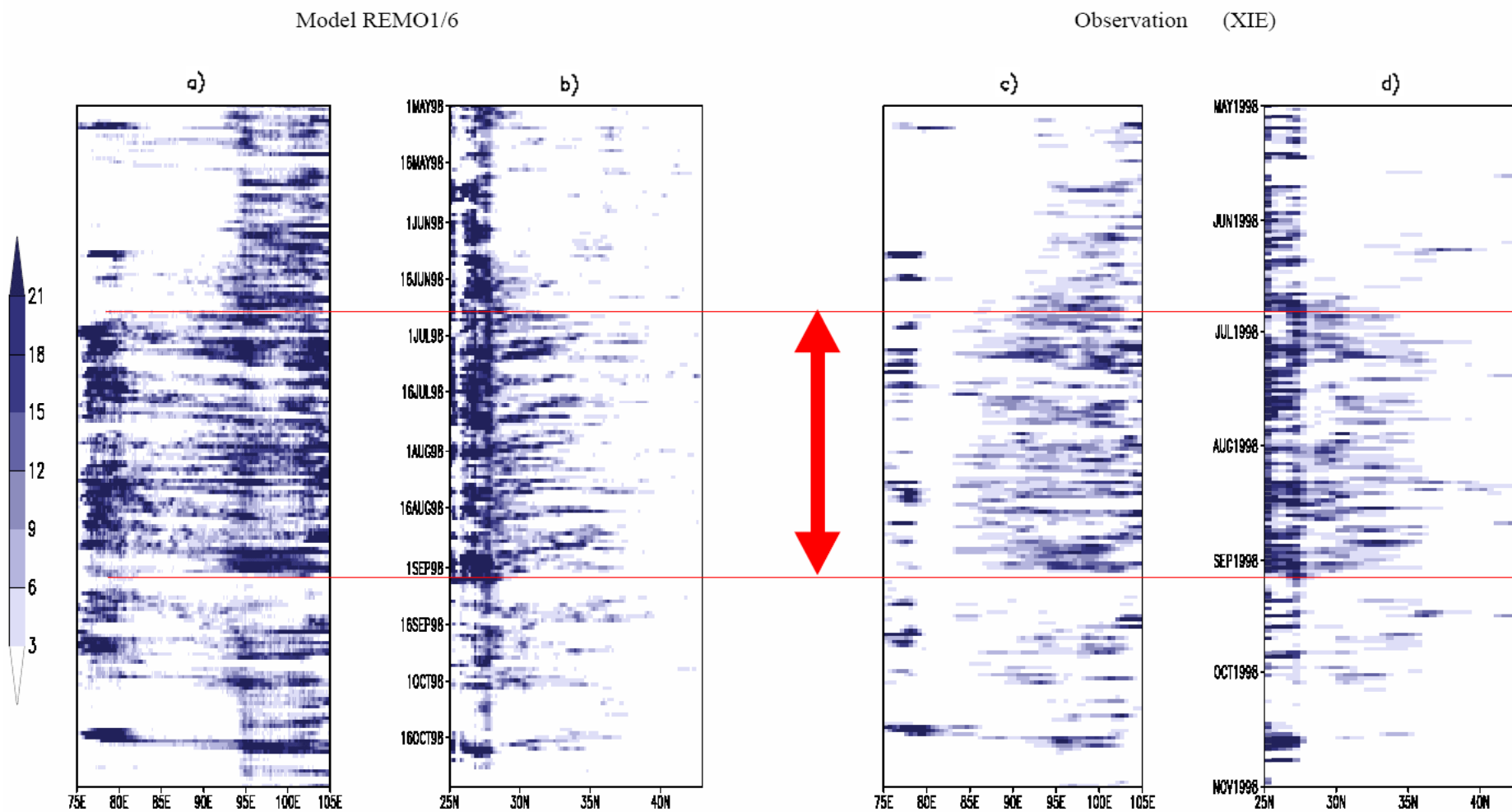


Figure 5.6. Longitude-time section along 30-32N (a, c) and Latitude-time section along 90-92E (b, d) of daily precipitation variation [unit: mm/day] from REMO1/6 simulation and XIE observation, respectively. The period is from 01 June to 31 October in 1998 shown in the y-axis. The red arrow covers the period between the two red horizontal lines representing the monsoonal period.

## 6. References

- Anyamba, A., C. J. Tucker, and R. Mahoney, 2002: From El Niño to La Niña: Vegetation response patterns over East and Southern Africa during the 1997-2000 period. *J. Climate*, 15, 3096-3103.
- Brinkop, S., E. Roeckner, 1996: Sensitivity of a general circulation model to parameterizations of cloud-turbulence interactions in the atmospheric boundary layer. *Tellus* 47A, 197-220.
- Christensen, J.H., O.B. Christensen, P. Lopez, E. van Meijgaard, and M. Botzet, 1996: The HIRHAM4 regional atmospheric climate model. Danish Meteorol. Institute, Copenhagen, Scientific Report 96-4, pp51.
- Cui, X., 2005: Evaluation of regional climate model REMO over East Asia monsoon. Diploma Thesis equivalent, University Hamburg.
- Fu, C., S. Y. Wang, Z. Xiong, W. J. Gutowski, D.-K. Lee, J. L. McGregor, Y. Sato, H. Kato, J.-W. Kim, and M.-S. Suh, 2005: Regional climate model intercomparison for Asia (RMIP), *Bull. Am. Meteorol. Soc.*, 86, 257-266.
- Giorgi, F. and L. O. Mearns, 1999: Introduction to special section: Regional climate modeling revisited. *J. G. R.*, 104 (D6): 6335-6352.
- Houghton, J. T., L. G. Meria Filho, B. A. Callender, H. Harris, A. Kattenberg, and K. Maskell (eds.), 1996: *The Science of Climate Change: Contribution of Working Group I to the Second Assessment of the Intergovernmental Panel on Climate Change*, Cambridge University Press, Cambridge, U. K., p. 572.
- Houghton, J. T., Y. Ding, D. J. Griggs, M. Noguer, P. J. van der Linden, X. Dai, K. Maskell, and C. A. Johnson (Eds.), 2001: *Climate Change 2001: The Scientific Basis*. Cambridge University Press, 881 pp.
- Jacob D and R. Podzun, 1997: Sensitivity studies with the regional climate model REMO. *Atmos. Phys.*, 63, 119-129.
- Jacob, D., 2001: A note to the simulation of the annual and inter-annual variability of the water budget over the Baltic Sea drainage basin. *Meteorology and Atmospheric Physics*, Vol.77, Issue 1-4, 61-73.
- Kang, H. S., D. H. Cha, and D. K. Lee, 2005: Evaluation of the mesoscale model/land surface model (MM5/LSM) coupled model for East Asian summer monsoon circulations, *J. Geophys. Res.*, 110, D10105, doi:10.1029/2004JD005266.
- Kato, H., H. Hirakuchi, K., Nishizawa, and F. Giorgi, 1999: Performance of the NCAR RegCM in the simulations of June and January climates over eastern Asia and the high-resolution effect of the model, *J. Geophys. Res.*, 104, 6455-6476.
- Leung, L.R., S. J. Ghan, Z.C. Zhao, Y. Luo, W.C. Wang and H. L. Wei, 1999 : Intercomparison of regional climate simulations of the 1991 summer monsoon in eastern Asia, *J. G. R.*, 104(D6): 6425-6454.
- Leung, L. R., L.O. Mearns, F. Giorgi, and R.L Wilby, 2003: meeting summaries on workshop of Regional climate research: Needs and opportunities. Available at <http://www.esig.ucar.edu/rcw/>.
- Liu, Y.Q., and R. Avissar, 1996: A simulation with the regional climate model RegCM2 of extremely anomalous precipitation during the 1991 East Asian flood: An evaluation study, *J. Geophys. Res.*, 101, 26,199-26,216.
- Majewski, D., 1991: The Europa Modell of the Deutscher Wetterdienst. ECMWF Seminar Proceedings, ECMWF Reading, UK, 147-191.
- New, M., D. Lister, M. Hulme, and I. Markin, 2002: A high resolution data set of surface climate over global land areas. *Clim. Res.*, 21, 1-25.

- Osborn, T.J., and M. Hulme, 1997: Development of a relationship between station and grid-box rain-day frequencies for climate model evaluation. *J. Climate*, 10, 1885-1908.
- Roeckner, E., K. Arpe, L. Bentsson, and et al., 1996: The atmospheric general circulation model ECHAM-4: Model description and simulation of present day climate. Max-Planck Institute for Meteorology report, No. 218: pp. 90. available at <http://www.mpimet.mpg.de>
- Seth, A., and F. Giorgi, 1998: The effects of Domain choice on summer precipitation simulation and sensitivity in a regional climate model. *J. Climate* 11, 2698-2712.
- Shimizu S., K. Ueno, H. Fujii, R. Shirooka, and L. Liu, 2001: Mesoscale characteristics and structures of stratiform precipitation on the Tibetan Plateau, *J. Meteor. Soc. Japan*, Vol. 79(1B), 435-461.
- Simmons, A.J., Gibson, J.K., 2000. The ERA40 Project Plan. ERA40 Project Report Series No.1, ECMWF, Reading, UK, pp. 63.
- Tang, M.-C., G. D. Cheng, and Z.-Y. Lin (Eds), 1998: Contemporary climatic variations over the Qinghai-Xizang (Tibet) Plateau and their influences on Environments (in Chinese). Guangdong Science and Technology Press, Guangzhou, 229pp.
- Tiedtke, M., 1989: A comprehensive mass flux scheme for cumulus parameterization in large-scale models. *Mon. Wea. Rev.* 117, 1779-1800.
- Ueno K., 1998: Characteristics of plateau-scale precipitation in Tibet estimated by satellite data during 1993 monsoon season, *J. Meteor. Soc. Japan*, 76, 533-548.
- Ueno K., H. Fujii, H. Yamada, and L. Liu, 2001: Weak and frequent monsoon precipitation over the Tibetan Plateau, *J. Meteor. Soc. Japan*, 79(1B), 419-434.
- Ueno K., and T. Ohata, 1996: The importance of the correction of precipitation measurements on the Tibetan Plateau, *J. Meteor. Soc. Japan*, 74, 211-220.
- Xie, P., A. Yatagai, and M. Chen, 2004: An analysis of daily precipitation over East Asia : Current status and future improvements. Proceedings of the 6th International Study Conference on GEWEX in Asia and GAME, December 3-5 2004, Kyoto, Japan.
- Xu, J., and S. Haginoya, 2001: An estimation of heat and water balances in the Tibetan Plateau. *J. Meteor. Soc. Japan*, 79(1B), 485-504.
- Yamada H. and precipitation-radar science group of GAME-Tibet, 1999: Features of radar echo over the Tibetan Plateau during the GAME-Tibet IOP, Proceedings of the first international workshop on GAME-Tibet, Xi'an, China, 133-136.
- Ye, D. Z., and Y. X. Gao, 1979: The meteorology of the Qinghai-Xiang (Tibetan) Plateau. Science Press, Beijing (in Chinese).
- Zhou, M. And Staff Members of Chinese Academy of Meteorological Science, 2000: Observational Analysis and Dynamic study of Atmospheric Boundary Layer on Tibet Plateau. Meteorology Press, Beijing, 125 pp (in Chinese).



## **Chapter VI:**

# **Conclusions and Outlook**

### **6.1 Conclusions**

During the last half century, the land cover over the Tibetan Plateau has been changed strongly. Tundra was gradually replaced by shrubland in the central plateau. Broad-leaved and coniferous forest at the southeastern Tibetan Plateau almost disappeared and changed mainly into cropland. Bare land shows up at the western border of the plateau replacing the original grassland over there. Considering the size and high elevation of the plateau, land cover changes on the Tibetan Plateau could influence dramatically the climate locally and regionally and even at global scale.

Several series of “equilibrium” climate simulations were conducted in this study using the most recent version of the Max Planck Institute for Meteorology atmospheric general circulation model ECHAM5 to investigate the interactions between climate and land cover changes over the Tibetan Plateau. By evaluation with reanalysis data, the ECHAM5 control simulation represents reasonably the Asian climate in terms of atmospheric circulation and surface climate parameters. However, the simulation results should be treated with caution, because of remaining uncertainties of model performance on the Tibetan Plateau.

Land cover changes on the Tibetan Plateau were caused by both natural and human factors (Zou et al. 2002). Therefore, a sensitivity experiment with replacing non-anthropogenic land cover on the Tibetan Plateau was conducted in chapter 2. The differences in comparison to the control simulation reveal that anthropogenic land cover changes are making the plateau drier and warmer. It is also found that it intensifies the Indian monsoon and weakens the East Asia monsoon in China as well.

The forest on the southeastern Tibetan Plateau has a crucial hydrological function both in and beyond China and it largely disappeared during the last 50 years. Recently forest cover increased in China benefitting from the new forest policy launched in China in 1998 (Zhang et al. 2000). Climate impacts of deforestation on the southeastern Tibetan Plateau were studied in chapter 3 by an experiment replacing coniferous forests over this area by cropland.

Decreased evaporation and increased precipitation are found on the southeast Tibetan Plateau due to deforestation, which would lead to increased runoff and influence downstream. Model results also demonstrate that deforestation on the southeastern Tibetan Plateau leads to a warmer Indian continent throughout the year and a cooler and wetter climate in South China in spring.

Besides the biogeophysical effect, land use change has modified the greenhouse warming signal through biogeochemical feedbacks (Stich et al. 2005). Climate scenario analyses show that the current vegetation on the Tibetan Plateau would shift westwards and northwards from the present position in a warming climate (Zhang et al. 1996). Interactions of land cover changes and climate warming were investigated in chapter 4 by performing an experiment of deforestation under a warmer climate assuming doubled CO<sub>2</sub> concentration in the atmosphere. It is found that the impacts of deforestation on the southeast Tibetan Plateau are modulated nonlinearly by the warmer climate conditions.

In summary, land cover changes on the Tibetan Plateau have a large impact on local weather and climate by modification of the water cycle and energy budget. They also impact on other areas, especially the Asian climate, mainly through teleconnections in atmospheric circulation changes. Global implications are small. Our model results demonstrate that effects of land cover changes on the Tibetan Plateau are modulated non-linearly in a warmer climate.

In order to downscale global model results, the regional climate model REMO was applied over the Tibetan Plateau and a “double-nesting” technique was implemented to solve the downscaling problems at the lateral boundaries. The 1998 summer was simulated driven by “perfect boundaries”. REMO can represent reasonably well the large-scale circulation and surface climate over the Tibetan Plateau. Comparing with observations from two stations, REMO can reproduce major precipitation events on daily scale and simulate the spatial differences. It is also found that REMO can reproduce well the monsoonal rainfall period. In summary, REMO can be applied in future for downscaling and for providing more realistic local response.

## **6.2 Outlook:**

### **a) Better scenarios?**

In this thesis, two scenarios of land cover changes (anthropogenic LUC and deforestation) on the Tibetan Plateau were investigated with respect to their impacts on regional and global climate. However, the land cover changes on the Tibetan Plateau are still uncertain due to lack of observations. Experiments with more realistic scenarios of historic land cover changes would be really interesting in order to compare with the observed local climate changes that occurred during the last half century. More investigations with possible future scenarios of land cover on the TP should also be conducted in future. For example, desertification has been a very severe problem on the TP recently, and might get worse in future, as projected by biomass model simulations. We have performed an experiment replacing the whole TP by a semi-desert when writing the thesis, however, it has not been included in this thesis due to limited time.

### **b) Coupled model?**

In our experiments, climatological SST and sea ice are applied aiming at a simpler detection of the interactions of deforestation and hydroclimatic processes. However, such experiments eliminate the response of the ocean in the climate system. Coupled GCMs are recommended to be applied for similar experiments in the future to test the hypotheses drawn in this study. Moreover, ensemble simulations with different models or different model assumptions are also recommended to reduce the uncertainty.

### **c) Nesting with regional model?**

It is noted that GCM results contain relatively large biases over the Tibetan Plateau. Meanwhile, the regional climate model REMO represents pretty well the regional characteristics and relatively well captures realistic precipitation variations driven by 'perfect boundaries', i.e. reanalysis data. This suggests a RCM/GCM nesting system can be implemented for more realistic investigations of the scientific issues in this study, providing the performances of GCM simulations are improved. The capacity of regional climate modelling is also critical for such nesting systems. Longer high quality observations are urgently needed to understand the vegetation dynamics, water recycling, and energy budgets over the Tibetan Plateau.

## Reference

- Stich, S., V. Brovkin, W. von Bloh, D. Van Vuuren, B. Eickhout, and A. Ganopolski, 2005: Impacts of future land cover changes on atmospheric CO<sub>2</sub> and climate. *Global Biogeochemical Cycles*, 19, GB2013, doi:10.1029/2004GB002311.
- Zhang X. S., D. A. Yang, G. S. Zhou, C. Y. Liu, and J. Zhang, 1996: Model expectation of impacts of global climate change on biomes of the Tibetan Plateau. In Omasa K., K. Kai, H. Taoda, Z. Uchijima, and M. Yoshino, (Eds.) *Climate Change and Plants in East Asia*. Tokyo: Springer-Verlag, pp. 25-38.
- Zhang, P., Shao, G., Zhao, G., Master, D.C. Le, Parker, G.R., Dunning, J.B. Jr., Li, Q., 2000: China's forest policy for the 21st century. *Science*, **288**, 2135-2136 (in policy forum).
- Zou, X., S. Li, C. Zhang, G. Dong, Y. Dong, and P. Yan, 2002: Desertification and control plan in the Tibet Autonomous Region of China. *J. Arid Environments*, **51**, 183-198.

## **Acknowledgement**

I would like to express my gratitude to my supervisor, Prof. Hans-F. Graf, for providing me the opportunity to work at MPI and for his continuous support and expert advices. His open-minded attitude and refreshing enthusiasm in the discussion of scientific subjects has been particularly motivating and stimulating.

I am very grateful to my supervisor, Dr. Baerbel Langmann, for her continuous support and always encouragement. Her friendly mentoring and unconditional support made my PhD study in Hamburg a brilliant and wonderful experience. Without her supervision, especially her continuous support and encouragement, this thesis would not have been so easy.

I greatly appreciate the supervision from my advisor panel chair, Prof. Hartmut Grassl, for his open-minded discussion and generous support. His broad acknowledge and expert advices always inspire me during the discussion. I am grateful for his strong interest in my work and for examining this dissertation.

I also wish to thank two other supervisors in China, Prof. Ronghui Huang and Prof. Wen Chen, for their support and arranging the opportunity for me to study at MPI. The financial support is acknowledged from Max Planck Society under the cooperation agreement between the Chinese Academy of Science and the Max Planck Society (CAS-MPG).

I am glad to be enrolled in the International Max Planck Research School on Earth System Modelling (IMPRS-ESM) and benefited a lot from it. I am grateful to the support from the school, including Prof. Guy Brasseur, Prof. Jochem Marotzke, Dr. Antje Weitz, Dr. Almut Arneth, Ms. Hanna Stadelhofer, Ms. Cornelia Kampmann.

I wish to thank all my colleagues at MPI and classmates/friends in IMPRS, who helped me during my PhD in several aspects, in particular. Especially, I thank Dr. Stefan Hagemann and Dr. Thomas Raddatz for their useful discussion about ECHAM5 application and experiment design. I would like to thank my colleagues/friends in my research group, Angelika Heil, Elina Marmer, Mellisa Pfeffer, Manu Anna Thomas, Dr. Claudia Timmreck, Rene Hommel, for their help both in working and living.

Especially, I would like to thank my parents and my sisters and brother for their life-long love and always confidence in me. Most importantly, I thank my beloved wife, Qian Li, for her love and company through the last 6 years. Without her, I cannot imagine the completion of this thesis.



**MPI-Examensarbeit-Referenz:**

Examensarbeit Nr. 1-82 bei Bedarf bitte anfragen:  
MPI für Meteorologie, Abtlg.: PR, Bundesstr. 53, 20146 Hamburg

**MPI-Report-Referenz:**

MPI-Report Nr. 1-351 bei Bedarf bitte anfragen:  
MPI für Meteorologie, Abtlg.: PR, Bundesstr. 53, 20146 Hamburg

---

**Beginn einer neuen Veröffentlichungsreihe des MPIM, welche die vorherigen Reihen "Reports" und "Examensarbeiten" weiterführt:**

**„Berichte zur Erdsystemforschung“ , „Reports on Earth System Science“, ISSN 1614-1199  
Sie enthält wissenschaftliche und technische Beiträge, inklusive Dissertationen.**

---

<b>Berichte zur Erdsystemforschung Nr.1</b> Juli 2004	<b>Simulation of Low-Frequency Climate Variability in the North Atlantic Ocean and the Arctic</b> Helmuth Haak
<b>Berichte zur Erdsystemforschung Nr.2</b> Juli 2004	<b>Satellitenfernerkundung des Emissionsvermögens von Landoberflächen im Mikrowellenbereich</b> Claudia Wunram
<b>Berichte zur Erdsystemforschung Nr.3</b> Juli 2004	<b>A Multi-Actor Dynamic Integrated Assessment Model (MADIAM)</b> Michael Weber
<b>Berichte zur Erdsystemforschung Nr.4</b> November 2004	<b>The Impact of International Greenhouse Gas Emissions Reduction on Indonesia</b> Armi Susandi
<b>Berichte zur Erdsystemforschung Nr.5</b> Januar 2005	<b>Proceedings of the first HyCARE meeting, Hamburg, 16-17 December 2004</b> Edited by Martin G. Schultz
<b>Berichte zur Erdsystemforschung Nr.6</b> Januar 2005	<b>Mechanisms and Predictability of North Atlantic - European Climate</b> Holger Pohlmann
<b>Berichte zur Erdsystemforschung Nr.7</b> November 2004	<b>Interannual and Decadal Variability in the Air-Sea Exchange of CO<sub>2</sub> - a Model Study</b> Patrick Wetzel
<b>Berichte zur Erdsystemforschung Nr.8</b> Dezember 2004	<b>Interannual Climate Variability in the Tropical Indian Ocean: A Study with a Hierarchy of Coupled General Circulation Models</b> Astrid Baquero Bernal
<b>Berichte zur Erdsystemforschung Nr.9</b> Februar 2005	<b>Towards the Assessment of the Aerosol Radiative Effects, A Global Modelling Approach</b> Philip Stier
<b>Berichte zur Erdsystemforschung Nr.10</b> März 2005	<b>Validation of the hydrological cycle of ERA40</b> Stefan Hagemann, Klaus Arpe and Lennart Bengtsson
<b>Berichte zur Erdsystemforschung Nr.11</b> Februar 2005	<b>Tropical Pacific/Atlantic Climate Variability and the Subtropical-Tropical Cells</b> Katja Lohmann

**MPI-Examensarbeit-Referenz:**

Examensarbeit Nr. 1-82 bei Bedarf bitte anfragen:  
MPI für Meteorologie, Abtlg.: PR, Bundesstr. 53, 20146 Hamburg

**MPI-Report-Referenz:**

MPI-Report Nr. 1-351 bei Bedarf bitte anfragen:  
MPI für Meteorologie, Abtlg.: PR, Bundesstr. 53, 20146 Hamburg

**Berichte zur  
Erdsystemforschung Nr.12**  
Juli 2005

**Sea Ice Export through Fram Strait: Variability and  
Interactions with Climate-**  
Torben Königk

**Berichte zur  
Erdsystemforschung Nr.13**  
August 2005

**Global oceanic heat and fresh water forcing  
datasets based on ERA-40 and ERA-15**  
Frank Röske

**Berichte zur  
Erdsystemforschung Nr.14**  
August 2005

**The Hamburg Ocean Carbon Cycle Model  
HAMOCC5.1 - Technical Description Release 1.1**  
Ernst Maier-Reimer, Iris Kriest, Joachim Segschneider,  
Patrick Wetzel

**Berichte zur  
Erdsystemforschung Nr.15**  
Juli 2005

**Long-range Atmospheric Transport and Total  
Environmental Fate of Persistent Organic Pollutants  
- A Study using a General Circulation Model**  
Semeena Valiyaveetil Shamsudheen

**Berichte zur  
Erdsystemforschung Nr.16**  
Oktober 2005

**Aerosol Indirect Effect in the Thermal Spectral  
Range as Seen from Satellites**  
Abhay Devasthale

